MODEL BASED SIMULATION OF BROACHING OPERATION:

CUTTING MECHANICS, SURFACE INTEGRITY AND

PROCESS OPTIMIZATION

By

SAYYED ALI HOSSEINI, B. Sc., M. Sc. (Mechanical Engineering)

A Thesis Submitted in Partial Fulfillment

of the Requirements for the Degree of

Doctor of Philosophy

in

The Faculty of Engineering and Applied Science

Department of Mechanical Engineering

University of Ontario Institute of Technology

April 2013

MODEL BASED SIMULATION OF BROACHING OPERATION:

CUTTING MECHANICS, SURFACE INTEGRITY AND

PROCESS OPTIMIZATION

DOCTORE OF PHILOSOPHY (2013)   University of Ontario Institute of

Technology (UOIT)

(Mechanical Engineering)   Oshawa, Ontario

TITLE: MODEL BASED SIMULATION OF BROACHING

OPERATION: CUTTING MECHANICS, SURFACE INTEGRITY

AND PROCESS OPTIMIZATION

AUTHOR: Sayyed Ali Hosseini

B. Sc. (Mechanical Engineering)

Ferdowsi University of Mashhad, Mashhad, Iran

M. Sc. (Mechanical Engineering)

Ferdowsi University of Mashhad, Mashhad, Iran

SUPERVISOR: Professor H.A. Kishawy,

NUMBER OF PAGES: xxi, 158

Abstract

Machining operations are widely used to produce parts with different shapes and complicated profiles. As a machining operation, broaching is commonly used for the machining of a broad range of complex internal and external profiles either circular or non-circular such as holes, keyways, guide ways, and slots on turbine discs having fir-tree shape. Broaching is performed by pushing or pulling a tapered tool through the workpiece to remove the unwanted material and produce the required profile. Broaching is also acknowledged because of its high productivity and attainable surface quality in comparison to the other machining processes.

The objective of this thesis is to simulate the broaching operation and use the results to present a methodology for optimum design of the broaching tools. In the course of the presented thesis, a new B-spline based geometric model is developed for broaching cutting edges followed by model validation using 3D ACIS modeller.

To study the mechanics of cutting and generated cutting forces during broaching operation, an energy based force model is presented which can predict the cutting forces based on the power spent in the cutting system. An experimental investigation is conducted in order to confirm the estimated forces.

The integrity of the broached surface is also investigated by focusing on surface roughness, subsurface microhardness, and subsurface microstructure as three major parameters of surface integrity.

An optimization procedure for broaching tools design is presented in this thesis. A mathematical representation of broaching tooth geometry is also

presented which is used to simulate the tooth as a cantilevered beam subjected to

a distributed load. The beam is solved considering the given design constraints to

achieve optimum geometric parameters for maximum durability and performance.

Acknowledgement

Many people supported the author and contributed to this thesis in countless ways. Primarily, the author would like to express his heartfelt appreciation to his research supervisor, Professor Hossam A. Kishawy, for his leadership, advice, support, and encouragement throughout the course of this research.

Sincere gratitude is expressed to the members of the examination committee: Professor Dan Zhang, Dr. Yuping He, and Dr. Philip Koshy, for their continuing interest and helpful discussions.

The financial support jointly provided by NSERC through Graduate Research Assistantship, the Department of Mechanical Engineering through Teaching Assistantship, and University of Ontario Institute of Technology through Dean's Graduate Scholarship are thankfully acknowledged.

A tremendous amount of gratitude is also expressed towards Dr. Behnam Moetakef-Imani, whom without his help facilitating the broaching tests would not have been possible. In addition, the author would also like to thank Mr. Richard Blackwell, general manager of Buehler Canada for his great support during the sample preparation and microhardness tests, Mr. Paul Dailleboust, operations manager of Signature Aluminum Canada Inc. for preparing the aluminum samples, and Mr. Nima Zarif Yussefian for his great helps during SEM imaging.

The author would like to thank Mr. Amirmohammad Ghandehariun, Mr. Mohsen Fallah, Mr. Morteza Tahamipour, and also his colleagues at the Machining Research Laboratory (MRL) and the staff at the Faculty of Engineering and Applied

Science, University of Ontario Institute of Technology for their help and support on various occasions.

Dedicated to my father, mother, sister and

my wife, Mahboobeh

without their support and sympathy none of this would have been

possible.

Table of Contents

List of Figures

List of Tables

Chapter 1:   Introduction

1-1   Preamble

Nowadays rapid development of industries increases the need to produce new parts and machines with different levels of complexity and sensitivity in order to satisfy the market demands. Due to their flexibility and availability, machining operations are one of the primary candidates to produce such complicated profiles which are frequent features of the mechanical parts in automotive, aerospace, and power plant industries. To achieve the maximum level of performance to survive in such a fast developing atmosphere, companies invest capital funds in research and development (R&D) to increase the productivity and decrease the waste of materials. Undoubtedly, manufacturing processes and more specifically machining technology are one of the most significant targets of these researches. Machining technology is a combination of several components running together to accomplish a specific task. Motion drivers and controllers, power transmitting components, machine tool structural components and finally cutting tools are all

working together to achieve a final goal which is producing parts and products with satisfactory quality and acceptable accuracy. Cutting tool is one of the key elements in the machining operations which is in the front line of cutting action. As a result, design, optimization, and reduction of the direct manufacturing costs associated with cutting tools and machining operations are never-ending jobs in industry.

The above mentioned jobs are accomplished by the utilization of advanced cutting tools, which allows higher material removal rates. They are also accomplished by high-productivity manufacturing lines and cells which are enhanced by intelligent process controllers. Furthermore, the jobs are achieved by improving the quality and reliability of machining operations. In doing such jobs, the fundamental concepts of the process, relating components, and direct tooling costs must be thoroughly analyzed and any possibility for improvement and cost reduction must be comprehensively investigated [1].

Among all of those machining operations in which the material is removed from workpiece surface by means of a cutting tool, there is a number of machining operations in which more than one cutting edge is engaged with the workpiece simultaneously. These machining operations are known as multi-toothed cutting operations. Milling, broaching and sawing are the most popular examples of multi-toothed cutting operations.

Broaching operation is one of the relatively expensive processes among the machining operations and more specifically among multi-toothed cutting

operations. A broad range of internal and external profiles can be produced by pulling or pushing the tapered multi-toothed broaching tool through the workpiece body.

Broaching has considerable advantages in comparison to the other machining processes. Roughing, semi finishing and finishing of complex profiles can be accomplished by one stroke of the broaching tool which may need many passes in other conventional machining processes such as turning and milling [2]. It can also produce parts with good surface quality and high tolerance accuracy in one stroke. Since the number of cutting edges which are simultaneously engaged with the workpiece is higher than the other cutting tools, the chip load on each of them will be smaller and tool life is distinctively longer in comparison to the other machining processes. In addition, broaching machines are not as complicated as CNC milling or CNC turning machines; thus they are considered as simple and easy to operate machines where no highly skilled operator is required. Although broaching machines are relatively simple, broaching tools are quite complicated and consequently expensive, and they must be built uniquely for each specific purpose.

1-2   Research Motivation

Tool manufacturers and specialists realized that the direct tooling cost associated with high-speed steel (HSS) tools may well exceed 50% in a modern automotive powertrain plant if it produces the full set of gears for transmissions.

Moreover, 80% of the direct tooling cost of HSS tools are related to helical and spline broaches, so the direct tooling cost associated with HSS broaches is enormous (Figure 1-1) [1].
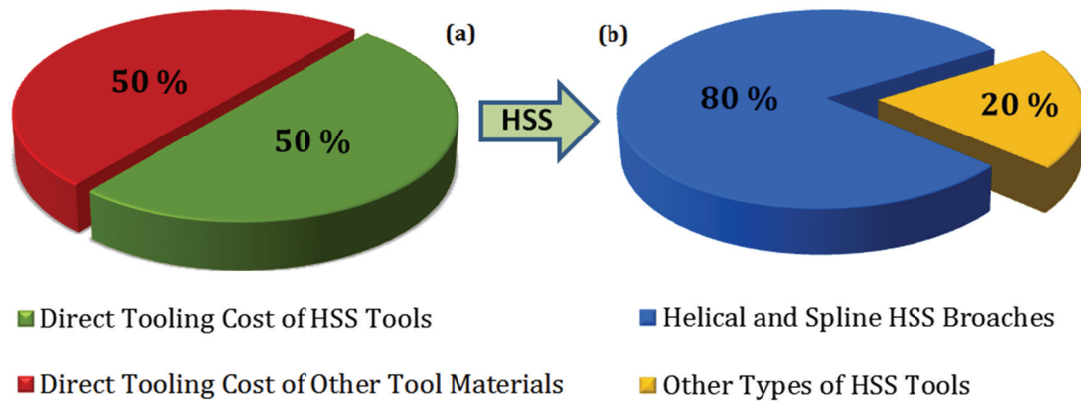
Figure 1-1: Percentage of direct tooling cost (a) HSS tools vs. other types of tool materials and (b) HSS helical and spline broaches vs. other types of HSS tools [1]

Investigating the total tooling cost of a six-speed rear wheel drive transmission with three rings demonstrates that more than half of the total tooling cost belongs to broaching tools. It clearly shows how large is the share of broaching cost among other tooling cost for a simple example. Detailed components of tooling cost for a six-speed rear wheel drive transmission are presented in Table 1-1.

Table 1-1: Total tooling cost of a six-speed rear wheel drive transmission with

three rings (Courtesy of the General Motors Business Unit of Production Service

Management)

Operation	Cost
Total tooling cost (all machining operations)	about $16
One stroke of the helical gear broach per each ring	$1.5
One stroke of the pot broach (outside spline) per each ring	$1.5
Total broaching cost	(1.5+1.5)*3 = $9

One of the main reasons for the expensive cost of broaching tools is that, unlike turning and milling tools which are available on the shelves, broaching tools must be ordered to be built based on the desired geometry of profile to be cut which imposes delay on the starting of the process and increases the total manufacturing costs.

In spite of its importance in industry, surprisingly, few research activities on HSS tools and more specifically on broaching have been carried out over the last twenty years [3-5]. No significant advances were made since the 1970s when powder metallurgy (PM) HSS was introduced. This is because of the common perception that HSS is an obsolete tool material (known since the end of the 19th century), which should have been substituted by more advanced tool materials a long time ago. Reality, however, shows otherwise, as HSS possesses a unique combination of properties (primarily hardness and toughness) which are essential for complex gear manufacturing tools. Compared to any other cutting tools, HSS

broaches are highly productive and precise tools that meet the requirements of the cycle time in mass production such as in the automotive industry. In addition it meets the requirements for high precision in the power and aerospace industries where slots for blades in the turbine disk are made using the so-called Christmas tree broaches [1].

Another important feature of HSS form broaches is their relatively low reliability that often makes broaching a bottle-neck operation in many modern powertrain plants. Generally, the low reliability of broaching operations is due to the absence of research on the design and geometry of such complex tools in spite of the fact that broaching tools and broaching operation are [1]:

- The most expensive and one of the most complex tools in the automotive industry that account for the significant tooling cost.

- Often producing the final surfaces to be used in service, i.e., directly responsible for quality and reliability of the product.

- Often bottle-neck operations due to low reliability of broaching tools.

Various broaching tools with different geometries are widely used in industry. Although the current state of knowledge in modelling the broaching operation is capable of simulating the cutting edges for broaching tools with simple geometry, like the tools which are utilized in keyways and holes broaching, the ability to achieve reliable simulation for more complicated broaching tool geometry is still limited. In order to design a broaching tool, a comprehensive

geometric model to simulate any desired geometry of cutting edge is essential and a reliable force model to predict the realistic cutting forces is required.

1-3   Scope of the Work and Thesis Outline

The mechanics of broaching operation is thoroughly investigated in this thesis. The thesis consists of four main sections.

The first part is focussed on geometric aspects of broaching operation and geometry of broaching tools. A model is proposed to express the cutting edge of a broaching tool as a B-spline parametric curve and utilizes the flexibility of parametric curves to calculate the geometry of engagement between tool and workpiece. The geometric model is further validated by utilizing 3D ACIS modeller as a geometric engine. As the broaching tool removes the material, the geometric engine creates the sweep volume of the cutting edges and updates the geometry of the workpiece. In the next step, the geometry of engagement between tool and workpiece is automatically extracted using the software capabilities. The results are then compared to check the validity of the geometric model.

In the second part, an energy based force model based on power spent in cutting system is proposed to predict the generated cutting forces during the broaching operation. The predicted cutting forces are further used to design the broaching tools.

In the third part of this thesis, newly generated broached surface is investigated by focusing on surface roughness, subsurface microhardness, and

subsurface microstructure. Integrity of broached surface is important because the broaching is considered as a finishing operation and normally no further process is performed to improve the surface quality. A three dimensional white light interferometer microscope is applied to provide a 3D pattern of the workpiece surface before, during, and after broaching. The effect of successive cutting edges on the variation of microhardness beneath the broached surface is also investigated. The machined surfaces are also examined using SEM to study the effect of broaching operation on the subsurface microstructure.

The fourth part of this thesis utilizes all of the developed works to present a methodology to optimize the design procedure of broaching tools.

Chapter 2:   Literature Review

2-1   Preamble

This chapter consists of five main sections describing the previously published work in the field of mathematical and geometric modelling of cutting edges, cutting force modelling, process optimization, and surface integrity with main focus on broaching operation, broaching tools, and their special features.

2-2   Mathematical Modelling of the Cutting Edge

Machining or in general metal cutting operation is the process of cutting or removing a layer of metal from the body of workpiece to obtain the desired geometry. Metal cutting is executed by means of a wedge shape cutting edge to separate a blank of workpiece into chip and part where the former is withdrawn and the latter is kept to perform the predefined task. Depending on the type of applied processes, the final part has a desired shape with a certain level of surface quality and dimensional accuracy. Regardless of the tool geometry and process

specification, machining can be classified under two main categories: orthogonal cutting and oblique cutting [6, 7]. Orthogonal cutting is defined by a straight cutting edge which is perpendicular to the direction of cutting velocity while in oblique cutting the cutting edge is considered a straight line, in the simplest form, which has an inclination angle with the normal direction to the cutting velocity.

Developing a mathematical model to express the geometry and shape of the cutting edge is always a matter of interest for many researchers and considerable efforts have been made to achieve it. Some of the most distinguished works toward achieving this goal are presented in the late 90's and early 2000's. A profile of the helical cutting edge for cylindrical flat end mill based on the number of flutes, helix angle, and tool diameter was presented by Budak et al. [8]. The geometry of cutting edge combined with milling force coefficients which are extracted from orthogonal cutting database were further utilized in the estimation of cutting forces for end milling operation. The same procedure was presented by Lee and Altintas [9] for simulation of ball end milling process. They presented a detailed mathematical description of ball end mill tool on a 3D Cartesian coordinate system. A general geometric simulation of any arbitrary end mill tool either helical or inserted was proposed and developed by Altintas and Engin [10-12]. They expressed the geometry of the helical cutting edge along the flute for any arbitrary inserts mathematically. This trend were followed by Merdol and Altintas [13] presenting a mathematical model for serrated cylindrical and serrated tapered ball end mill. They considered the effect of serrations on the geometry of helical cutting edge for

rough end mills where removing a bulk load of material is required. The same geometric models can be found for turning, drilling [14] and boring operation [15] where the geometry of the applied tools is discussed in detail. These are just a few samples of published paper about milling, turning, drilling and boring as examples of conventional machining processes.

Although broaching is well defined in industry, a limited number of research works have been reported in the open literature. In 1960 Monday [16] presented the most comprehensive source describing the broaching technology, geometry of cutting tool, and different applicable types of machines in broaching. The collection of works representing the usefulness of the broaching operation was edited and published by Kokmeyer [17].

Generally speaking, in comparison to milling and turning operation, the number of published studies investigating broaching operation is quite limited and no mathematical model was presented by the above mentioned research works that can be used to generate a cutting edge for a sample broaching tool.

2-3   Geometric Modelling of the Cutting Edge

Geometric modeling techniques offer a broad range of capabilities to complete a 3D representation of cutter and workpiece [18] where the appropriate geometric simulation of machining process need to be accurately represented. Geometric modelling can be divided into three main categories: Wire-frame modelling, Surface modelling and Solid modeling. Wire-frame modelling is the

simplest category which represents the object using points and lines. The surface modelling is more complete in comparison to the wire-frame modelling and it can be used for representing open objects like sculptured and free form surfaces. Solid modelling is the most complete and state of the art category in which an object can be presented in its real and complete form. Solid modelling can be achieved using three different approaches. Spatial enumeration by means of octrees, Constructive solid geometry (CSG) and Boundary representation (B-rep) [19].

Solid modeling techniques in their early applications were mostly applied to represent engineering components with very simple geometric features such as cuboids, quadrics and the torus [20]. However, development of computers over the years, introduced high capabilities in graphical representation, and has promoted the applicability of computer aided design (CAD) systems and solid modeling techniques. Nowadays, representation and manipulation of blended and complicated surfaces is one of the major outstanding abilities of solid modeling systems.

The application of CAD systems and solid modeling techniques in the simulation of cutting operations is extensively investigated by Wang [21], Takeuchi et al. [22], Altintas et al. [23], Spence [24], Boogert et al. [25], Imani [19], Imani et al.[18], Sadeghi et al. [26], Fleisig and Spence [27] and Merdol and Altintas [28].

The only research works applying parametric representation and solid modelling techniques to simulate broaching operation are presented by Hosseini and Kishawy [29] and Hosseini et al. [30].

2-4   Prediction of Cutting Forces

Prediction of cutting forces is an essential part of each machining simulation. The machining tests are normally expensive and time consuming. Performing the simulations in a virtual environment is an economic way to alter the variables, repeat the tests, and achieve optimum cutting conditions. It can be also utilized for design of the cutting tools as well as the optimization.

One of the earliest researches in this field was performed by Gilormini et al. [31] who compared the cutting forces in a single broaching to the forces in slotting and tapping process. Sutherland et al. [32] proposed a force model for broaching based on the oblique analysis to determine the forces in the gear broaching process. Their model showed the relationship between contact area, chip load and cutting force. Sajeev et al. [33, 34] investigated the effects of broaching parameters on the tool and workpiece deflections and the final shape of the broached geometry. Budak [35] examined the performance of broaching tools used for broaching of waspaloy turbine discs with fir-tree profile based on the monitoring of force and power. It has been shown that for majority of the investigated tools, the distribution of load among the different sections of broaching tool was not uniform which leads to uneven tool wear. The research on condition monitoring of

broaching tools was followed by Axinte and Gindy [36] and Axinte et al. [37]. They monitored the condition of broaching tool by mounting several sensors in different positions of the tool. The chipped or worn out tooth was identified by analysing the extracted force pattern. Recently Hosseini and Kishawy [29] presented a general force model for orthogonal broaching using B-spline interpolation of cutting edge. By taking geometric flexibility of B-spline curves, their model was capable of modeling any arbitrary orthogonal broaching cutting edge geometry as well as calculating the chip load for different cutting conditions. The above mentioned model was further developed by Kishawy et al. [1] by considering the energy spent on the cutting system.

2-5   Broaching Tool Design and Optimization

The ultimate goal of each simulation is to enhance the level of understanding about the process and utilize it to promote the design procedure. One of the key factors that makes the design of broaching tool a very critical job is adjustability of the cutting parameters.

In other conventional machining process e.g. milling and turning, cutting parameters like speed, feed, and depth of cut can be easily changed during the operation; therefore, in case the cutting tool is not properly selected, these parameters can be adjusted to improve the process and make the production line running efficiently. Figure 2-1compares the adjustability of cutting parameters in broaching versus turning and milling.

Turning	Adjustability	Milling	Adjustability	Broaching	Adjustability
Spindle Speed (rpm)	✓	Spindle Speed (rpm)	✓	Cutting Speed (mm/min)	✓
Feed (mm/rev)	✓	Feed (mm/rev)	✓	Feed	✗
Width of Cut (mm)	✓	Axial Depth of Cut (mm)	✓	Axial Depth of Cut	✗
		Width of Cut	✓	Width of Cut	✗
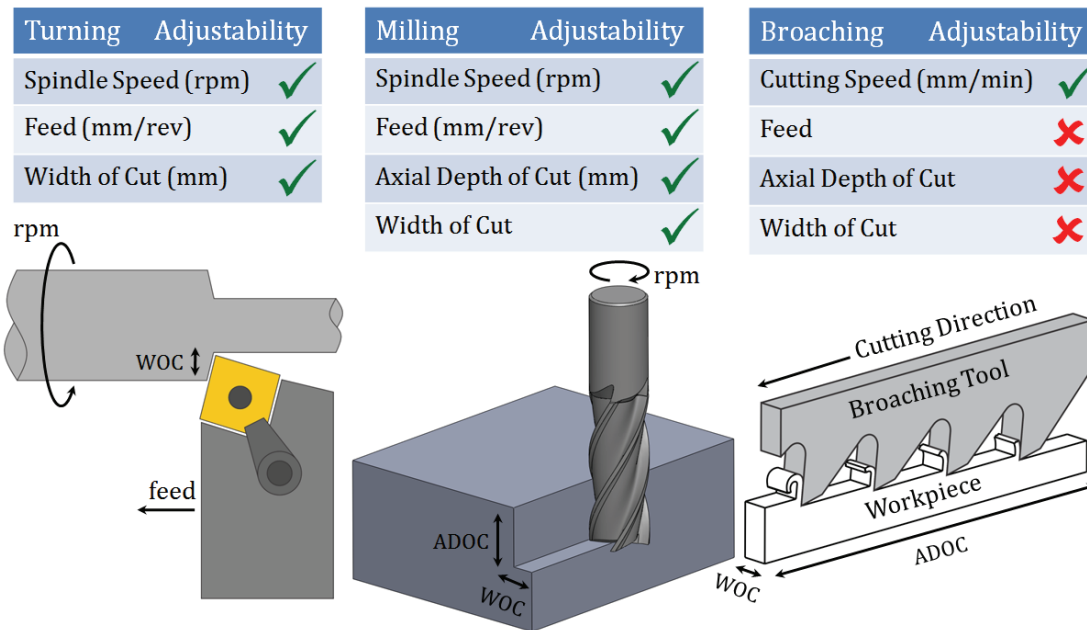
Figure 2-1: Adjustability of cutting parameters in turning, milling and broaching

As it can be seen in Figure 2-1, in broaching operation, none of the cutting parameters but cutting speed can be altered during the process when a certain broaching tool is applied. Feed cannot be changed because the feed action in broaching operation is performed by the difference between heights of the successive teeth. The axial depth of cut (axial length of the engagement between tool and workpiece) and width of cut cannot be altered because these parameters are determined by the length and width of the workpiece (or profile to be cut). As a result of all of the above mentioned restrictions, proper design of a broaching tool plays an important role in saving money and optimizing the production process.

Terry et al. [38] presented a system for optimal design of broaching tools. They presented the factors that affect productivity in broaching operation. They

also explained the design constraints and the priority and importance of each one and how to select these constraints. A finite element was also used to predict the tooth deflection and verify the experimental data in order to create the general rules for designing broaching tools. Recently Ozturk and Budak [39, 40] performed Finite Element Analysis to calculate the stresses in the broaching tool during the cutting process. The developed model was used to simulate the broaching process and predict the generated stresses in the tool to improve the tool design. They studied broaching of fir-tree profiles, simulated the cutting forces as well as the tool stresses, and applied the results to improve the broaching tool design. Later, Kokturk and Budak [2, 41] performed an optimization on the front profile of the broaching tooth. The cutting conditions were changed in their study, until the predefined constraints can be satisfied. The optimized conditions are then used to improve the broaching process.

2-6   Surface Integrity

Surface integrity is a term which is usually applied to define the quality of the workpiece surface after being manufactured. The surface and subsurface layer of workpiece is highly affected by a combination of stress and generated temperatures during machining operations [42]. This harsh situation can lead to defects, alterations of the microstructure or microhardness. It may cause plastic deformation, craters, inclusions, surface cracking, folds, and residual stresses in the finished part [5, 43]. The amount of these imperfections is related to the

mechanical and thermal energy generated on the machined surface during machining operations. The machining induced defects can considerably change the reliability and durability of the machined part [44]. Hence, it is necessary to understand the effects of each machining operation and its parameters on the surface characteristics of machined part before new machining process is deployed.

The classification of surface integrity parameters is not consistent through the open literature; however, it can be generally divided into two main categories: Surface topography and Surface layer characteristics. Surface roughness, waviness, and form errors are the major contributors of surface topography while subsurface microhardness, residual stress, phase changes, recrystallization, and cracks determine the surface layer characteristics [43].

In 1990, Konig et al. [4] presented a research work investigating the machining of hard materials with geometrically defined cutting edges. They also studied the mechanics of chip formation and surface integrity in hard machining. The residual stresses beneath the turned surface of austenitic stainless steel was investigated by Jang et al. [45]. Effects of several cutting parameters such as depth of cut, feed, cutting speed, and tool geometry were investigated in this research work. A comprehensive research work about the advancement in different techniques of surface integrity measuring was published by Lucca et al. [46]. Several research works that studied machining and their effects on the integrity of machined surface can be found in [47-52].

Broaching has not received considerable attention in the field of surface integrity. In 1985, He et al. [3] studied the effects of broaching operation on the surface integrity of titanium alloy. Generally, plastic deformation and diffusing oxygen and nitrogen due to the high temperature (600°C- 700°C) during machining are two major factors affecting the subsurface microhardness of titanium and its alloys; however, when broaching is performed on titanium and its alloys, subsurface microhardness is predominantly affected by plastic deformation where the temperature is not as high as other machining operations due to low cutting speed [3]. Kishawy et al. [1] measured the subsurface microhardness beneath the broached surface for brass and steel AISI 12L14. The results confirmed the trend of the previously published work by He et al. [3] where almost 100 μm beneath the broached surface is highly affected by plastic deformation increasing the microhardness locally.

2-7   Summary

Most of the above mentioned studies dealt with milling and turning operations as two widely used machining processes. Broaching is still suffering due to a lack of knowledge about mechanics of the process, tool geometry, design procedure, and the resultant surface integrity. The presented thesis is an attempt to broaden the knowledge about broaching operation through analysing the geometry of process and presenting a design procedure for broaching tools considering the generated cutting force and surface integrity.

Chapter 3: Broaching Tool Geometry

3-1   Preamble

Cutting tool is the heart of any machining operation which serves in the front line of cutting action. The broaching tools are manufactured based on the fact that roughing, semi-finishing, and finishing must be accomplished by one stroke of the machine. This chapter presents the different possible types of broaching tools and their basic geometric features.

3-2   Geometry of Broaching Tool

Geometry of broaching tool is quite complicated due to the nature of the process. In other conventional machining operation such as turning and milling, the desired workpiece geometry is generated by the relative motion of tool and workpiece; therefore, the final geometry of the part is not similar to the geometry of cutting tool. As a result, milling tools either helical or inserted are generally similar with some slight differences in their geometry. Having known the tool

diameter, number of flutes, and helix angle, the helical milling tool can be geometrically built. The simpler procedure can be followed for the inserted milling or turning tools where the cutting edges consist of one or more inserts which are normally linear, circular, square, or triangular. Figure 3-1 demonstrates the geometric simplicity of milling and turning tools.
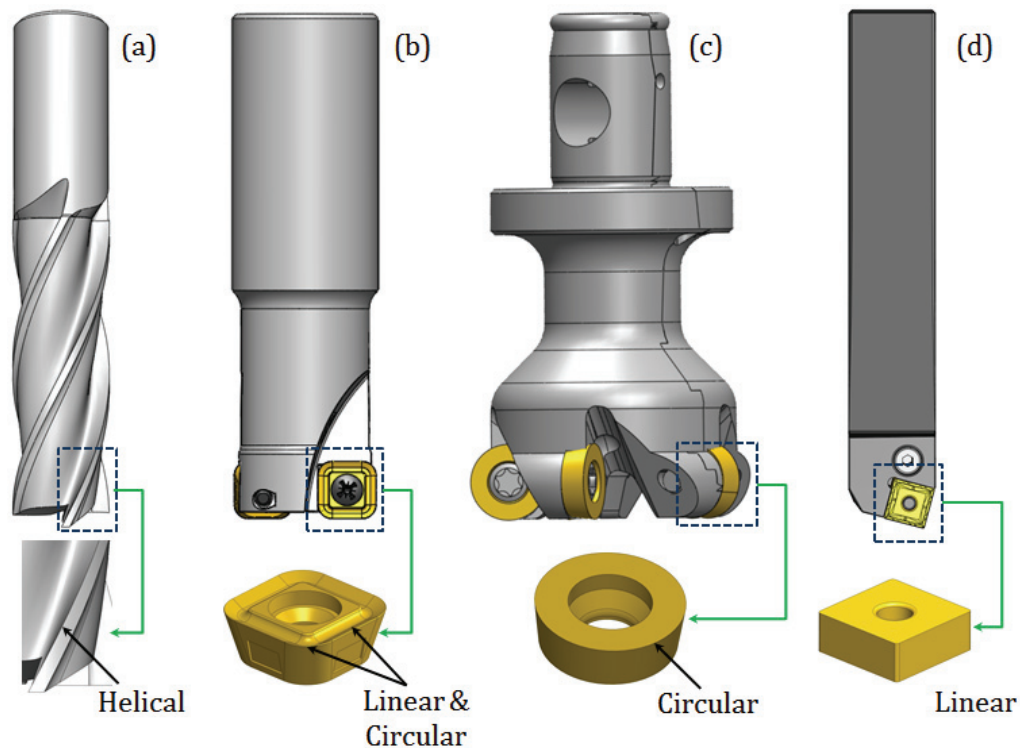
Figure 3-1: Geometric simplicity of cutting edge for (a) end mill tool. (b) indexable end mill tool. (c) face mill tool. (d) turning tool

In contrast with the above mentioned tools, broaching tools have different geometries corresponding to the profile to be formed on the workpiece. Two main categories are distinguished among broaching tools which are internal and external (surface) broaches [16]. Internal broaching is performed by means of a

tool with the exterior shape matching the required profile to be cut on the workpiece. This tool is pushed or pulled through a hole which is previously drilled or cored on the workpiece to let the tool go through and generate the requested profile. In external broaching, the workpiece is clamped firmly to the machine table using a fixture and tool which has a profile to suit the required external profile passes over it to remove the material from the workpiece surface [16].

Each broaching tool has two different profiles: a side profile and a front profile. The front profile varies according to the broad range of geometry to be cut while the side profile is almost similar in all broaching tools. Figure 3-2 demonstrates the variety of front profile in broaching tools.
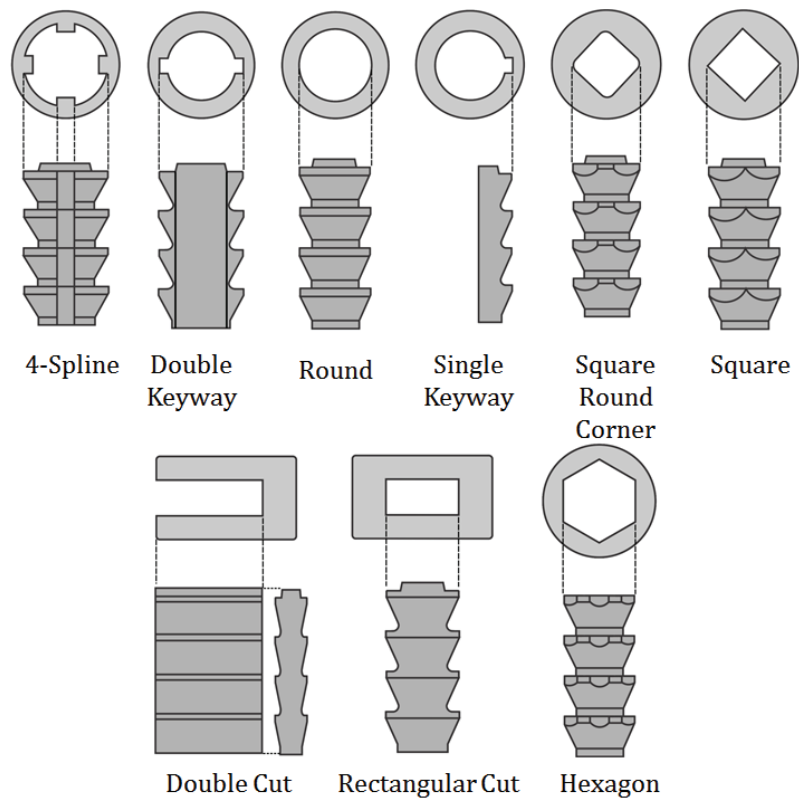
Figure 3-2: Variety of front profiles in broaching tools [53]

As it can be seen from Figure 3-2, the front profile categorically depends on workpiece geometry and must be designed accordingly. The front profile of broaching tools varies from a single keyway to hexagonal shapes. It can be even more complicated when machining of fir tree on turbine disks is required. However, as it was previously mentioned, the side profiles are almost similar in the broaching tools. Figure 3-3 shows the geometry of side profile for a typical broaching tool.
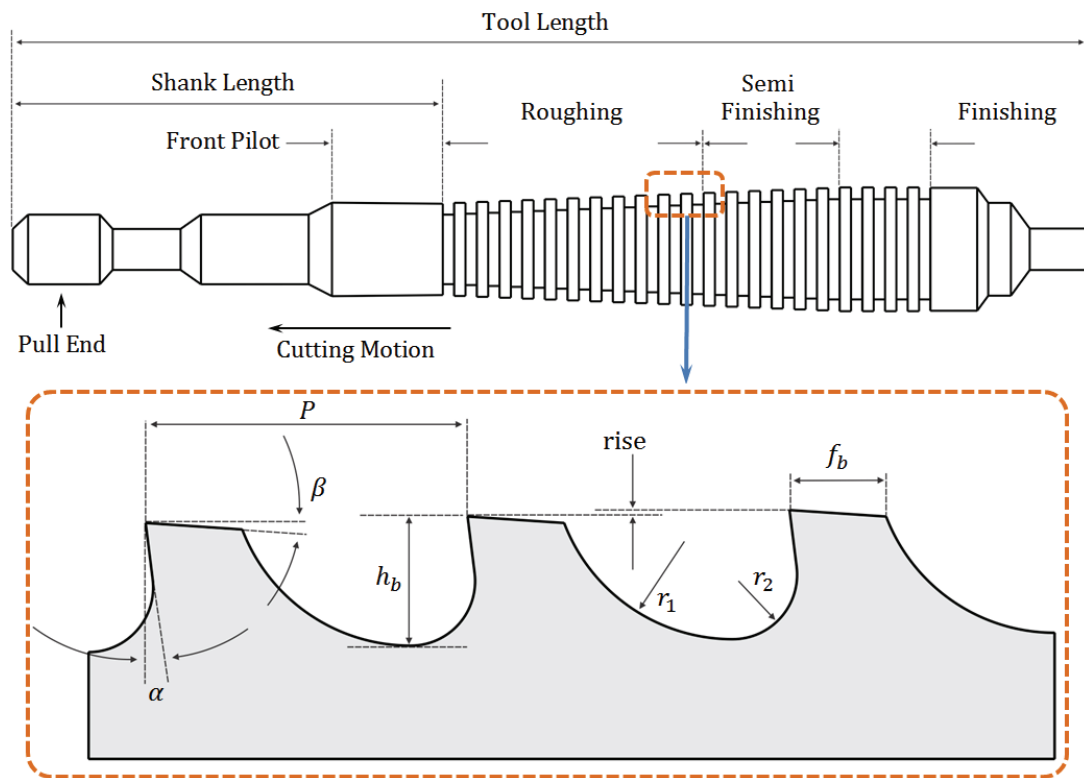
Figure 3-3: Typical geometry of side profile for broaching tools

The side profile of the broaching tool is determined by the key features of the tool such as pitch length (P), tooth height (h_b), land (f_b), rake angle (α), clearance angle (β) and rise per tooth.

3-2-1 Tool Length

The length of a broaching tool is determined by the amount of material to be removed and mechanical properties of the workpiece [54]. The length is limited by the parameters of broaching machine such as power, stiffness, maximum length of stroke, and maximum length of the tool that can be fitted into the machine's ram.

3-2-2 Pitch Length

Pitch length (P), is the distance between two successive teeth on a broaching tool which is determined by the cutting length and greatly influenced by the type of workpiece material. Greater pitch length is required during broaching long workpieces to accommodate the produced chip. Tooth pitch on semi-finishing and finishing teeth may be smaller to reduce the overall tool length. To preserve the dynamic stability of the process and prevent chatter vibration, the pitch is calculated so that at least two or preferably more teeth are engaged with the workpiece simultaneously [16, 55]. The pitch length is an important parameter because the total number of teeth, the construction of teeth on a broaching tool, and the number of simultaneously in-cut teeth are directly determined by this parameter [43].

3-2-3 Land Length

The thickness of the tooth at its tip level is called land length (f_b) which determines the tooth strength against the stresses during broaching operation.

3-2-4 Rake Angle

Rake angle (α), is the angle between the cutting face and the normal direction to the workpiece surface. Although positive, negative, and zero rake angles are commonly used in machining operations, the rake angle in broaching tools is normally positive. The positive rake angle sharpens the cutting tool, reduces the power requirement and helps the chip flow over the rake face. It must be noted that small rake angles increase the tooth strength and cutting forces while big rake angles decrease the cutting force and tooth strength. In order to strike a balance between having moderate cutting forces and adequate strength the rake angle must be selected within optimum range (see Table 3-1)

Table 3-1: Rake angle for cutting and finishing teeth of broaching tools [55]

Work Material	Rake Angle α (deg)	
	Cutting	Finishing
Steel	15	5
Grey cast iron	10	5
Malleable iron	10	-5
Aluminum and its alloy	20	20
Bronze and brass	5	-10

3-2-5 Clearance Angle (Relief Angle)

The clearance angle (β), is the angle between the back of the tool and the horizontal line (normally parallel to the machined surface) [16]. Clearance angle is built to provide sufficient space between the workpiece and back of the tool to

eliminate interference and reduce friction. Normally the entire land is relieved by grinding to produce clearance angle on roughing and semi finishing teeth. However, on the finishing teeth, only a part of the land at the far side is grounded to form the clearance angle and another part of the land immediately behind the cutting edge is left straight [55] which allows re-sharpening without altering the tooth size. The clearance angles for cutting teeth of a broaching tool are presented in Table 3-2.

Table 3-2: Clearance angle for cutting, semi finishing, and finishing teeth of broaching tools [55]

Type of Broach	Clearance Angle β (deg)		
	Cutting	Semi Finishing	Finishing
Round and spline	3	2	1
Keyway	3	2	2
External surface	3	2	2
Adjustable table	3 to 4	3 to 4	3 to 4
Non- adjustable table	3 to 4	2	1 to 2

3-2-6 Rise per Tooth

The rise per tooth, also known as tooth rise, or feed per tooth is the difference between the heights of the two successive teeth which determines the undeformed chip thickness or depth of material to be removed by each tooth. A large tooth rise increases the amount of material removed by each tooth and imposes a higher level of cutting force and stresses to the cutting edge. It also

increases the required machine power. In contrast, too small rise per tooth causes rubbing between the tooth and the workpiece surface and will result in glazed or galled surface finish.

3-2-7 Gullet Space

Gullet space which is the empty space between two following teeth is defined by (r_1) and (r_2) (see Figure 3-4). Gullet space is mainly used to retain the chip during cutting until the tooth leaves the workpiece. Once the broaching tool engages with the workpiece, chip is captured between tool and workpiece and it is maintained in the gullet space until the tooth finishes the cut and leaves the workpiece. Small gullet space may cause tool breakage due to the lack of space to keep the removed chip and may also lead to poor surface finish due to the rubbing of removed chip to the machined surface. In contrast, a large gullet space makes the tooth very slender and decreases the strength and stability of the broaching tool.

3-3   Mathematical Model of Side Profile

A broaching tool must be accurately designed to achieve optimum geometry. In order to design a broaching tool, rake angle, clearance angle, land, pitch length, tooth height, gullet space, number of teeth and finally tool length must be identified by relating these geometric parameters mathematically. A mathematical model is presented in this section. The presented model expresses the geometry of

side profile mathematically and it can be used for further design and optimization of the broaching tool. Figure 3-4 demonstrates the design parameters of the side profile for sample broaching tool. The land length and tooth height are normally considered as a function of pitch length and their magnitudes are selected as $f_b = 0.3P$ and $h_b = 0.4P$ [55].

Figure 3-4: Design parameters of the side profile for sample broaching tool

To calculate the gullet space, (r_1), (r_2), (A), and (B) must be identified. (r_2) is the smaller radius of gullet which can be expressed as:

$$r_2 = \frac{h_b}{2} = \frac{0.4P}{2} = 0.2P \tag{3-1}$$

The vertical distance between the end of the land (o'') and the bottom of the gullet (o) (see Figure 3-4) is represented by (B) as follows:

$$B = o''c = h_b - f_b \times \tan\beta - rpt = 0.4P - 0.3P \times \tan\beta - rpt =$$
$$P[0.4 - 0.3 \times \tan\beta] - rpt \tag{3-2}$$

In equation 3-2, (rpt) is the rise per tooth which is corresponding to the feed in Figure 3-4. In addition to the (B), (A) is the horizontal distance between the end of the land (o'') and the bottom of the gullet (o). The point (o) is located where circle (c_1) with radius (r_1) and circle (c_2) with radius (r_2) meet each other tangentially. The distance (A) can be written as:

$$A = P - f_b - (r_2 - x'') \tag{3-3}$$

$$x'' = x + x' = [r_2 \times \tan\alpha\,(1 - \sin\alpha)] + [r_2(1 - \cos\alpha)] = r_2[\tan\alpha + 1 - \sec\alpha]$$

$$5° \leq \alpha \leq 20° \Rightarrow \sec\alpha \approx 1 \Rightarrow x'' = r_2 \times \tan\alpha \tag{3-4}$$

Parameter (A) will be revealed by replacing (x'') from equation 3-4 into equation 3-3.

$$A = P - f_b - \left(r_2 - x^{''}\right) = P - 0.3P - (r_2 - r_2 \tan \alpha) =$$

$$P(0.5 + 0.2 \tan \alpha) \tag{3-5}$$

The next step in the completion of mathematical simulation of the broaching tool is finding the bigger radius of the gullet (r_1). Using triangle $c_1 oo'$ knowing that o' is located at the middle of oo'':

$$oo'' = \sqrt{A^2 + B^2} = \sqrt{(0.5P + 0.2P \tan \alpha)^2 + (0.4P - 0.3P \tan \beta - rpt)^2} \tag{3-6}$$

In triangle $c_1 oo'$

$$\sin \gamma = \frac{oo'}{c_1 o} = \frac{oo'}{r_1} \Rightarrow r_1 = \frac{oo'}{\sin \gamma} = \frac{oo''}{2 \sin \gamma} = \frac{oo''}{2 \left(\dfrac{B}{oo''}\right)} = \frac{oo''^2}{2B} \tag{3-7}$$

In equation 3-6, the terms containing $(\tan^2 \alpha)$ and $(\tan^2 \beta)$ are very small and consequently negligible as follows:

$$5° \leq \alpha \leq 20° \rightarrow 3.1 \times 10^{-4} \leq 0.04 \times \tan^2 \alpha \leq 5.3 \times 10^{-3}$$

$$\tag{3-8}$$

$$1° \leq \beta \leq 4° \rightarrow 2.7 \times 10^{-5} \leq 0.09 \times \tan^2 \beta \leq 4.4 \times 10^{-4}$$

As a result, by substituting equation 3-6 into equation 3-7, the bigger radius of the gullet can be expressed as follows:

$$r_1 = \frac{oo''^2}{2B} = \tag{3-9}$$

$$\frac{P^2(0.41 + 0.2 \tan \alpha - 0.24 \tan \beta) + rpt^2 - 0.8P \times rpt + 0.6P \tan \beta \times rpt}{2P[0.4 - 0.3 \tan \beta] - rpt}$$

Thickness of the cutting edge is another important feature of the broaching tool which is varying along the tooth from tip to root. Thickness must be clearly identified for each section of the tooth and must be used in designing the tool features to provide the required strength during the cutting process. The tooth can be divided into three main segments: (a) tooth tip, (b) tooth body and (c) tooth base. Figure 3-5 depicts the variation of thickness along a tooth for a broaching tool from tip to root. As can be seen from previously developed equations, all of the geometric features of a broaching tool are mathematically expressed as a function of pitch length, rake angle and clearance angle.
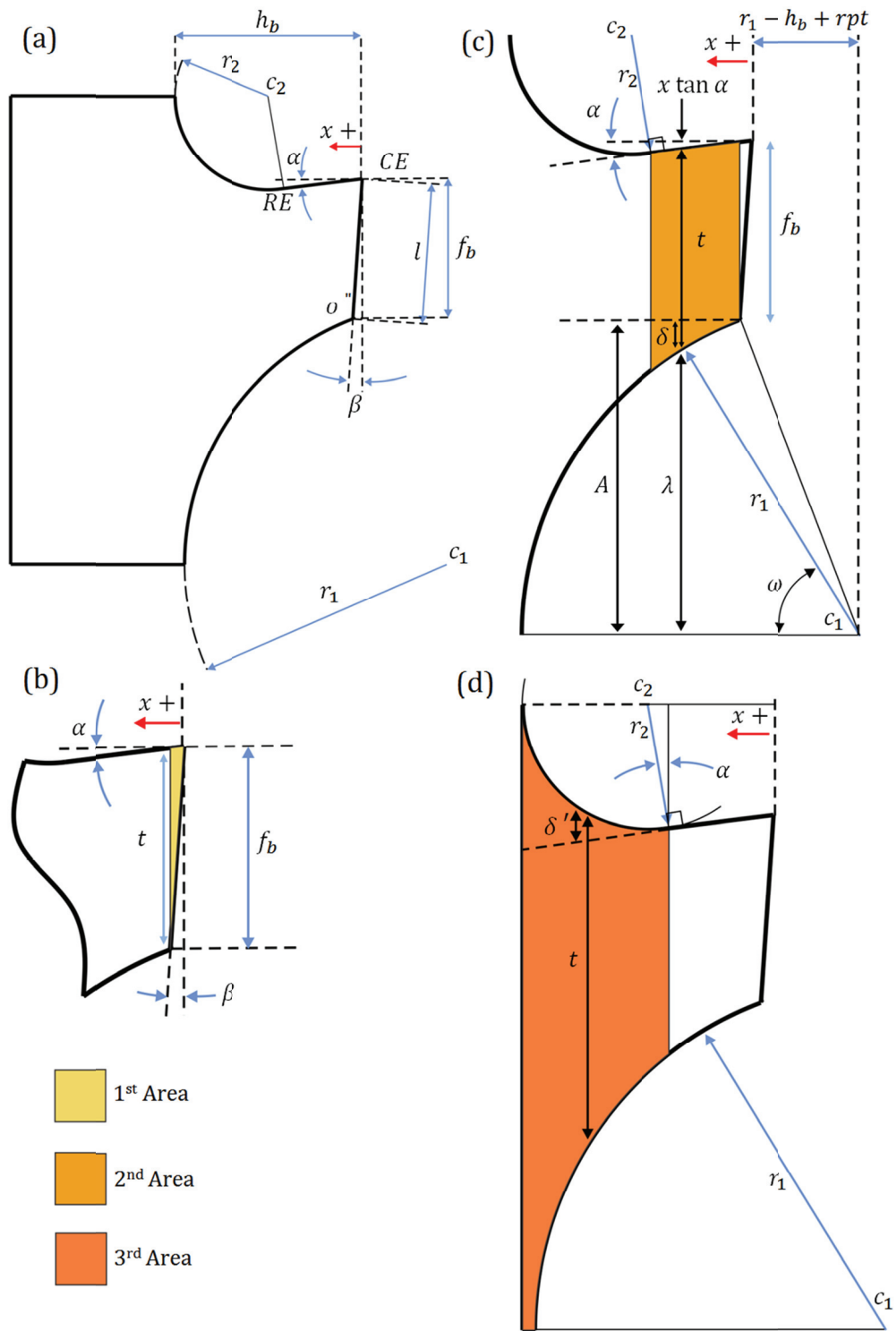
Figure 3-5: Variation of thickness for a single tooth. (a) general geometry and coordinate system. (b) tooth tip. (c) tooth body. (d) tooth root

The variation of tooth thickness can be mathematically modelled by selecting the tool tip as the origin of the coordinate system. Considering

$$t = x(\cot\beta - \tan\alpha) \qquad 0 \le x < f_b \tan\beta$$

$$t = f_b - x\tan\alpha + \delta \qquad f_b\tan\beta \le x < r_2(1 - \sin\alpha) \qquad \text{(3-10)}$$

$$t = f_b - x\tan\alpha + \delta + \delta' \quad r_2(1 - \sin\alpha) \le x \le h_b(= 2r_2)$$

In equation 3-10,

$$\delta = A - \lambda$$

$$\lambda = r_1\sin\omega = r_1\sin\left[\cos^{-1}\left(\frac{x + r_1 - h_b + rpt}{r_1}\right)\right] \qquad \text{(3-11)}$$

$$\delta' = r_2\cos\alpha + [x - r_2(1 - \sin\alpha)]\tan\alpha - \sqrt{r_2^2 - (r_2 - x)^2}$$

3-4   Summary

A mathematical formulation is presented in this chapter to describe the geometry of the side profile for a sample broaching tool. The mathematical model formulates the geometry of side profile and it can be further used in optimization process.

Chapter 4:   Geometric Simulation of Cutting in Broaching Operation

4-1   Preamble

In this chapter, general aspects of cutting in broaching operation are presented. A single cutting edge of a broaching tool is expressed as a B-spline parametric curve and chip load and length of the engagement between tool and workpiece is calculated. The presented model has a great flexibility to simulate any geometry and it can be applied for the entire broaching tools.

4-2   Mechanics of Cutting in Broaching

Similar to almost all of the cutting processes, the cutting force in broaching can be expressed generally by three differential components which are directly related to chip load area and the contact length between cutting edge and workpiece such as [56]:

$$df_t = K_{tc} \times h_i \times dl_i + K_{te} \times dl_i$$

$$df_f = K_{fc} \times h_i \times dl_i + K_{fe} \times dl_i \qquad (4\text{-}1)$$

$$df_r = K_{rc} \times h_i \times dl_i + K_{re} \times dl_i$$

Figure 4-1 depicts the main features of oblique broaching and shows the force components generated during the chip removal process.
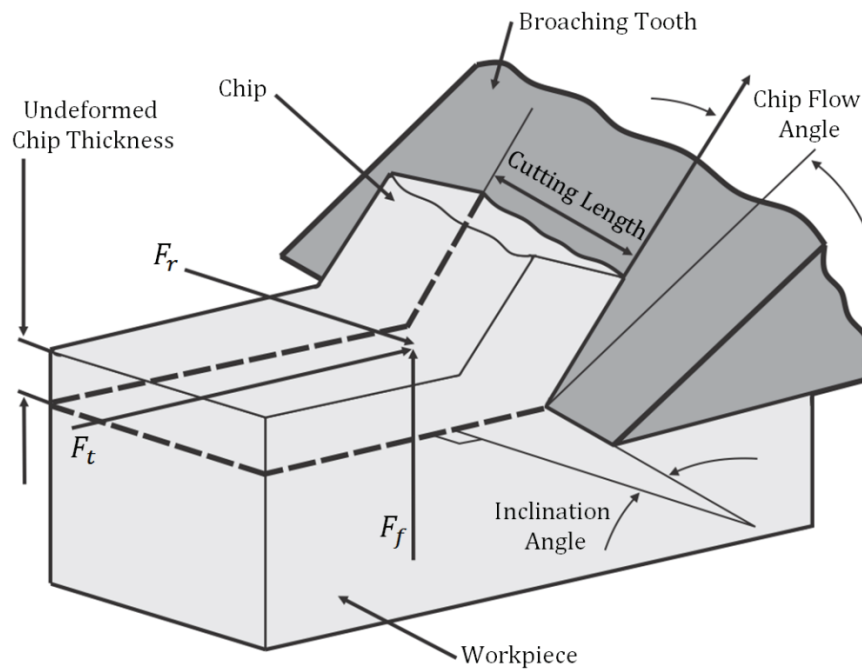
Figure 4-1: Mechanics of oblique broaching

In equations 4-1, (df_t) is the differential component of tangential force, (df_f) is the differential component of feed force and (df_r) is the differential component of radial force. (dh_i) and (dl_i) are chip thickness and length of the cut for infinitesimal element along the cutting edge respectively. (K_c) and (K_e) are cutting and edge constants while the subscripts (t, f, r) refer to the tangential, feed and

radial directions [56]. (df_r) appears when cutting edge has an oblique (inclination) angle with the cutting direction which is the case in oblique broaching. The total tangential, feed and radial components of cutting force for each edge can be calculated by integrating those components along the cutting edge. Equation 4-2 shows the force integration along the cutting edge from the start to the end of engagement.

$$F_t = K_{tc} \int_{i=0}^{l} h_i \times dl_i + K_{te} \int_{i=0}^{l} dl_i$$

$$F_f = K_{fc} \int_{i=0}^{l} h_i \times dl_i + K_{fe} \int_{i=0}^{l} dl_i \qquad (4\text{-}2)$$

$$F_r = K_{rc} \int_{i=0}^{l} h_i \times dl_i + K_{re} \int_{i=0}^{l} dl_i$$

In equation 4-2, $(h_i \times dl_i)$ represents a differential element of the chip area which is removed by the cutting edge. Equation 4-2 can be re-written in the following format:

$$F_t = K_{tc} \int_{i=0}^{l} dA_i + K_{te} \int_{i=0}^{l} dl_i$$

$$F_f = K_{fc} \int_{i=0}^{l} dA_i + K_{fe} \int_{i=0}^{l} dl_i \qquad (4\text{-}3)$$

$$F_r = K_{rc} \int_{i=0}^{l} dA_i + K_{re} \int_{i=0}^{l} dl_i$$

In the above equation, $(\int dA_i)$ is chip load in front of the cutting edge and $(\int dl_i)$ is the length of engagement between cutting edge and workpiece. Figure 4-2 demonstrates the infinitesimal element of cutting edge, chip load and contact length for an arbitrary fir tree broaching tool.
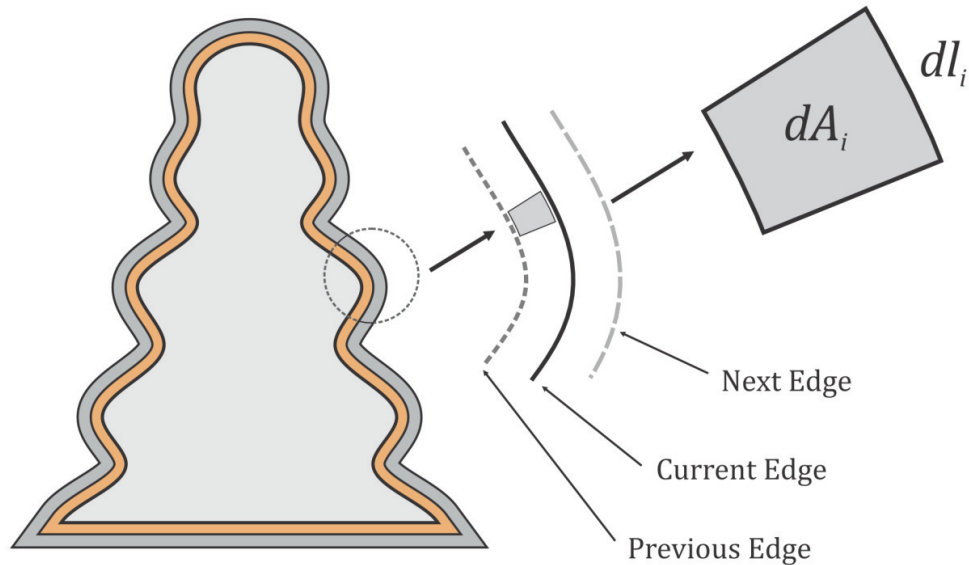
Figure 4-2: Infinitesimal element of cutting edge

Since the chip load distribution along the cutting edge of broaching tool may not be uniform, it must be divided into small sections where the local thickness can be assumed as constant. Since there is no relative motion between broaching teeth on the same tool, the total chip area can be calculated as a surrounded area between two successive teeth. Cutting forces are then obtained without segmenting the edge into elements. However, expressing the geometry of broaching cutting edge by an explicit function is problematic and consequently the calculation of $(\int dA_i)$ and $(\int dl_i)$ is a challenging task. Parametric representation

of the broaching cutting edge by B-spline curves simplifies the calculations and makes integration and derivation along the cutting edge easier.

4-3   Parametric Representation of Cutting Edges

The parametric model of cutting edges for broaching tool is presented in this section. The geometry of cutting edges is then used to develop a model for the chip load and contact length calculation. Such a geometric model for broaching must have the capability to cover all of the different possible geometries of broaching tools. The primary solution is dividing the cutting edge into a number of sections and expressing each section by a certain function. The best solution is implementing parametric functions which have the capability to represent a broad range of geometries. In this case the geometry of each cutting edge can be presented by equation 4-4:

$$\begin{cases} x = C_x(u) \\ y = C_y(u) \\ z = C_z(u) \end{cases} \tag{4-4}$$

where (x, y, z) are coordinates of points along the cutting edge. If the simulations are performed on an existing tool, the required coordinates can be obtained by digitizing or 3D scanning. However, these simulations are normally executed by the tool designers before manufacturing the tool. In such cases there is no tool to be digitized or scanned. Therefore, data points are selected by the tool designers based on their design criteria and fed into the simulation software to

achieve optimum features for maximum durability and performance. In order to define parametric functions for cutting edge, B-spline parametric functions are implemented in this research. A B-spline of degree p which is able to interpolate $(n + 1)$ data points $(D_0, D_1, \ldots, D_n)$ along the cutting edge is defined by $(n + 1)$ control points $(P_0, P_1, \ldots, P_n)$ and expresses the cutting edge by a parametric curve [57]. The control points $(P_0, P_1, \ldots, P_n)$ control the geometry of the curve which is passing through data points $(D_0, D_1, \ldots, D_n)$ and generate the cutting edge. Figure 4-3 demonstrates sets of data points, control points and interpolating B-spline for a sample curve.
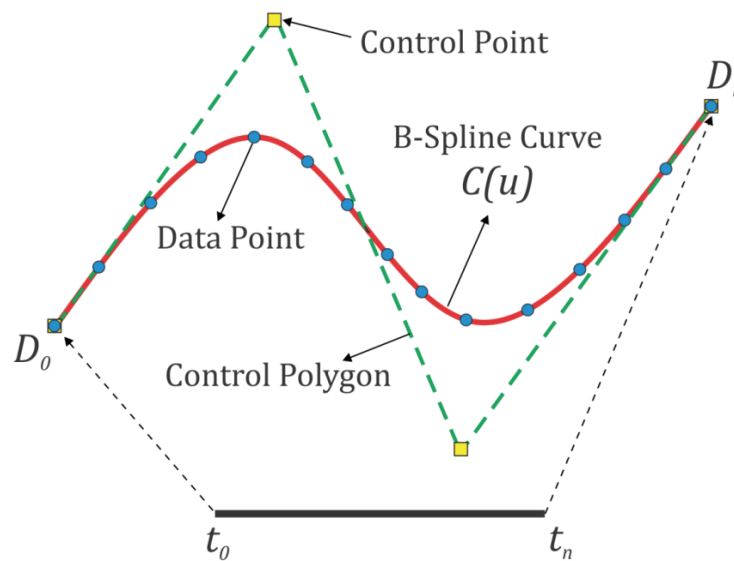
Figure 4-3: Schematic view of data points, control points and interpolating B-spline for a sample curve

This parametric representation of cutting edge can be easily utilized to perform derivation and integration along the edge to find chip load area and engagement

length. The cutting edge of a broaching tool which is interpolated by B-spline of degree (p) can be expressed as follows [58]:

$$C(u) = \sum_{i=0}^{n} N_{i,p}(u)P_i \rightarrow \begin{cases} C_x(u) = \sum_{i=0}^{n} N_{i,p}(u)P_{xi} \\ C_y(u) = \sum_{i=0}^{n} N_{i,p}(u)P_{yi} \\ C_z(u) = \sum_{i=0}^{n} N_{i,p}(u)P_{zi} \end{cases} \qquad (4\text{-}5)$$

In equation 4-5, $C(u)$ is interpolating B-spline curve of degree (p), (P_i) are control points and $N_{i,p}(u)$ are B-spline Basis functions. The basis functions $N_{i,p}(u)$ can be calculated by applying the following recursive algorithm [57, 58].

$$N_{i,0}(u) = \begin{cases} 1 & if \ u_i \leq u < u_{i+1} \\ 0 & otherwise \end{cases}$$

$$\qquad (4\text{-}6)$$

$$N_{i,p}(u) = \frac{u - u_i}{u_{i+p} - u_i} N_{i,p-1}(u) + \frac{u_{i+p+1} - u}{u_{i+p+1} - u_{i+1}} N_{i+1,p-1}(u)$$

where (u_i) is a B-spline knot from the knot vector of $[u_0, u_m]$. The $(n + 1)$ unknown control points must be found to solve equation 4-5. By presenting a parameter like (t_k) which can be selected using three different methods namely uniformly spaced, chord length, and centripetal the control points can be related to the data points. Each parameter (t_k) corresponds to data point (D_k) [57, 58]

$$D_k = C(t_k) = \sum_{i=0}^{n} N_{i,p}(t_k)P_i \qquad 0 \leq k \leq n \qquad (4\text{-}7)$$

Equation 4-7 has $(n+1)$ B-spline basis functions $[N_{i,p} \quad i = 0, \dots, n]$ and $(n+1)$ parameters $[t_k \quad k = 0, \dots, n]$ that can be organized into a $(n+1) \times (n+1)$ matrix (N) by substituting t into $N_{i,p}(u)$ [58]. Data points and control points can be also expressed in a similar way.

$$N = \begin{bmatrix} N_{0,p}(t_0) & \cdots & N_{n,p}(t_0) \\ \vdots & \ddots & \vdots \\ N_{0,p}(t_n) & \cdots & N_{n,p}(t_n) \end{bmatrix}$$

$$D = \begin{bmatrix} d_{0x} & d_{0y} & d_{0z} \\ d_{1x} & d_{1y} & d_{1z} \\ \vdots & \vdots & \vdots \\ d_{nx} & d_{ny} & d_{nz} \end{bmatrix} \tag{4-8}$$

$$P = \begin{bmatrix} P_{0x} & P_{0y} & P_{0z} \\ P_{1x} & P_{1y} & P_{1z} \\ \vdots & \vdots & \vdots \\ P_{nx} & P_{ny} & P_{nz} \end{bmatrix}$$

Matrix (D) in equation (4-8) is constructed using data points along the cutting edge which has been previously acquired by either digitizing or 3D scanning when the tool is available or generated by tool designers when the tool is still under design. Data points, basis functions and control points can be presented in a system of linear equations where (D) and (N) are known and (P) is the only unknown parameter. The desired control points and consequently the cutting edge which is interpolated by B-spline curves are revealed by solving equation 4-9 for the unknown parameter (P).

$$\begin{bmatrix} d_{0x} & d_{0y} & d_{0z} \\ d_{1x} & d_{1y} & d_{1z} \\ \vdots & \vdots & \vdots \\ d_{nx} & d_{ny} & d_{nz} \end{bmatrix} = \begin{bmatrix} N_{0,p}(t_0) & \cdots & N_{n,p}(t_0) \\ \vdots & \ddots & \vdots \\ N_{0,p}(t_n) & \cdots & N_{n,p}(t_n) \end{bmatrix} \times \begin{bmatrix} P_{0x} & P_{0y} & P_{0z} \\ P_{1x} & P_{1y} & P_{1z} \\ \vdots & \vdots & \vdots \\ P_{nx} & P_{ny} & P_{nz} \end{bmatrix} \qquad (4\text{-}9)$$

Figure 4-4 shows the control points and the desired interpolated broaching cutting edge using B-spline curves for a sample fir tree profile.
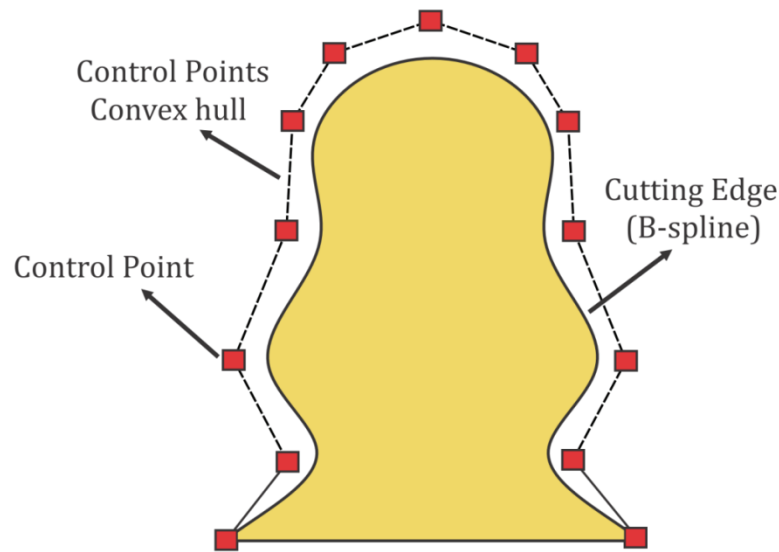
Figure 4-4: B-spline interpolation of cutting edge

4-4 Calculation of Chip Load and Contact Length

As it was previously stated, regardless of the method utilized to estimate the cutting forces, calculation of chip load and contact length is essential. Like other machining operations, broaching can be classified into orthogonal and oblique categories. In orthogonal broaching, all of the cutting edges are parallel together and perpendicular to the cutter axis; therefore, the third column of matrixes (D)

and (P) in equation 4-9 are zero and only the two parameters of $C_x(u)$ and $C_y(u)$ in equation 4-5 are needed to represent the cutting edge. Figure 4-5 depicts the typical Cartesian coordinates in orthogonal and oblique broaching. In contrast with orthogonal broaching in which all teeth are perpendicular to the cutter axis, the cutting edges in oblique broaching have an inclination angle with the cutter axis; however, they are still parallel to each other. In this case $C_x(u)$, $C_y(u)$, $C_z(u)$ and all of the coordinates in the third column of matrixes (D) and (P) are non-zero. A B-spline interpolation of 3D curves is possible but it is time consuming; hence, it is preferred to transform the 3D coordinates to 2D and follow the 2D interpolation procedure after transformation.
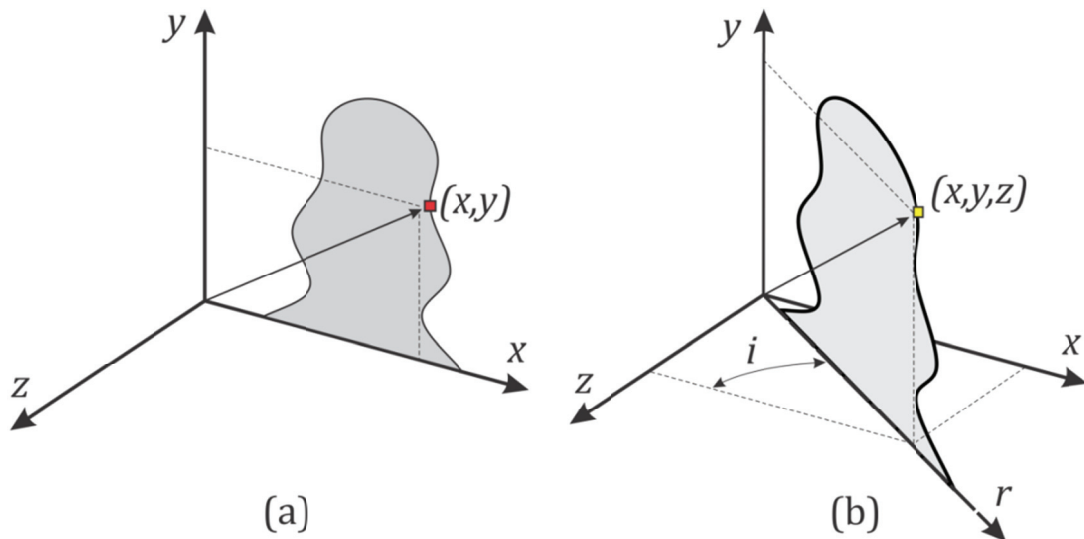
Figure 4-5: Cartesian coordinates for (a) orthogonal and (b) oblique broaching

Coordinates of point (x, y, x) in Cartesian coordinates can be expressed by (r, y) in (ry) plane as follows:

$$r = \sqrt{x^2 + z^2} \; and \; y = y \qquad\qquad\qquad (4\text{-}10)$$

The above transformation can be done for all of the cutting edge data points and in the new coordinate system matrix (D) is as follows:

$$D = \begin{bmatrix} d_{0x_{new}} & d_{0y_{new}} & 0 \\ d_{1x_{new}} & d_{1y_{new}} & 0 \\ \vdots & \vdots & \vdots \\ d_{nx_{new}} & d_{ny_{new}} & 0 \end{bmatrix} = \begin{bmatrix} r_{0x} & d_{0y} & 0 \\ r_{1x} & d_{1y} & 0 \\ \vdots & \vdots & \vdots \\ r_{nx} & d_{ny} & 0 \end{bmatrix} \qquad (4\text{-}11)$$

Once matrix (D) is presented in the new coordinate system, the interpolation process can be completed.

The total chip load $(\int dA_i)$ and contact length $(\int dl_i)$ for each cutting edge can be calculated based on the parametric nature of cutting edge representation. The chip load is the area perpendicular to the direction of cutting which is removed by the currently engaged cutting edge. Therefore, it can be geometrically considered as the area between the two successive cutting edges. Calculation of chip load and contact length in broaching operation can be basically divided into two different cases. The first case is encountered when each tooth is completely larger than its predecessor. In this case the chip load can be obtained by calculating the area between two curves (edge) from the beginning to the end. The second case which is slightly more complicated occurs when the current cutting edge is not completely bigger than the previous one. In other words, this case appears when only some parts of the current cutting edge are bigger than the previous one. In this case the chip load cannot be calculated by integrating the whole area between the two curves because upper and lower limits of integration

are not the same as the beginning and the end of the curves. For this reason the chip load must be calculated by projecting two successive cutting edges in one plane, determining the intersection of those curves and integrating the intersection area. Figure 4-6 shows the above mentioned categories for the two sample geometries.
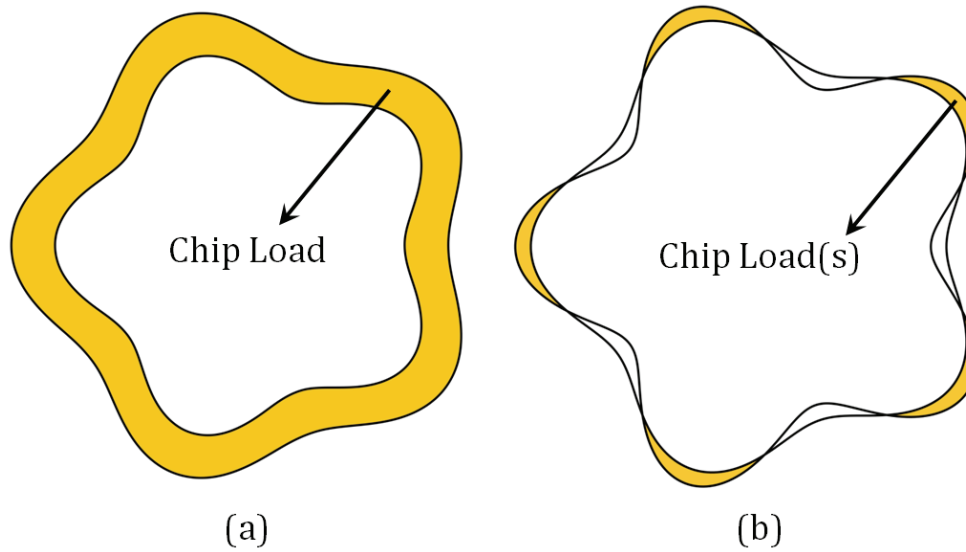
Figure 4-6: Classification of Cutting Edges: (a) without intersection and (b) with intersection

Assuming two successive cutting edges as follows:

$$C_1(u) = \begin{cases} C_{x1}(u) \\ C_{y1}(u) \\ C_{z1}(u) \end{cases} \quad u \in [0,1]$$

$$C_2(u) = \begin{cases} C_{x2}(u) \\ C_{y2}(u) \\ C_{z2}(u) \end{cases} \quad u \in [0,1]$$

(4-12)

To calculate the intersection points for the two cutting edges, they must be subdivided into a number of Bezier curves. A complete description of subdivision algorithm can be found in [57]. After subdividing the B-spline curve into Bezier curves, the intersection conditions are checked for each two pairs of Bezier curves. The problem of finding the intersection of curves can be simplified into solving a system of algebraic equations [59]. This system of equations can be represented as follows:

$$\begin{cases} C_{x1}(u) - C_{x2}(u) = 0 & u \in [0,1] \\ C_{y1}(u) - C_{y2}(u) = 0 & u \in [0,1] \\ C_{z1}(u) - C_{z2}(u) = 0 & u \in [0,1] \end{cases} \tag{4-13}$$

Finding the roots of the above equations will lead to finding the intersection points of the two curves. It must be noted that these curves are actually the cutting edges and they are in two different but parallel planes. By projecting two curves in one plane and finding the (x, y) coordinates of intersection points, the boundary of integration for calculation of chip load is revealed. However, these coordinates cannot be directly used as the upper and lower limits of integration. These curves are parametric; consequently the corresponding parameter of intersection points must be identified on each curve separately. These parameters are not necessarily similar on both curves depending on the geometry and parameter selection method which were discussed before. The corresponding parameter (u) can be found by substituting the (x) and (y) of the intersection points in the B-spline function and solving them to find (u). Once the cutting edge is presented by B-

spline curves and the upper and lower limit of integration are defined, the cutting length for the currently engaged cutting edge and chip load for two successive cutting edges are calculated using mathematical relation for parametric functions.

Current edge: $C_i(u) = \begin{cases} C_{xi}(u) \\ C_{yi}(u) \end{cases}$ $u \in [0,1]$

$$(4\text{-}14)$$

Previous edge: $C_{i-1}(u) = \begin{cases} C_{x(i-1)}(u) \\ C_{y(i-1)}(u) \end{cases}$ $u \in [0,1]$

Area: $A_t = \int_{u_{s_i}}^{u_{e_i}} C_{y_i}(u)\frac{dC_{x_i}(u)}{du} du - \int_{u_{s_{i-1}}}^{u_{e_{i-1}}} C_{y_{i-1}}(u)\frac{dC_{x_{i-1}}(u)}{du} du$

$$(4\text{-}15)$$

Length: $L_t = \int_{u_{s_i}}^{u_{e_i}} \sqrt{\left[\frac{dC_{x_i}(u)}{du}\right]^2 + \left[\frac{dC_{y_i}(u)}{du}\right]^2} du$

where $(s, e, i, i-1)$ indicate start of the cut, end of the cut, current cutting edge, and previous cutting edge, respectively. Equations 4-14 and 4-15 are 2D parametric equations and can be utilized in the calculation of chip load and contact length for orthogonal broaching tools which consists majority of broaching tools. However, the model can be further developed for oblique broaching given that the cutting edges with an oblique angle are still in parallel planes.

4-5   Geometric Verification of the Model Using MATLAB

In order to confirm validity and reliability, the proposed model is geometrically certified using MATLAB and 3D ACIS modeller. Certain geometry (Figure 4-6) which is a very common profile for oil pump gears is selected and

simulated using the proposed model in MATLAB. The generated coordinates for the data points are then imported into the 3D ACIS modeller which is capable of interpolating a set of data points, measuring the length of the curves, and computing the surrounded area. The resultant area and length which are calculated by the model in MATLAB are then compared to the results of ACIS to check the validity of the model. Table 4-1 presents the mathematical formulations of the desired geometry for two different cases. It must be noted that the presented equations in Table 4-1 are only arbitrary equations to generate data points and they can be replaced by any other equation or given set of data points.

Table 4-1: Utilized formulation for generating the data points

$Case\ 1: without\ intersection$ $0 \le \theta \le 2\pi$	$r_1 = 4 - 0.5 \times \sin(5\theta) \rightarrow \begin{cases} x_1 = r_1 \sin(\theta) \\ y_1 = r_1 \cos(\theta) \end{cases}$
	$r_2 = 5 - 0.5 \times \sin(5\theta) \rightarrow \begin{cases} x_2 = r_2 \sin(\theta) \\ y_2 = r_2 \cos(\theta) \end{cases}$
$Case\ 2: with\ intersection$ $0 \le \theta \le 2\pi$	$r_1 = 4 - 0.5 \times \sin(5\theta) \rightarrow \begin{cases} x_2 = r_2 \sin(\theta) \\ y_2 = r_2 \cos(\theta) \end{cases}$
	$r_2 = 4 - 0.8 \times \sin(5\theta) \rightarrow \begin{cases} x_2 = r_2 \sin(\theta) \\ y_2 = r_2 \cos(\theta) \end{cases}$

Figure 4-7 and Table 4-2 demonstrate the 3rd degree interpolation for two different categories of cutting edges and the obtained results respectively. The required data points were generated using the mathematical formulation presented in Table 4-1. It must be mentioned that the presented procedure is applicable where no explicit function is available to represent the cutting edge

which is a very common case. The above mathematical formulas have been only applied to generate data points for model validation.
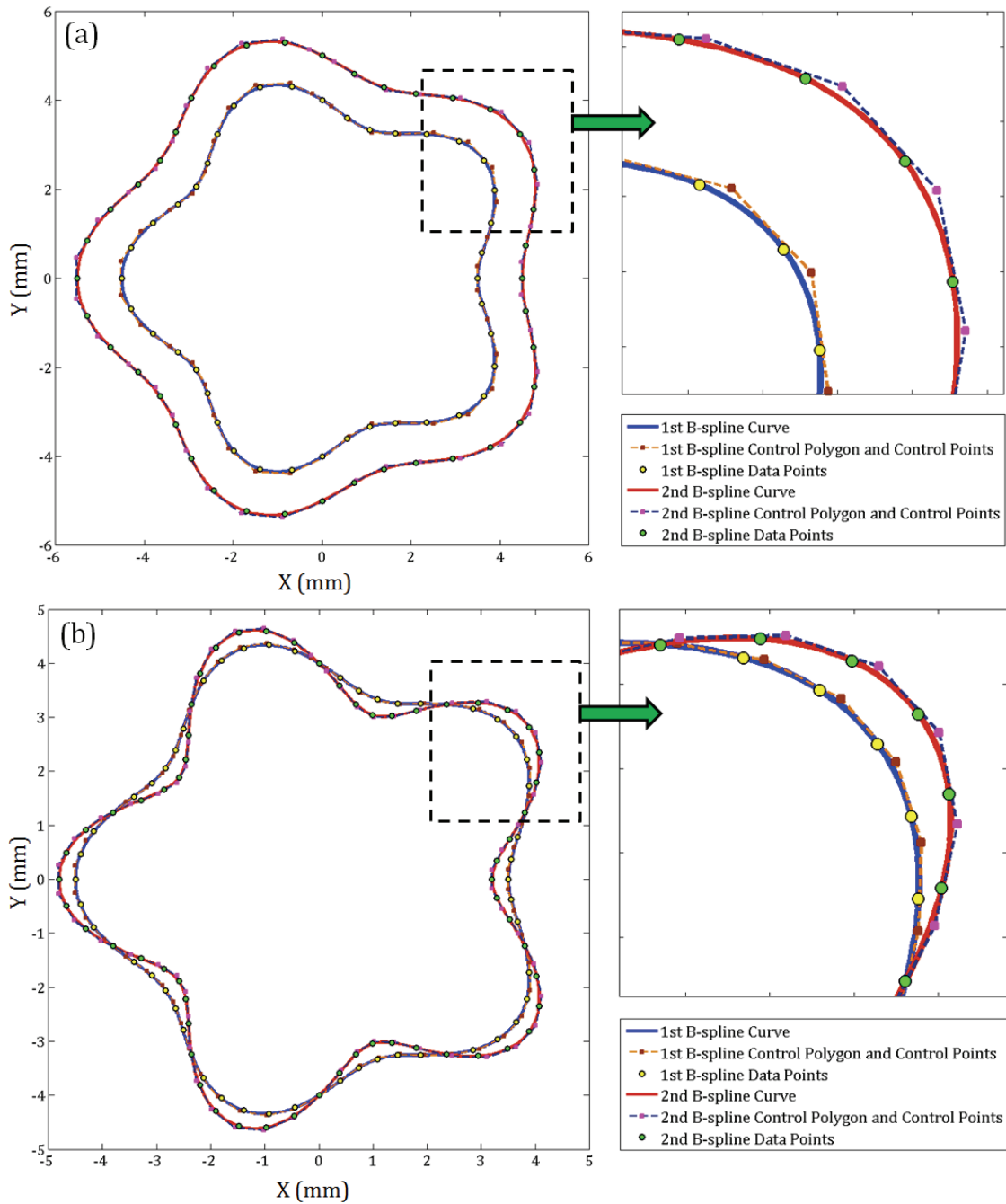
Figure 4-7: Parametric representation of cutting edges: (a) without intersection and (b) with intersection

Table 4-2: Simulation results using MATLAB

	Without Intersection		With Intersection	
	Inner Curve (1st edge)	Outer Curve (2nd edge)	Inner Curve (1st edge)	Outer Curve (2nd edge)
Length (mm)	27.4396	33.3005	2.9406	3.3482
Area (mm^2)	28.2743		0.5413	

Accuracy of the interpolation and consequently the final results are highly affected by the number of data points and degree of B-spline; however, it must be noted that the accuracy is not linearly increased or decreased by increasing or decreasing the number of data points and degree of the B-spline. In other words, the accuracy of the results is not necessarily promoted by increasing the number of data points and the degree of B-spline curves. The effect of the number of data points and the degree of B-spline on the accuracy of the interpolation results is demonstrated in Figure 4-8. As can be seen from Figure 4-8, the 1st degree B-spline (linear interpolation) is simple but not accurate enough. The accuracy of 1st degree interpolation can be increased by increasing the number of data points which is not desirable. The 2nd degree is more accurate but in comparison to the 3rd degree it needs more data points to achieve the same accuracy especially for the complex geometries. It has been shown that the best result can be achieved by applying 3rd degree B-spline. The higher degrees of interpolation are vulnerable to the number of data points and oscillation may occur specially at the beginning and end of the curve where it is constrained to the first and last data points. This can be referred

to the Runge's phenomenon which is an oscillation problem especially at the borders of the interpolation interval when a higher degree of interpolation is applied.
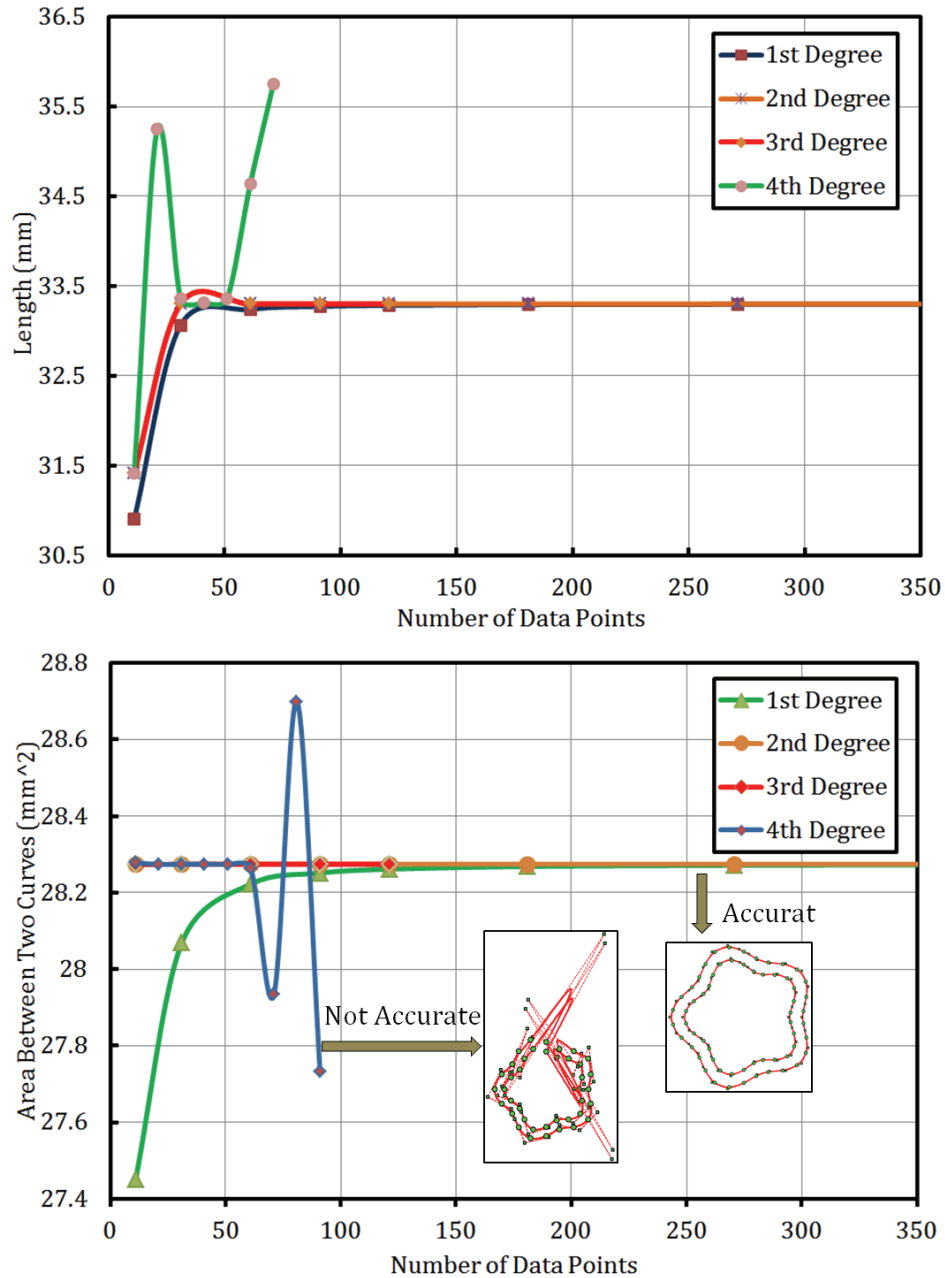
Figure 4-8: Effect of B-spline degree and number of data points on the length and area between interpolated curves

In order to check the validity of the presented model in simulation of cutting edges with sharp corners, a simple keyway profile which was previously presented by Kokturk [2] was selected and examined as a real case in addition to above mentioned profiles in Figure 4-7. The geometric features of the keyway broaching tool are presented in Figure 4-9 and Table 4-3 respectively.
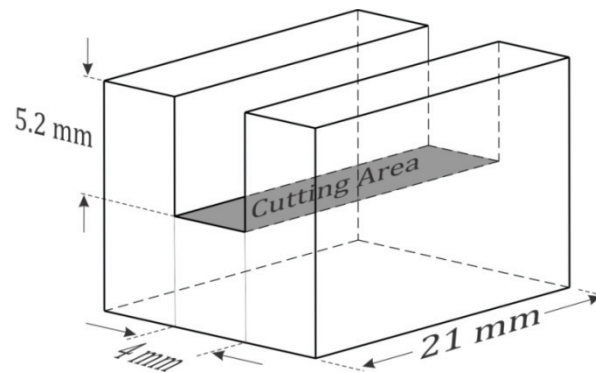
Figure 4-9: Final dimensions of the keyway

Table 4-3: Geometry of broaching tool to make a keyway [2]

Cutter Type	Orthogonal	Oblique
Number of Teeth	20	20
Pitch Length	5 mm	5 mm
Height of the First Tooth	4 mm	4 mm
Upper Length of the Tooth	4 mm	$4/\cos 15$ mm
Base length of the Tooth	4 mm	$4/\cos 15$ mm
Upper Surface Raise	0.06 mm	0.06 mm
Inclination (Oblique) Angle	0	15

The broaching tool has 20 teeth; each removes 0.06 mm from the workpiece body to increase the depth of keyway from 4 mm to 5.2 mm. It is clear that when inclination angle is 0°, the length of engagement between tool and workpiece

(contact length) for each tooth is equal to the upper length of the tooth which is 4 mm. Also, the chip load (area between two successive teeth) in front of each cutting edge is 0.24 mm^2 which is equal to the contact length (4 mm) multiply by rise per tooth (0.06 mm). Two successive teeth are interpolated using 1st and 2nd order B-spline parametric curves and the chip load as well as tool-workpiece contact length were calculated. Results are presented in Figure 4-10 and Table 4-4.
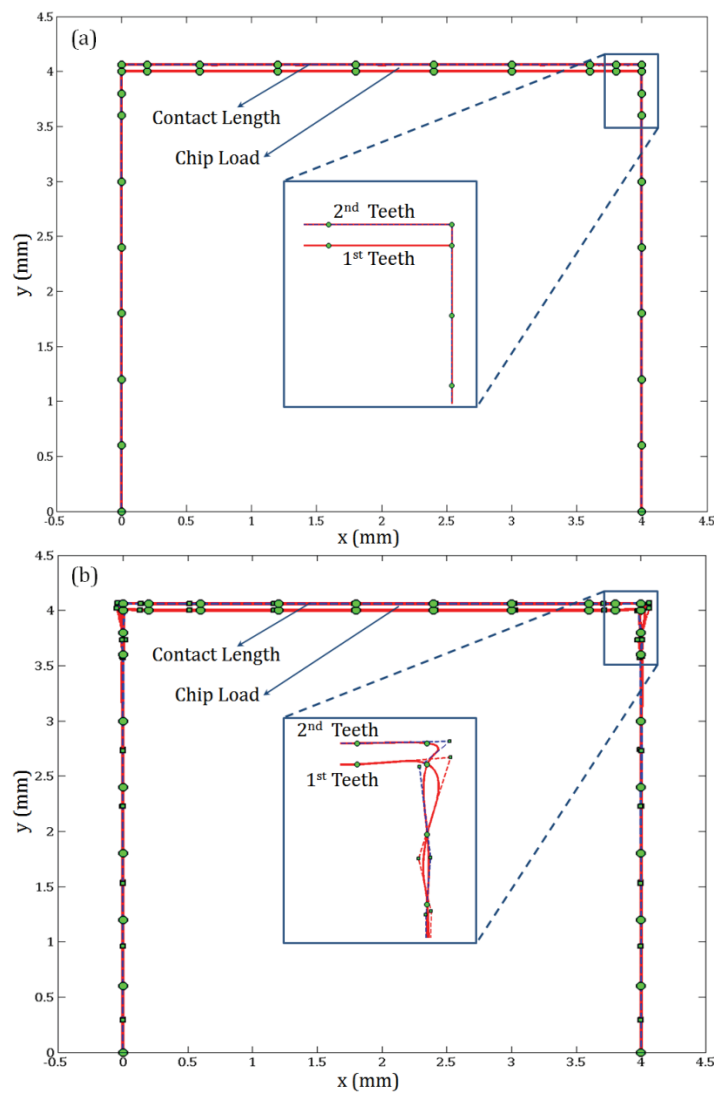
Figure 4-10: B-spline interpolation of two teeth (a) 1st order and (b) 2nd order

Table 4-4: Simulation results for keyway tool using 1st and 2nd order interpolation

	Exact Amount	Interpolation (1st order B-spline)	Interpolation (2nd order spline)
Contact Length (mm)	4.0000	4.0000	4.0229
Area Beneath the 1st Teeth (mm^2)	16.0000	16.0000	16.0081
Area Beneath the 1st Teeth (mm^2)	16.2400	16.2400	16.2399
Chip Load Area (mm^2)	0.2400	0.2400	0.2319

As can be seen from Figure 4-10, the best results for keyway broaching tool is achieved by utilizing 1st order interpolation, despite oil pump geometry with smooth profile (Figure 4-7), where the 3rd order interpolation yields the best results. It must be noted that smooth geometries with no prompt curvature variations are not sensitive to the number of data points. In this case, the interpolating B-spline can follow the data points precisely. In contrast, the inaccuracy occurs in geometries with instantaneous change in slope and curvature which is a common case in profiles with sharp corners (Figure 4-10). In such cases, an acceptable accuracy and time efficiency can be achieved by applying lower degree of interpolating curve and more data points at the sharp corners.

4-6   Geometric Verification of the Model Using ACIS

As it was previously stated, in broaching, the cutting tool is fed towards a stationary workpiece. Since there is no feed motion in broaching operation (the difference between heights of teeth plays the role of feed), the only relative motion

between tool and workpiece is the linear cutting motion of the tool. Therefore, the chip load can be assumed constant after complete engagement between the tool and the workpiece.

The ACIS 3D solid modeller was utilized as a geometric engine to simulate the cutting edges, tool motion, engagement between tool and workpiece, and to update the part. The data points can be imported into ACIS or generated using software capability. The cutting edges are created by defining a wire body from the data points and the workpiece is created as a block or cylinder.

4-6-1 Modeling of the Chip Load and Updating the Part in ACIS

The geometry of chip is calculated based on the B-rep model of the tool, workpiece and their relative motion. The updated part is built by doing a Boolean subtraction between the tool and workpiece. The instantaneously engaged segment of the cutting edge during cutting action is modeled by following these steps:

- Constructing the boundary of workpiece as a solid block

- Constructing the wire frame model of the cutting edges

- Translating the cutting edges into their initial position

- Moving the cutting edges toward the workpiece by a linear increment along the tool axis (z-axis)

- Finding the intersection of cutting edge with the boundary of workpiece block

- Updating the part geometry by performing Boolean subtraction between workpiece block and cutting edges using the following command:

(bool:subtract workpiece block Tool)

Starting with the primary contact of the generated cutting edges with the workpiece block, the chip geometry is computed automatically by subtracting the geometry of cutting edge from the geometry of workpiece block. The procedure continues at each updating stage to determine the chip load for one complete stroke of broaching cutting tool. Figure 4-11 shows the B-rep model of the cutting edges, solid body of the workpiece and general aspects of cutting action which is simulated by the 3D ACIS modeller.
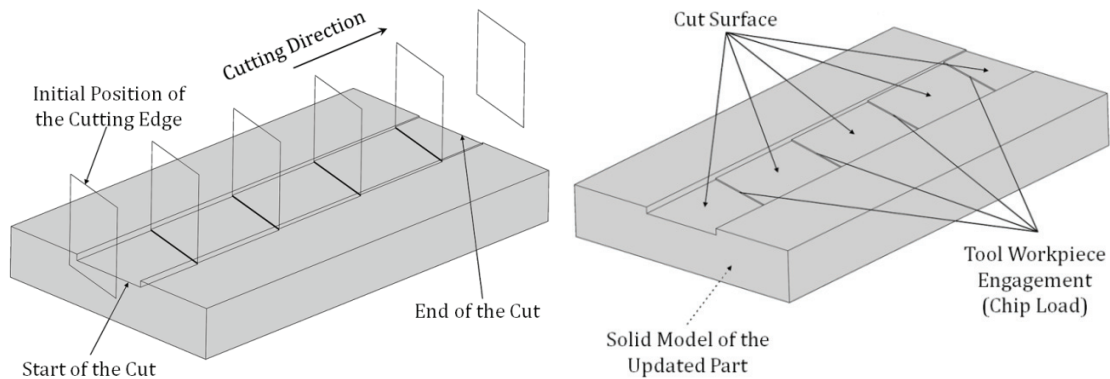
Figure 4-11: Solid model of the workpiece, B-rep model of the cutting edges, updated part, and tool-workpiece engagement

Figure 4-12 describes the algorithm which was used to simulate the cutting action and calculate the chip load during the simulated broaching operation.

Setting ACIS primary Parameters

Set Environment Properties
(Color, Tolerance …)

Create Working Coordinate System

Input Broaching Tool Geometry

Define Leading Edge Reference Point

Define Workpiece Block (WPB)

For position = Begining of the Cut

To Postion = End of the Cut

Transform the Tool Toward the
Workpiece and Check the Intersection
Until the Tool Exit the Workpiece

if Tool Intersect the

Workpiece

No

Yes

Subtract the Cutter form the Workpiece
Keep the Intersection Area as Chip Load

Next

Figure 4-12: Simulation algorithm in ACIS

The previous geometries which were simulated in Figure 4-7 and Figure 4-10 are also simulated using 3D ACIS modeller. The simulation process for oil pump profile is presented in Figure 4-13.
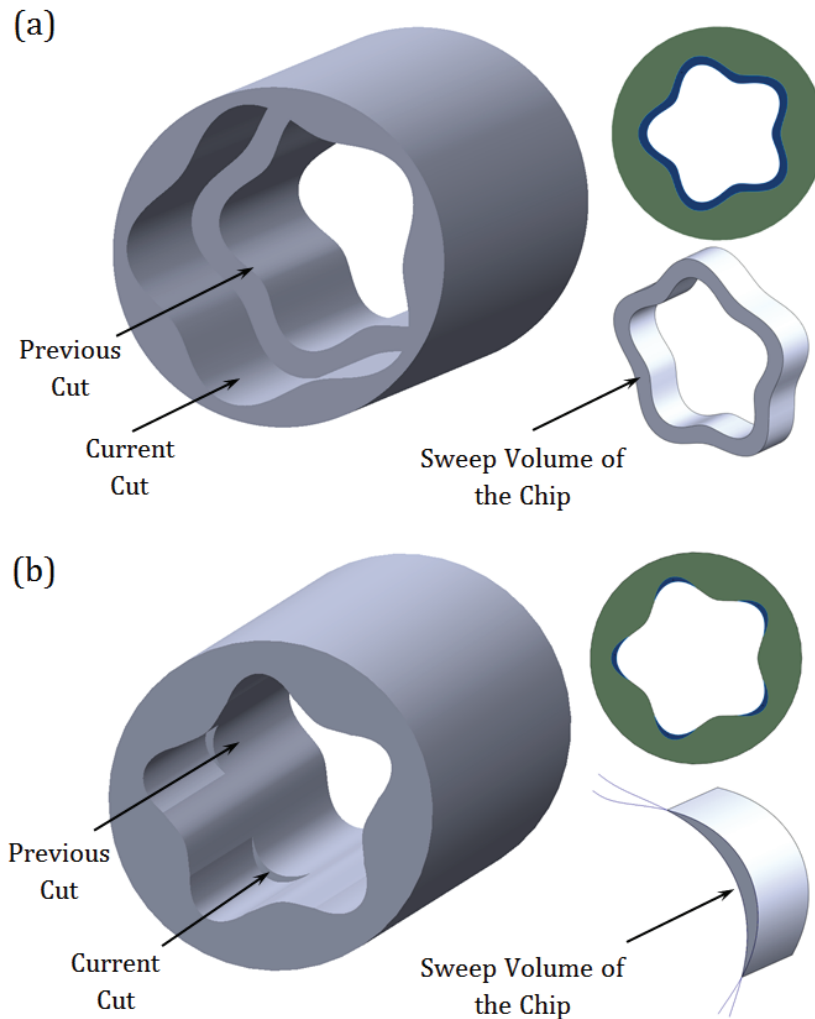
Figure 4-13: Simulation of two successive cutting edges in ACIS: (a) without intersection and (b) with intersection

As can be seen in Figure 4-13, both categories of cutting edges in broaching where the successive cutting edges have no intersections or intersect each other

can be simulated in 3D ACIS modeller. Table 4-5 compares the results of ACIS and MATLAB.

Table 4-5: Comparing the results of MATLAB and ACIS

		Without Intersection		With Intersection	
		Inner Curve (1st edge)	Outer Curve (2nd edge)	Inner Curve (1st edge)	Outer Curve (2nd edge)
MATLAB	Length (mm)	27.4396	33.3005	2.9406	3.3482
	Area (mm^2)	28.2743		0.5413	
ACIS	Length (mm)	27.4287	33.2846	2.9314	3.3437
	Area (mm^2)	28.2735		0.5412	

A comparison of the results in Table 4-5 demonstrates that the presented model in MATLAB is capable of calculating the tool-workpiece contact length and chip load with acceptable accuracy. The same procedure can be followed for keyway broaching tool. Figure 4-14 and Figure 4-15 show the simulation of keyway broaching with and without inclination angle (oblique angle) in the 3D ACIS modeller.

Start of the Cut

Middle of the Cut

Solid Model of
the Workpiece

End of the Cut

B-rep Model of
the Cutting Edges
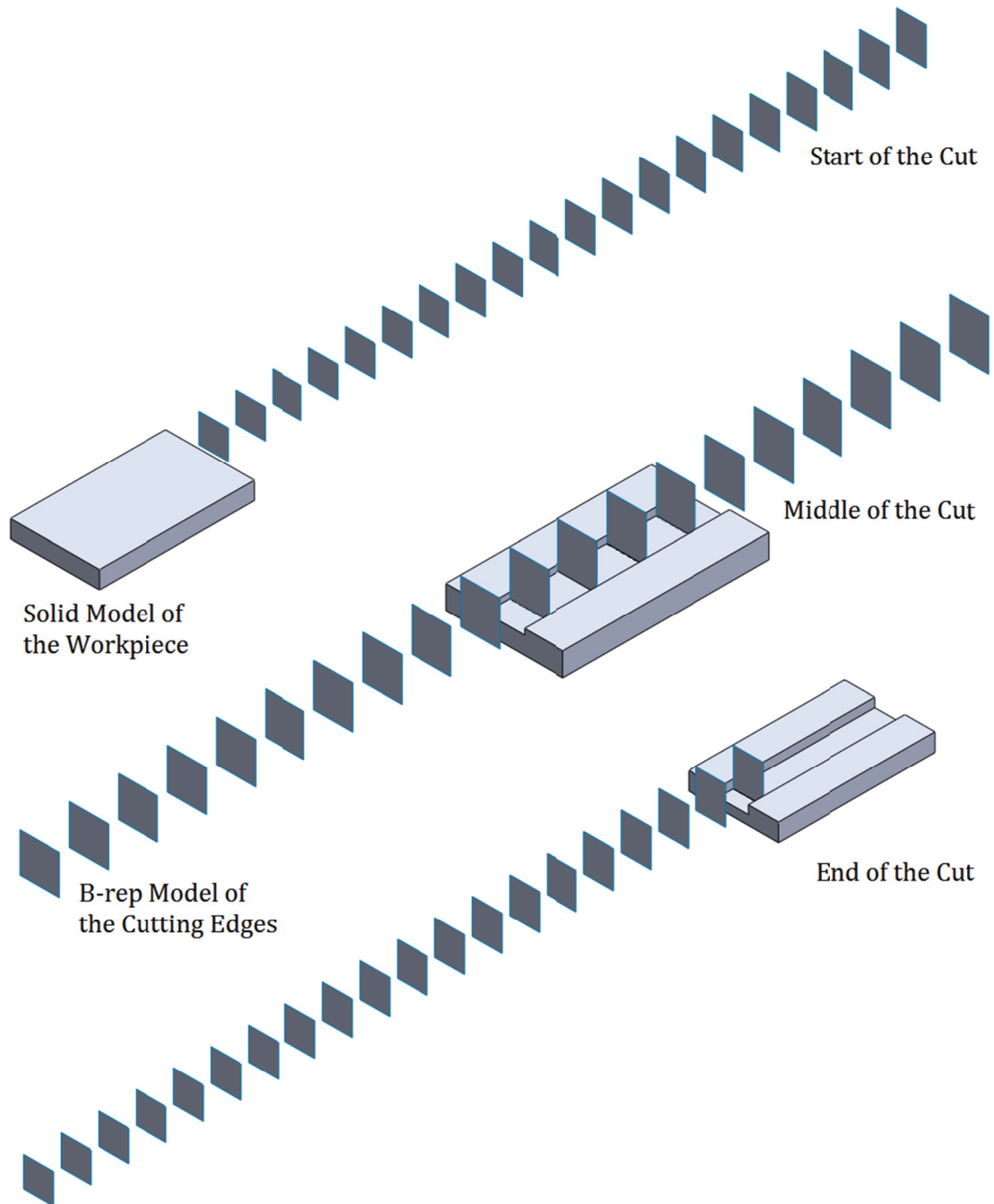
Figure 4-14: Simulation of a complete stroke of the broaching tool with no oblique

angle

Start of the Cut

Middle of the Cut

Solid Model of
the Workpiece

End of the Cut

B-rep Model of
the Cutting Edges
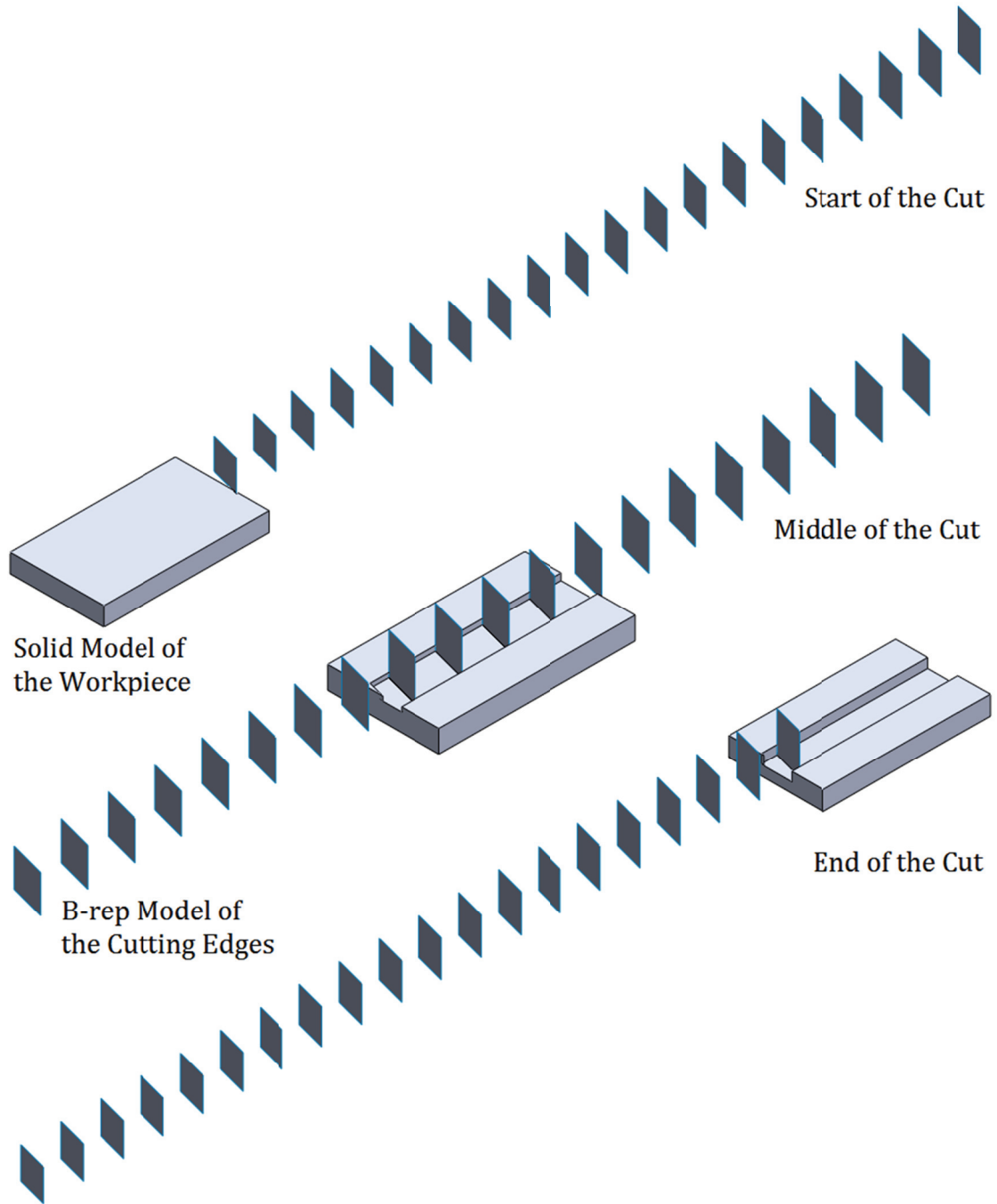
Figure 4-15: Simulation of a complete stroke of the broaching tool with oblique

angle

Table 4-6 shows the simulated contact length and chip load area for the keyway broaching tool for both orthogonal and oblique case.

Table 4-6: Simulation results for keyway broaching tool using 3D ACIS modeller

		Orthogonal	Oblique
Exact Amount	Length (mm)	4.0000	4.1411
	Area (mm^2)	0.2400	0.2485
ACIS	Length (mm)	4.0117	4.1621
	Area (mm^2)	0.2451	0.2497

As can be concluded from table 4-6, ACIS is able to calculate the contact length and chip load within the acceptable range of accuracy. However, ACIS was only utilized to confirm the results of the proposed model in MATLAB and it will not be used for further calculation.

4-7 Results and Discussions

The chip load and tool-workpiece contact length must be calculated for each single tooth at each step and then multiplied by the number of the simultaneously engaged teeth to achieve the total contact length and chip load which is removed by tool at the given moment of time. The pitch length for the keyway broaching

tool is 5 mm (see Table 4-3) and the length of the keyway to be broached is 21 mm (see Figure 4-9); therefore, the maximum number of teeth that can be simultaneously engaged with the workpiece is five teeth. When the tool starts the cut, the chip load and length of the engagement are gradually raised until the maximum number of teeth is engaged with the workpiece.

In order to check the capability of the proposed geometric model, the generated cutting force during the broaching of the above mentioned keyway was simulated and compared to the results of the previously published work by Kokturk [2]. The mechanistic method of force modelling is utilized and cutting constants are selected according to [2] . The cutting constants are presented in table 4-7 and the cutting conditions and geometry of the tool and workpiece can be found in Figure 4-9 and Table 4-3.

Table 4-7: Cutting constants

Workpiece Material	Waspaloy	Waspaloy
Oblique angle	0 deg	15 deg
K_t	5281 (N/mm^2)	5393 (N/mm^2)
K_f	2889 (N/mm^2)	2900 (N/mm^2)
K_r	0 (N/mm^2)	353 (N/mm^2)

The mathematical formulation for mechanistic cutting force modelling was previously presented in this chapter (see equations 4-1 to 4-3). The results of mechanistic force modelling are presented in Figure 4-16 and Figure 4-17.
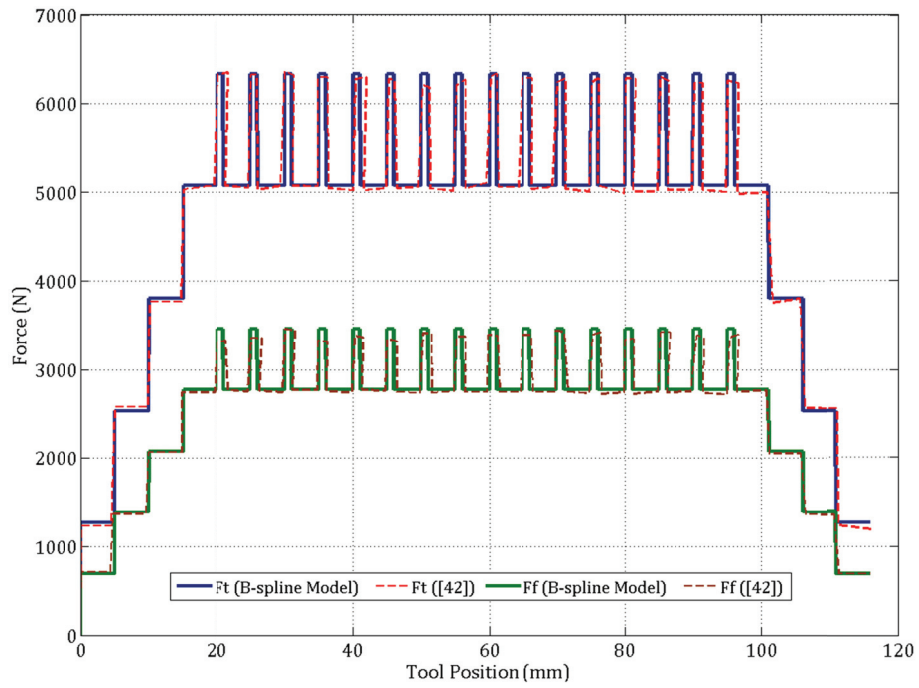
Figure 4-16: Simulated and experimental cutting forces for orthogonal broaching
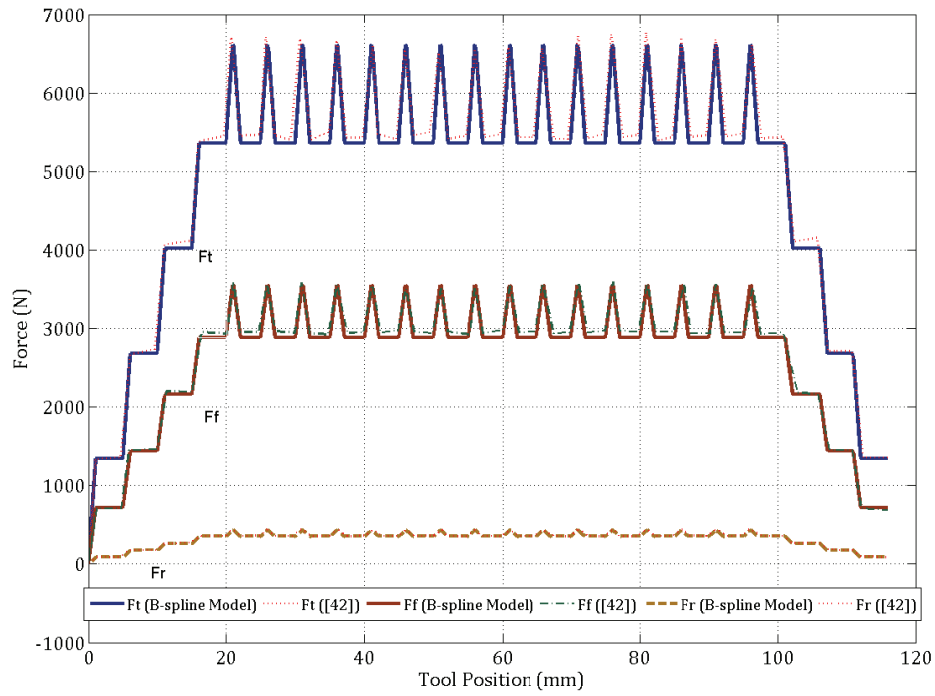
Figure 4-17: Simulated and experimental cutting forces for oblique broaching

4-8   Summary

A simulation of the broaching operation including calculation of the chip load and tool-workpiece contact length was presented. The results of the proposed model were also verified utilizing 3D ACIS modeller. The presented procedures are fundamental and they can be used for the modelling of broaching operations with any arbitrary profile of cutting tool.

Chapter 5:   Prediction of Cutting Forces in Broaching Operation

5-1   Preamble

This chapter aims to develop an energy based force model to be used for any kind of broaching tools. The force model is needed for design of broaching tools, broaching machines and desired fixtures to meet high requirements to broached parts. The cutting force model has been developed using the advanced cutting mechanics and its authenticity was verified by a multi-facet comparison of the simulated and the measured forces.

5-2   Background of Force Modelling

The theoretical basis of the force prediction in metal cutting was originally constructed by Merchant's model [60]. Based on the work published by Ernst and Merchant [61] the cutting action occurs when the level of stress acting on the shear plane reaches or become higher than the shear strength of the workpiece material.

However, further researches showed that shear strength is not a reliable factor in the simulation of cutting action. It has been shown [62] that instead of shear strength, shear flow stress which is somehow higher than the yield strength of the workpiece material must be considered.

Another classical approach for the modelling of cutting processes is the mechanistic method which is also based on Merchant's theory. The cutting forces in mechanistic approach, are related to the geometry of contact between tool and workpiece and also cutting coefficients [8, 9, 56, 63]. Geometry of contact (engagement) between tool and workpiece is generally defined by the length of the cut and undeformed chip thickness for any infinitesimal element along the cutting edge. The effects of mechanical properties of tool and workpiece are also taken into consideration using cutting coefficients which can be achieved experimentally [8]. However, Merchant's model is too idealistic since the characteristic stresses of the workpiece material cannot be considered in the absence of corresponding strains especially in metal cutting where the strain rate is extremely high. Merchant's method is criticized by Astakhov and Xiao [62] when it comes to accurate prediction of the cutting forces. A force model was presented by Astakhov and Xiao [62] in which the cutting forces are calculated based on the power balance in the cutting system. The bigger the strain rate is, the more power is required to perform the task. As a result, by considering the power (energy) balance in a cutting system, the strain rate is automatically reflected. This

approach is primarily introduced for turning but it can be also applied to broaching operation with some modifications.

5-3 Energy Based Cutting Force Modelling

According to that methodology presented by Astakhov and Xiao [62] the cutting force can be represented as a function of cutting power as follows:

$$F_t = \frac{P_c}{v} = \frac{P_{pd} + P_{fR} + P_{fF} + P_{ch} + P_{mn-ce}}{v}$$

(5-1)

In equation 5-1, (P_{pd}) is the power spent on the plastic deformation of the surface layer being removed by cutting tool, (P_{fR}) is the power spent at the tool-chip interface, (P_{fF}) is the power spent at the tool-workpiece interface, (P_{ch}) is the power spent in the formation of new surfaces, and (P_{mn-ce}) is the energy spent due to the combined influence of the minor cutting edge [62].

In order to predict the cutting force in broaching operation each of the above mentioned components of cutting power must be accurately identified. Figure 5-1 shows the components of the cutting forces.
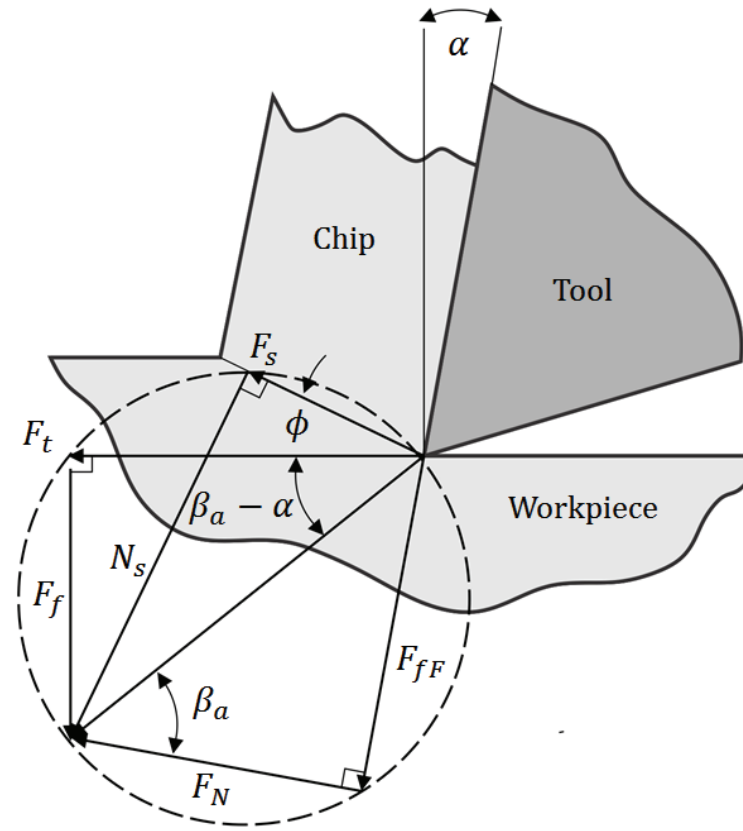
Figure 5-1: The force system in cutting

5-3-1 Power Spent on the Plastic Deformation Zone

This component of cutting power is calculated as:

$$P_{pd} = \frac{K(1.15 \times ln\xi)^{n+1}}{n+1} \times v \times A_w \qquad (5\text{-}2)$$

where (K) is the strength coefficient (N/m²), (n) is the hardening exponent of the work material. The (K) and (n) are obtained using true stress–strain curve. The latter is generated using engineering stress-strain curve by assuming that the volume change in the specimen is negligible.

$$\sigma_T = \sigma_E(1 + \epsilon_E)$$

$$\epsilon_T = \ln(\epsilon_E + 1)$$

<div align="right">(5-3)</div>

In equation 5-3, (σ_T) is true stress, (σ_E) is engineering stress, (ϵ_T) is true strain and (ϵ_E) is engineering strain. The most common formula that relates true stress to true strain is a power expression [64] as presented in equation 5-4 where (K) is the stress at $(\epsilon_T = 1)$ and (n) is the slope of a log–log plot of equation 5-4. It must be noted that equation 5-4 is valid before necking occurs [65].

$$\sigma_t = K \times (\epsilon_T)^n \qquad (5\text{-}4)$$

In addition to (K) and (n), in equation 5-2, (A_w) is uncut chip cross-sectional area (m^2), (v) is cutting velocity (m/s), and (ξ) is the chip compression ratio.

$$\xi = \frac{t_2}{t_1} = \frac{v}{v_1} \qquad (5\text{-}5)$$

In equation 5-5, (v_1) is chip velocity over the rake face.

5-3-2 Friction at the Tool-Chip Interface

The power spent at the tool-chip interface due to friction between tool and chip on the rake face can be calculated as:

$$P_{fR} = \tau_c \times l_c \times b_{1T} \times \frac{v}{\xi}$$

$$l_c = t_{1T} \times \xi^k$$

<div align="right">(5-6)</div>

where $(\tau_c = 0.28 \times \sigma_R)$ (N/m^2) is the average shear stress at the tool-chip interface [66], (σ_R) is the ultimate tensile strength of the workpiece material (N/m^2), and (b_{1T}) is the true chip width (m). The tool-chip contact length (l_c) is calculated based on equation 5-6 where (t_{1T}) is the true uncut chip thickness (m) and $(k = 1.5)$ when $(\xi < 4)$ and $(k = 1.3)$ when $(\xi \geq 4)$ [66].

5-3-3 Friction at the Tool-Workpiece Interface

The power spent because of friction at the tool-workpiece interface is calculated as presented in [62]. In equation 5-7, (v) is the cutting velocity (m/s) and (F_{fF}) is the friction force on the tool–workpiece interface.

$$P_{fF} = F_{fF} \times v \tag{5-7}$$

$$F_{fF} = 0.625 \times \tau_y \times \rho_{ce} \times l_{ac} \times \sqrt{\frac{B_r}{\sin \beta}} \tag{5-8}$$

$$B_r = \frac{\cos \alpha}{\xi - \sin \alpha} \tag{5-9}$$

In equations 5-8, (B_r) is the Briks similarity criterion [67], (τ_y) is the shear strength of the workpiece material (N/m^2), (ρ_{ce}) is the radius of the cutting edge (m), (β) is the normal clearance angle (deg), (α) is the normal rake angle (deg), (l_{ac}) is the length of the active part of the cutting edge (the length of the cutting edge engaged in cutting) (m).

5-3-4 New surface Formation and influence of the minor cutting edge

The power spent due to the formation of new surfaces (P_{ch}) is negligible in broaching as the cutting speed, and thus the frequency of chip formation is small. The energy spent due to the influence of the minor cutting edge (P_{mn-ce}) is assumed to be zero because broaching tool does not have minor cutting edge.

5-4   Force Model Verification

In order to check the validity of the proposed force model, four different materials were chosen and broaching tests were performed using the selected materials.

5-4-1 Obtaining Mechanical Properties of Workpiece Materials

AISI 1045, AISI 12L14, AL 7075, and Brass were used as workpiece materials and standard tensile tests were carried out to determine their mechanical properties. Figure 5-2 depicts the prepared samples for tensile tests. The engineering and true stress strain curves for the test materials are presented in figures 5-3 to 5-6.
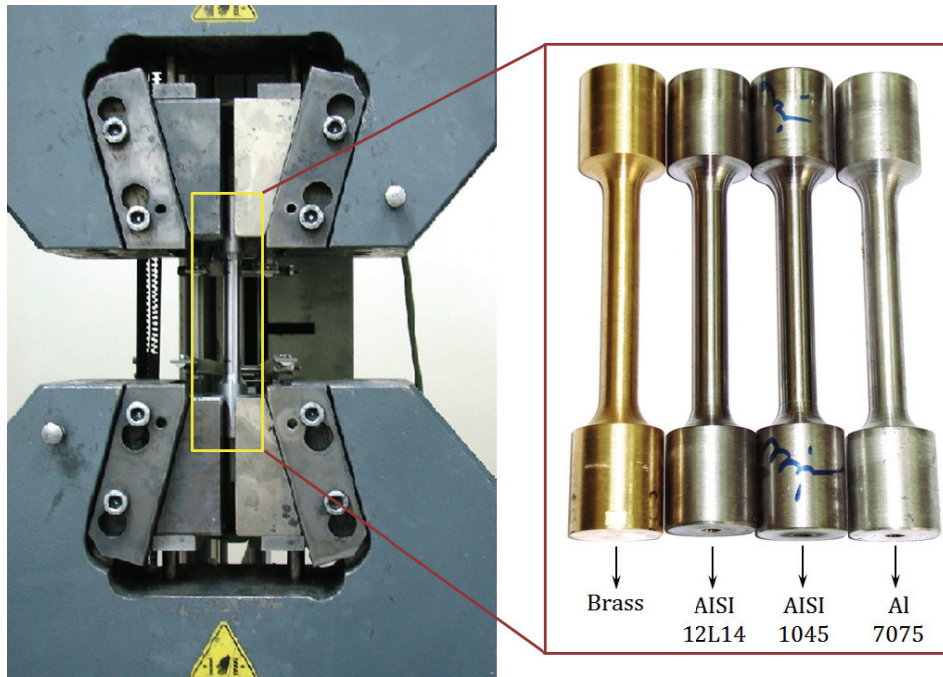
Figure 5-2: Tensile tests and prepared samples
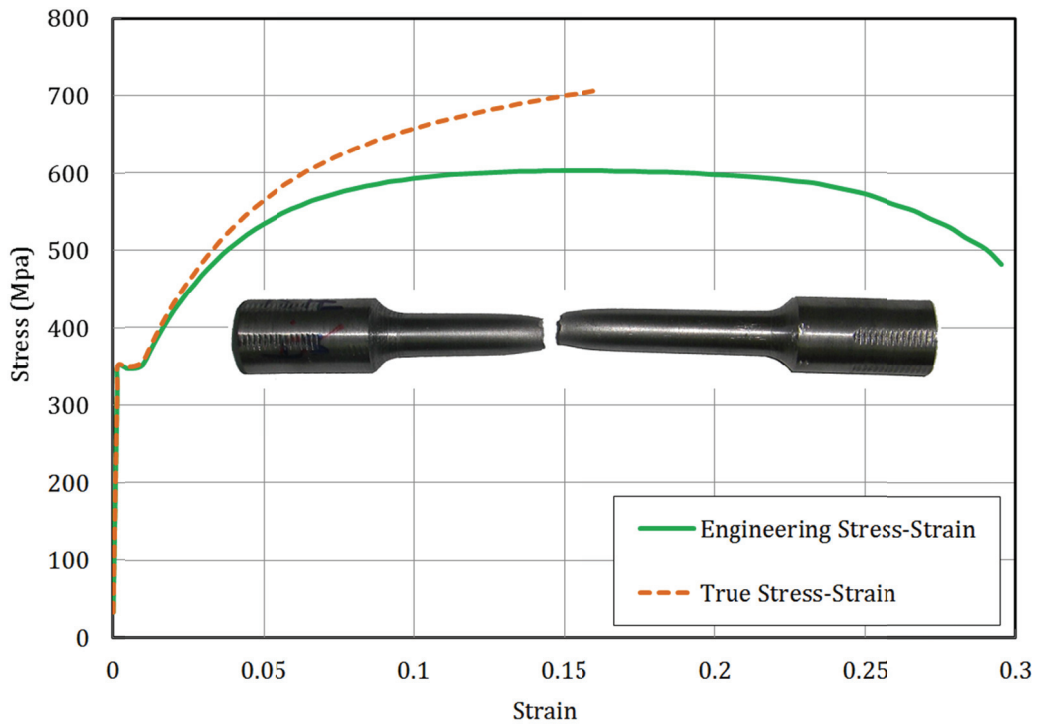
Figure 5-3: Stress-strain curves for AISI 1045
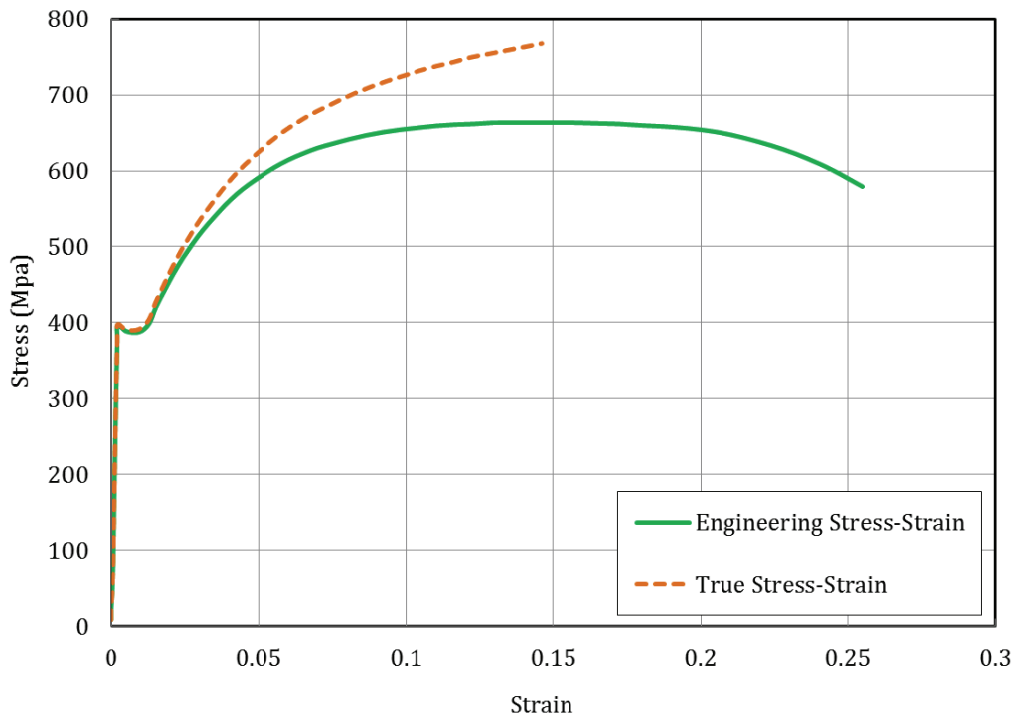
Figure 5-4: Stress-strain curves for AISI 12L14
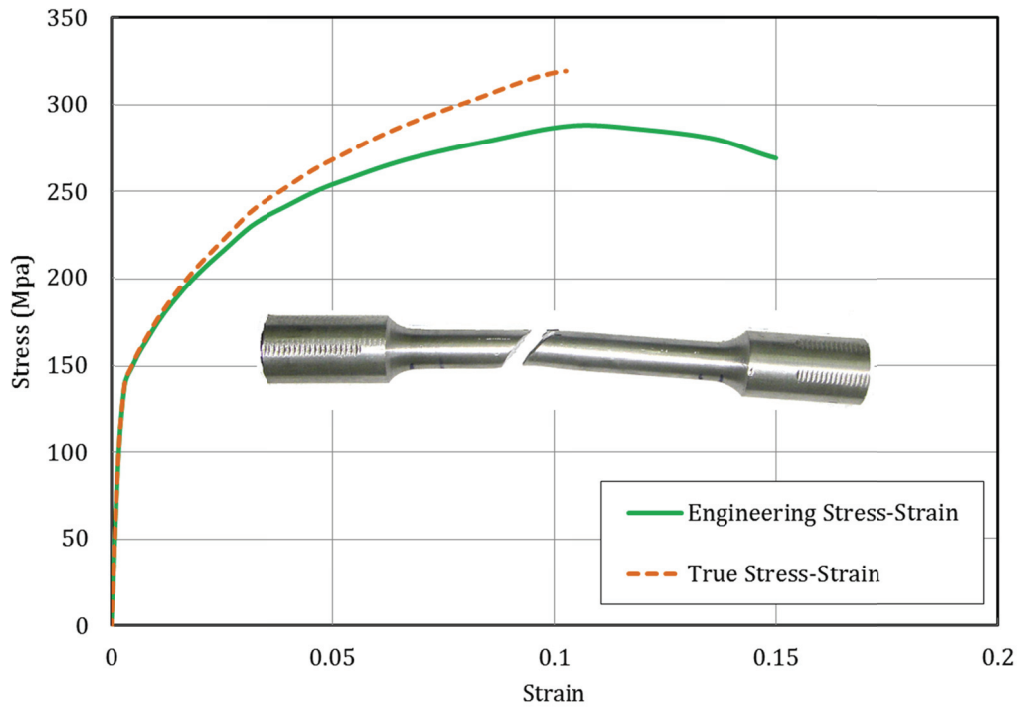
Figure 5-5: Stress-strain curves for Al 7075
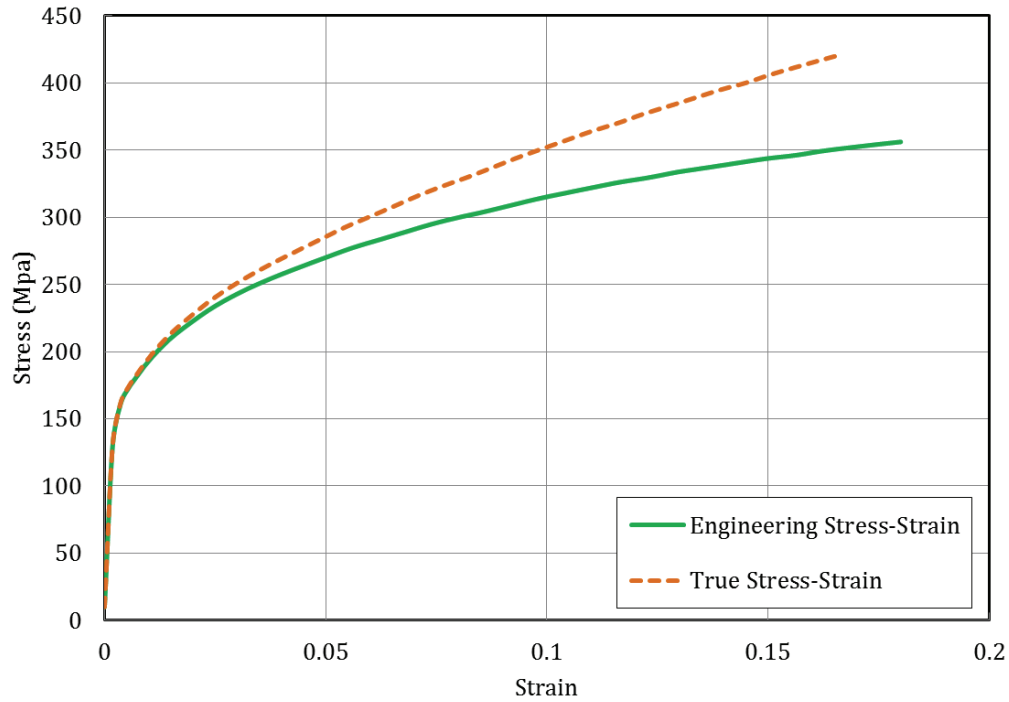
Figure 5-6: Stress-strain curves for Brass

Table 5-1 shows the mechanical properties and the other required parameters for workpiece materials extracted from stress-strain curves.

Table 5-1: Mechanical properties of workpiece materials

	AISI 1045	AISI 12L14	Al 7075	Brass
E (GPa)	210	200	64	80
σ_{yield} (MPa)	346	397	135	147
$\sigma_{R(ultimate)}$ (MPa)	605	663	280	356
K (GPa)	0.96	1.07	0.45	0.54
n	0.17	0.18	0.24	0.30
ξ	9	5	6	4
τ_y (MPa) [68]	$0.75\,\sigma_R$	$0.75\,\sigma_R$	$0.65\,\sigma_R$	$0.65\,\sigma_R$
τ_c (MPa)	169	186	78	100

5-4-2 Experimental Setup and Test Configuration

A broaching machine with 5000 kg maximum pull load capacity and 1000 mm maximum length of stroke was utilized to perform the tests. A number of continuous and interrupted broaching tests were conducted to validate the model and to investigate the effects of broaching operation on the surface integrity of the machined surface. The generated cutting forces were collected using a KISTLER 9255B table dynamometer equipped with a 5070 charge amplifier.

5-4-2-1   Workpiece Geometry

The results of an experiment are reliable when the tests are performed in a real situation. For this reason a wheel hub which is a common part in automotive industry was selected as sample geometry for the workpiece. Figure 5-7 illustrates the geometry of the above mentioned wheel hub before and after broaching.
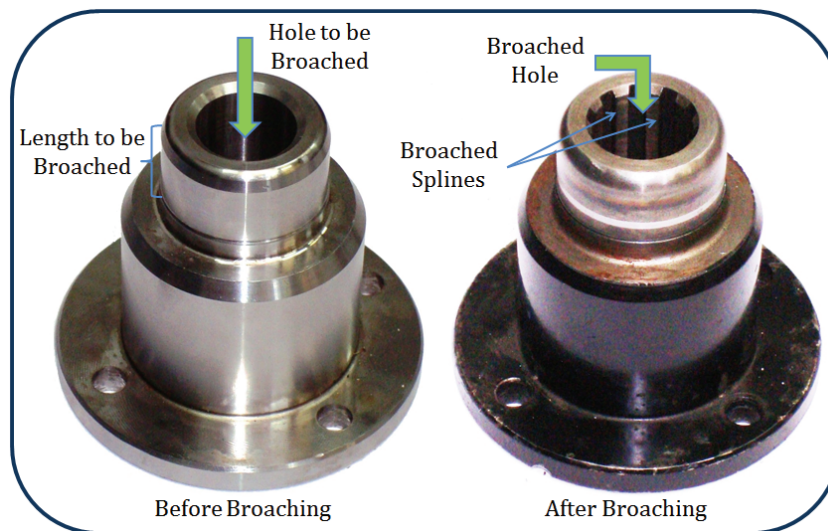
Figure 5-7: Geometry of the selected wheel hub before and after broaching

According to Figure 5-7, the only part of the wheel hub to be broached is the upper part; therefore, cylindrical workpieces were prepared with the same length equal to the length of the part to be broached from the coupling and pre-drilling and boring was performed to make the initial hole to let the broaching tool go through the workpiece and start the cutting action. Figure 5-8 depicts the geometry of the prepared sample.
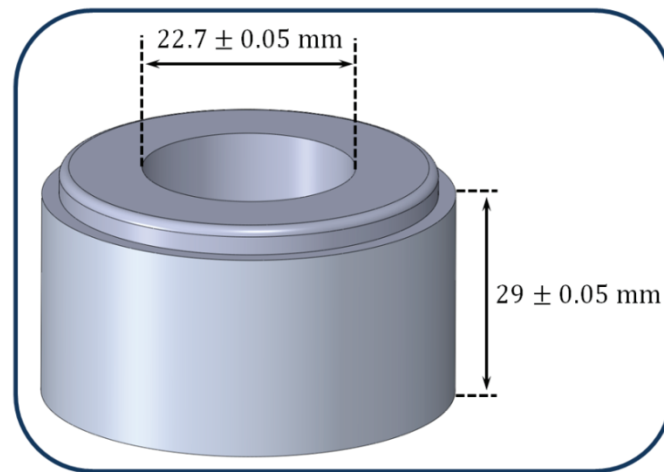
Figure 5-8: Geometry of the prepared samples for broaching tests

5-4-2-2   Broaching Tool

A spline broaching tool made up of HSS (ASP2023) was employed to run the experiments. The spline broaching tools are commonly utilized in automotive industries to produce internal gears for power trains. The broaching tool was digitized by RENISHAW Cyclone digitizer with 1 μm accuracy and the obtained set of data was used to extract the geometric features of cutting edges. Figure 5-9 and Table 5-2 demonstrate the geometric features of the utilized broaching tool.
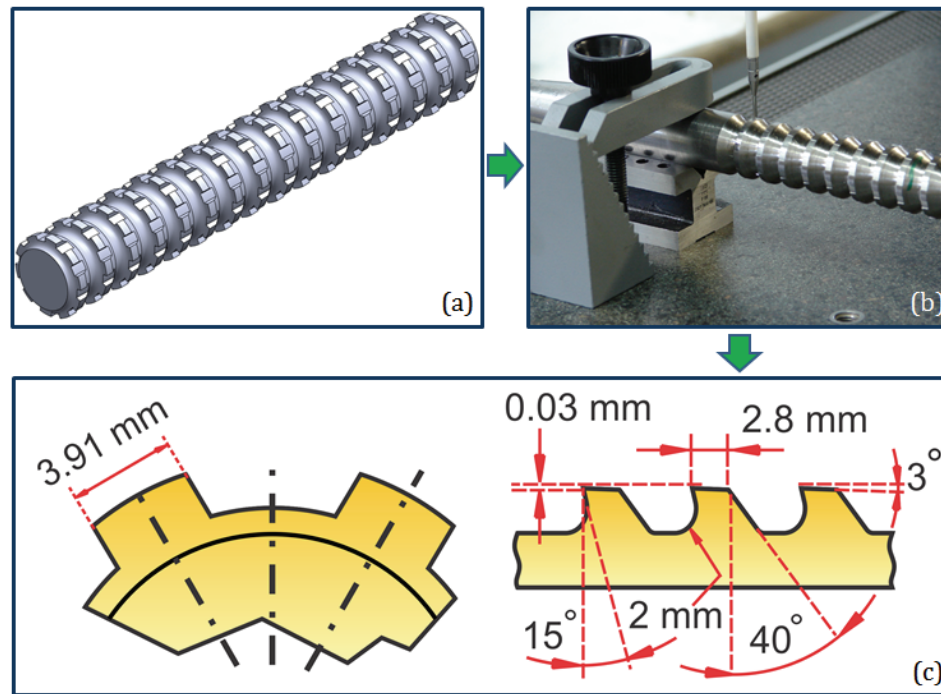
Figure 5-9: (a) Schematic view of the broaching tool. (b) Digitizing the tool. (c)

Extracted geometry of the broaching tool

Table 5-2: Geometric features of broaching tool

Tool type	Full form- pull end
Minor diameter	22.6 mm
Number of splines on each tooth	10
Spline width	3.91 mm
Number of teeth	44
Rise per tooth	0.03 mm
Pitch	10 mm
Land	2.8 mm
Rake angle	15°
Clearance Angle	3°
R_1	2 mm
R_2	N/A
Tooth height	3 mm
Edge radius	5 µm
Length of broach	965.2 mm
Distance to first tooth	304.8 mm

5-4-2-3 Fixture

In order to hold the workpieces against the broaching tool during machining, a fixture was designed and manufactured which includes a base plate and hood to keep the workpiece aligned with the tool and prevent any lateral motion during broaching. The fixture has the capability to be mounted either directly on the broaching machine table or on the dynamometer when cutting force acquisition is required. Figure 5-10 displays the fixture and its components.
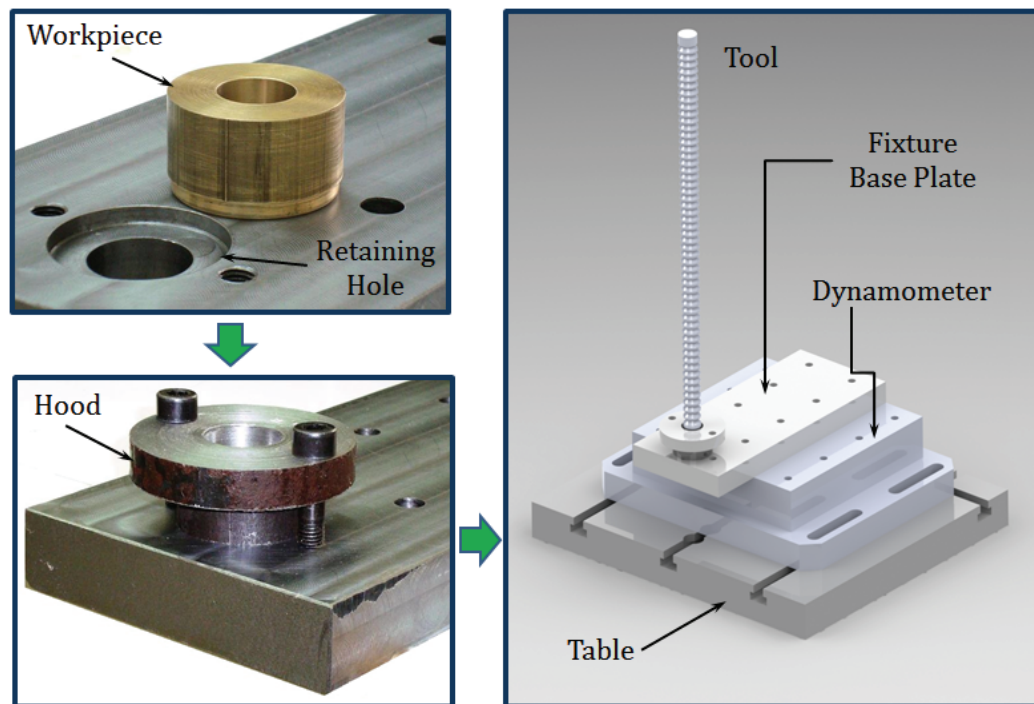
Figure 5-10: Fixture and its components

5-4-3 Cutting Tests

Broaching tests were performed at the cutting speed of 1 m/min. The cutting operation is assumed plain strain; therefore, the difference between chip width

before and after cutting is negligible. As a result, b_{1T} is equal to the length of cutting edge $(l_{ac} = b_{1T} = 3.91 \text{ mm})$. The true uncut chip thickness t_{1T} is also assumed equal to difference between the heights of two successive cutting edges $(t_{1T} = rise\ per\ tooth = 0.03 \text{ mm})$. These values also verified utilizing the proposed geometric model in chapter 4. Figure 5-11 shows the interpolation of two successive cutting edges for the applied spline broaching tool.
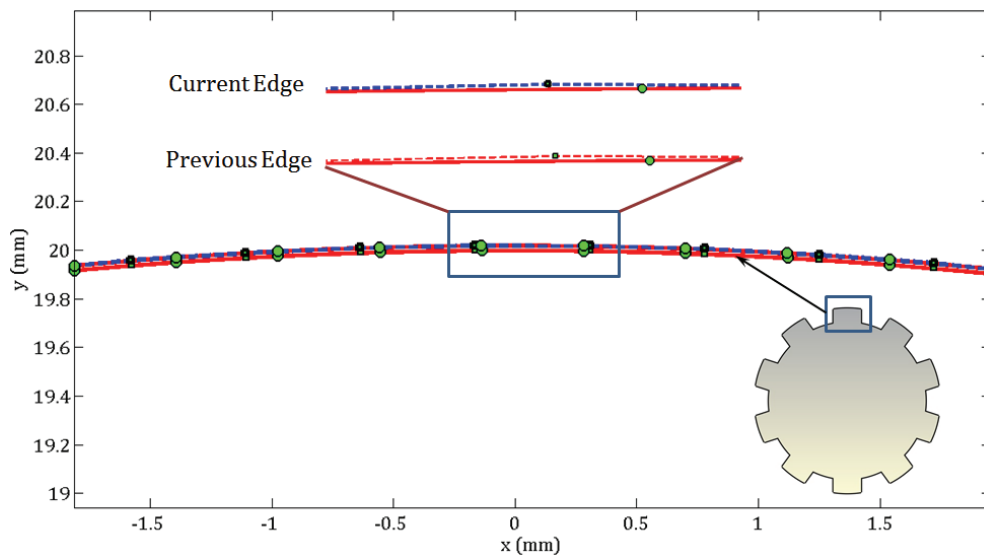
Figure 5-11: B-spline interpolation of two successive teeth for utilized spline broaching tool

The total cutting force is calculated by multiplying the force per tooth calculated using equation 5-1 by the number of splines on each tooth and then by the number of teeth simultaneously engaged with the workpiece. Figure 5-12 demonstrates the test configuration. The simulated cutting force (along the cutting velocity) has been plotted versus measured forces in figures 5-13 to 5-16.
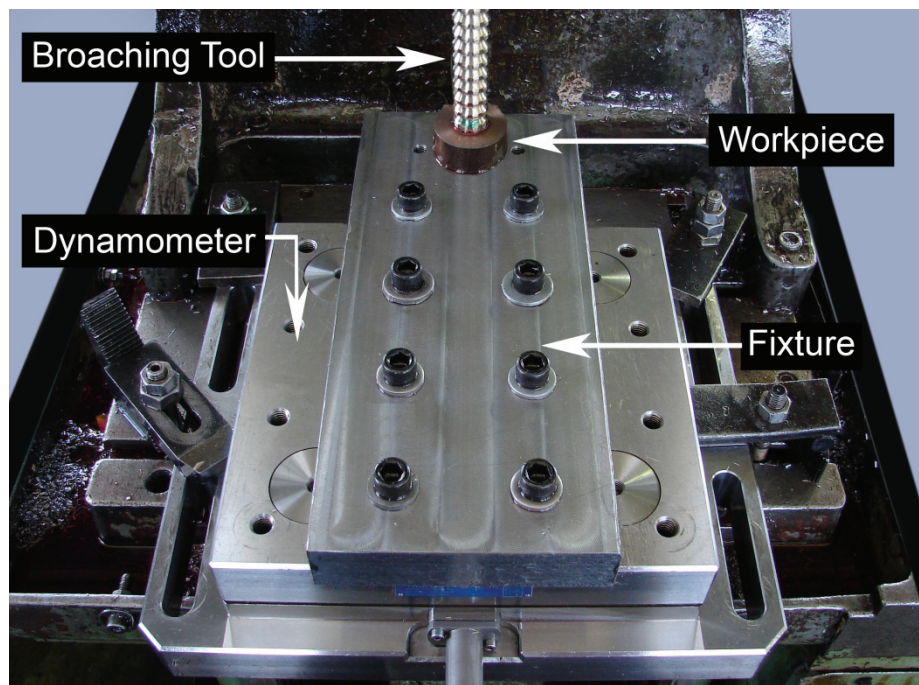
Figure 5-12: Broaching test configuration
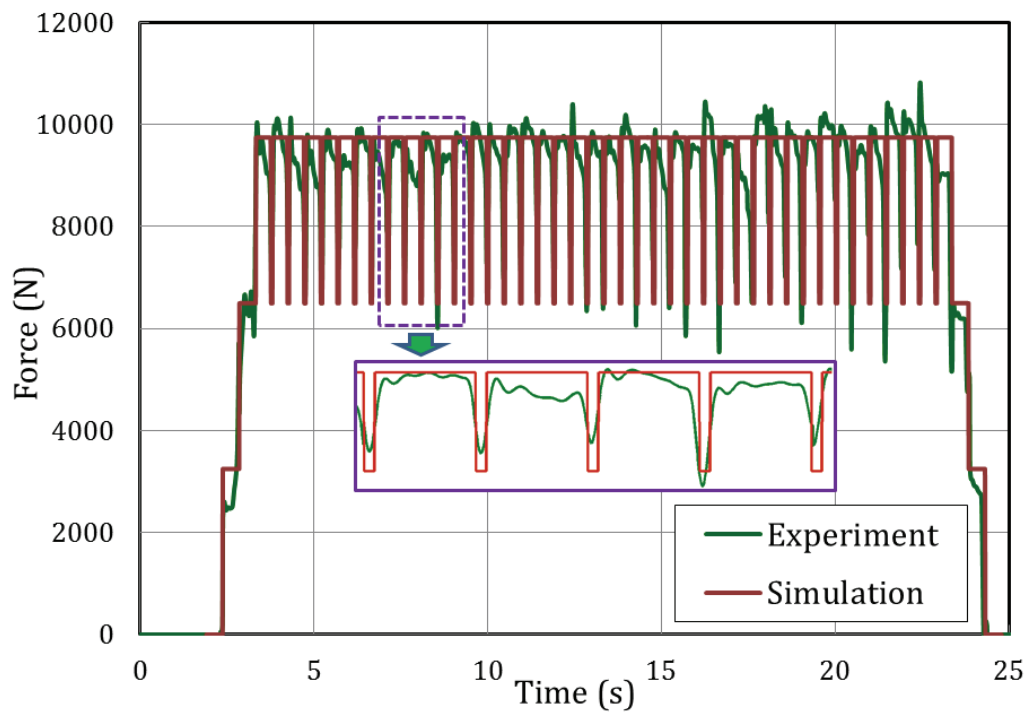
Figure 5-13: Simulated and measured cutting force for AISI 12L14
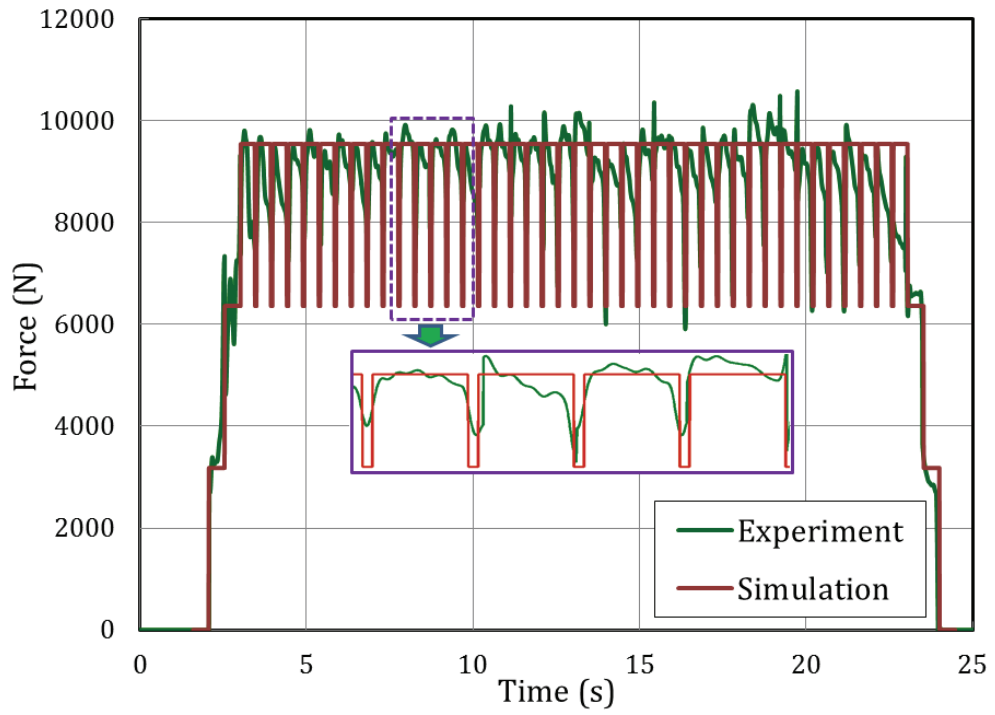
Figure 5-14: Simulated and measured cutting force for AISI 1045
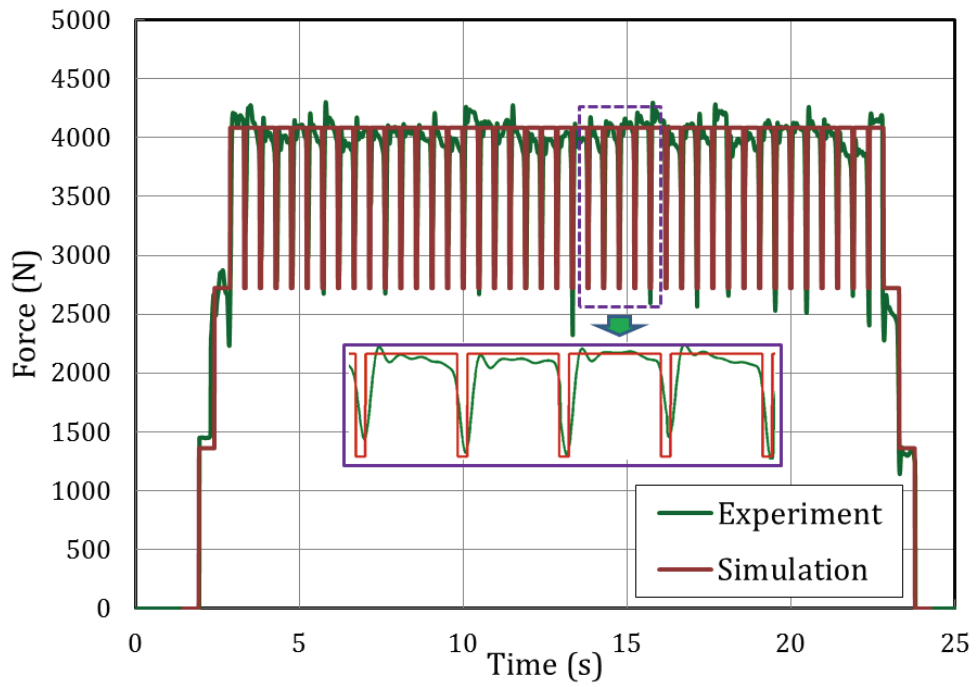
Figure 5-15: Simulated and measured cutting force for Al 7075
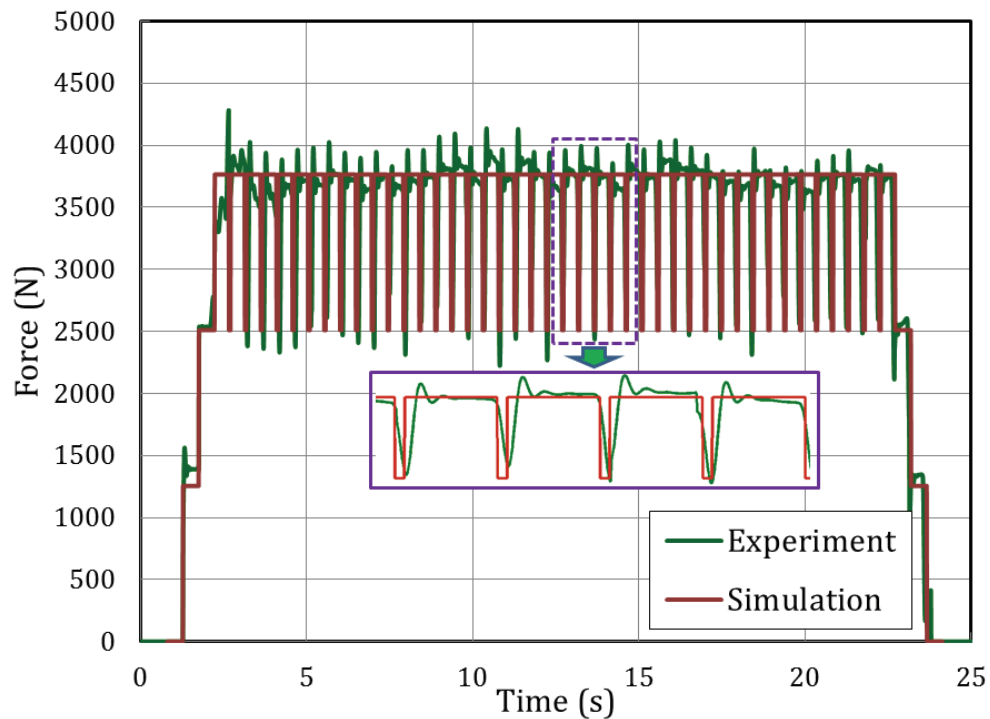
Figure 5-16: Simulated and measured cutting force for brass

As it can be seen, once the tool engages with the workpiece the cutting force increases progressively until the maximum possible number of teeth is in engagement. Then, cutting force oscillates between its maximum and minimum during the stable phase of cutting. Once the last tooth engages with the workpiece, the cutting force gradually drops as the tool leaves the workpiece. Figures 5-12 to 5-15 verify the good agreement between the simulated and the measured data.

5-5   Summary

An energy-based methodology for simulating the cutting force during the broaching operation has been presented in this chapter. The mathematical

formulation applied for the cutting force simulation is based on quantifying the contribution of different power components spent in the cutting system. The simulated cutting force and measured results are reasonably close; therefore, the proposed force model can be used for designing the broaching tool as well as optimizing the process.

Chapter 6: Effects of Broaching Operation on the Integrity of Machined Surface

6-1 Preamble

The strength and durability of machined parts are the highly influential factors to fulfil the growing requirements of industries especially where safe performance under severe condition is a matter of concern. The main objective of this chapter is to investigate the effects of broaching operation on the integrity of machined surface. Several samples were prepared and used to study the effects of broaching operation and the successive teeth of broaching tool on the subsurface microhardness, subsurface plastic deformation and surface roughness of the broached parts.

6-2 Surface Integrity and Its Importance

Mechanical components are typically designed based on their mechanical and physical properties. However, during machining operations some changes are

introduced to the workpiece which alter its mechanical and physical properties near the surface region. Mechanical properties such as creep resistance, corrosion resistance, fatigue limit, and cracking are among those properties that are highly influenced by surface characteristics. It has been determined [47, 54, 69, 70] that fatigue failure occurs near or on the surface of the machined part. Surface integrity becomes the principal factor where the part is subjected to continuous dynamic loading and severe environmental conditions. Power generation and aerospace industries are significant examples of the structures subjected to dynamic stresses and high temperatures. For these reasons the surface characteristics must be acquired to promote the design process. In addition, the corresponding cutting parameters that will generate the best surface quality must be also identified [71].

Generally, the surface integrity refers to the excellence and functionality of the machined surface; hence, proposing a unique definition for it is not easy. "Surface integrity is commonly described as the topographical, mechanical, chemical and metallurgical state of a machined surface and its relationship to functional performance" [5]. Surface integrity can be generally divided into two main categories: surface texture (surface topography) and surface metallurgy (surface layer characteristics) [42, 44, 47, 72]. Surface texture refers to the entire surface features associated with the geometry of machined surface such as surface roughness, form errors and surface waviness. Surface metallurgy or the characteristics of the surface layer includes any types of changes introduced to the

part surface base metal like subsurface plastic deformation, subsurface microhardness, residual stress, phase changes, recrystallization, and cracks.

Surface integrity, in spline broaching of automotive components such as sun gears, is important since this operation is a finishing operation and thus directly determines the nose and reliability of the whole transmission. Moreover, because sun gears are subjected to heat treatment after broaching, plastic deformation beneath the broached surface (depth of cold-working) determines the distortion due to the heat treatment. Therefore, the heat treatment regime should be adjusted correspondingly knowing this depth [1].

Among all of the previously mentioned integrity parameters, surface roughness, subsurface plastic deformation, and subsurface microhardness were selected and studied before and after performing broaching operation.

6-3   Experimental Procedure

A number of continuous and interrupted broaching tests were conducted on four different workpiece materials to investigate the effects of broaching and successive teeth on the integrity parameters of machined surface. Broaching tests were performed using spline broach made of HSS ASP2023.

To examine the broached surface and sub-surface, small pie shape specimens were cut from the workpiece. Specimens were cut from the workpiece using wire EDM in a manner which minimizes the effects of the removal process on the surface integrity and leads to the least possible surface alteration or burning.

In continuous broaching tests, the tool was permitted to complete its stroke while in interrupted tests; the tool was stopped at the middle of the cut and was retracted slowly. Due to the conical shape of the broaching tool, slow retraction of the tool does not have a significant damaging effect on the surface. The interrupted tests were performed in order to keep the feed marks of broaching tool on the workpiece and to study the effect of each individual tooth on the integrity of the broached surface. Figure 6-1 illustrates the mechanism of the interrupted tests and the geometry of samples used for the surface integrity investigations.
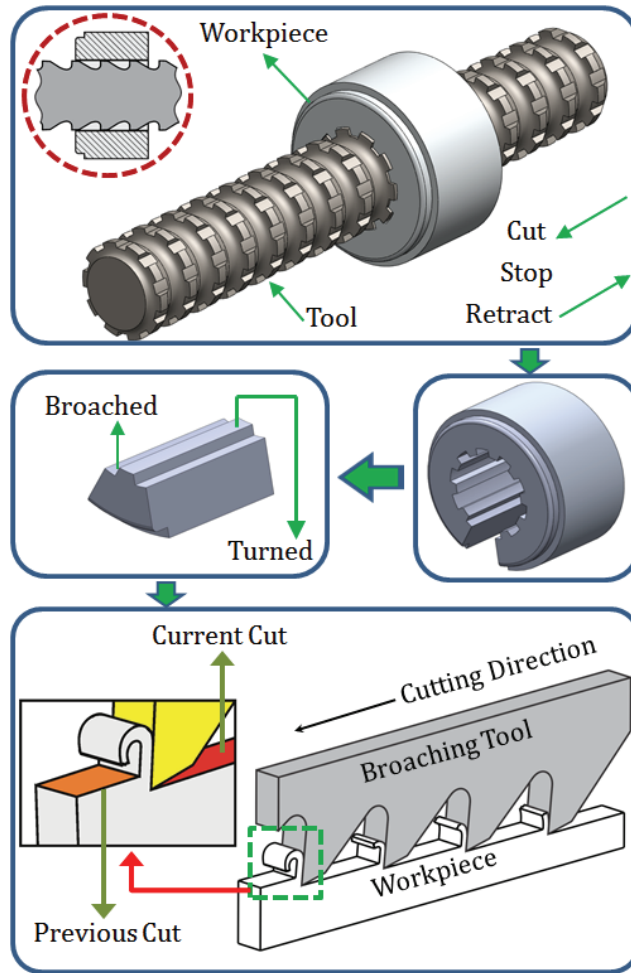
Figure 6-1: Interrupted cutting and geometry of the samples

The samples are washed gently using Isopropyl Alcohol to remove the dust and rust from the surface. At this step the samples are ready for surface roughness measurements. Finishing the surface roughness tests, the samples were mounted in a thermoplastic acrylic which is recommended for general metallurgy and then polished in order to get a smooth and flat surface to investigate the plastic deformation and variation of microhardness beneath the broached surface. The polishing steps for AISI 12L14, AISI 1045, Al7075, and brass are selected according to Buehler catalogue presented in Table 6-1 and Table 6-2.

Table 6-1: Four-step polishing procedure for AISI 12L14 and AISI 1045

(Courtesy of BUEHLER Canada)

		Surface	Abrasive	Lubricant	Time	Force / Sample
1	Grinding	CarbiMet	180 Grit	Water	1:00 min	31N
2	Polishing	UltraPol	9 μm Diamond	N/A	5:00 min	31N
3	Polishing	TexMet	3 μm Diamond	N/A	3:00 min	31N
4	Polishing	MasterTEX	0.05 μm Alumina	N/A	1:00 min	31N

Table 6-2: Five-step polishing procedure for Al 7075 and brass

(Courtesy of BUEHLER Canada)

		Surface	Abrasive	Lubricant	Time	Force / Sample
1	Grinding	CarbiMet	240 Grit	Water	1:00 min	31N
2	Grinding	CarbiMet	320 Grit	Water	1:00 min	31N
2	Polishing	UltraPol	6 μm Diamond	N/A	5:00 min	31N
3	Polishing	TriDent	3 μm Diamond	N/A	3:00 min	31N
4	Polishing	VelTEX	0.05 μm Alumina	N/A	2:00 min	31N

6-4   Effects of Broaching on the Roughness of Machined Surface

Running the machines at their highest level of performance and maintaining product quality at the same time are desired practices in each manufacturing system. Achieving the above mentioned goals simultaneously is a challenging job specifically when machining (cutting of metals) where several sophisticated phenomena tack place is a matter of interest. To overcome these problems, the cutting tools must be accurately designed and the value of machining parameters must be precisely selected to reach the desired level of part quality and keep the production rate high.

One of the broadly used indexes for describing the quality of part surface is surface roughness [73] which plays an important role in the performance of part under different types of loading. Several roughness parameters of the broached surfaces were measured using white light interferometry microscope at different steps given that the broaching tool enters the cut until it leaves the workpiece. Table 6-3 shows the definition of different roughness parameters. In Table 6-3, (S_a) describes the average distance to the mean, (S_q) describes the standard deviation of the surface, (S_{sk}) describes the asymmetry of the height distribution, (S_{ku}) describes the width of the height distribution, (S_v) represents the depth of the deepest valley, (S_p) shows the height of the highest peak, (S_t) describes the distance between the deepest valley to the highest peak evaluated over the entire surface and finally (S_z) represents the distance from the deepest valley to the highest peak evaluated over base surface and averaged.

Table 6-3: Definition of the roughness parameters

Parameter	Name	Definition
S_a	Average Roughness	$S_a = \dfrac{1}{MN} \displaystyle\sum_{m=1}^{M} \sum_{n=1}^{N} |z_{mn} - \bar{z}|$
S_q	Root-Mean Square Roughness	$S_q = \sqrt{\dfrac{1}{MN} \displaystyle\sum_{m=1}^{M} \sum_{n=1}^{N} (z_{mn} - \bar{z})^2}$
S_{sk}	Skewness	$S_{sk} = \dfrac{1}{MNS_q^3} \displaystyle\sum_{m=1}^{M} \sum_{n=1}^{N} (z_{mn} - \bar{z})^3$
S_{ku}	Kurtosis	$S_{ku} = \dfrac{1}{MNS_q^4} \displaystyle\sum_{m=1}^{M} \sum_{n=1}^{N} (z_{mn} - \bar{z})^4$
S_v	Valley Depth	$S_v = |\min(z_{mn})|$
S_p	Peak Height	$S_p = |\max(z_{mn})|$
S_t	Total Roughness	$S_t = S_v + S_p$
S_z	Average Total Roughness	$S_z = \langle S_v + S_p \rangle_{eval.surf}$

As it has been previously mentioned, the initial hole to let the broaching tool go through the workpiece and start the cut was made using drilling followed by boring to increase the diameter and acquire the required dimension. Similar to the

turning operation, the main factors that affect the surface roughness generated in boring are geometry of cutting tool, feed rate, material properties of workpiece, eccentricity of spindle, rotation errors, and chatter vibration [74]. Assuming that machine and cutting tool are in perfect condition and there is no room for error and chatter vibration, the surface roughness in turning and boring is dominantly generated along the axial direction of the workpiece through a recurrence of the tool geometry at feed per revolution span [74]. This profile can be exactly seen for the four different test materials before broaching (see Appendix A).

When the broaching tool starts the cut, the teeth enter the workpiece after each other and remove a certain amount of material from workpiece surface. In the absence of feed motion in broaching, feed action is performed by the rise per tooth; hence, the generated surface by the current tooth is completely swept by the next one. In this case, the dominant parameters affecting the surface integrity are tool nose radius and the quality of cutting edge. Any imperfection of cutting edges like chipping and cracks leave its footprints on the generated surface. The footprint of broaching teeth is usually removed by finishing teeth at the end of the cut to promote the surface quality. In the case of imperfection on the finishing teeth, the trail of the imperfection will remain along the machined surface from the beginning to the end of the cut. The average roughness (S_a) which is the most widely used parameter among the surface roughness parameters is presented in Table 6-4 for AISI 12L14, AISI 1045, Al 7075, and brass.

Table 6-4: S_a for test materials before, during, and after broaching

Stage	AISI 12L14	AISI 1045	Al 7075	Brass
Before Broaching	$3.18\ \mu m$	$3.09\ \mu m$	$1.3\ \mu m$	$0.808\ \mu m$
After 21st Tooth	$2.6\ \mu m$	$3.9\ \mu m$	$1.4\ \mu m$	$1.03\ \mu m$
After 22nd Tooth	$2.9\ \mu m$	$1.37\ \mu m$	$1.66\ \mu m$	$0.946\ \mu m$
After 23rd Tooth	$1.8\ \mu m$	$2.99\ \mu m$	$0.803\ \mu m$	$0.774\ \mu m$
After complete Stroke	$1.24\ \mu m$	$1.2\ \mu m$	$1.3\ \mu m$	$0.806\ \mu m$

As can be seen from **Error! Reference source not found.**, the average roughness for AISI 12L14 and AISI 1045 is almost the same. However, the same machining operation results in much smoother surface for softer material like Al 7075 and brass. When comparing Al7075 and brass, the surface roughness for brass is smaller due to its softness and better machinability. General trend during broaching is to decrease the surface roughness and increase the surface quality. However, no significant change can be seen for Al 7075 and brass. This may occur because the size of the chips which are trapped in the gullet space during broaching of Al 7075 and brass is smaller than that of AISI12L14 and AISI 1045. In comparison to the other test materials, brass has smaller chip thickness ratio (ξ) which results in smaller chip size. The smaller chips can be accommodated in the gullet space easier than the large chips which prevent the chips from being trapped between the cutting tooth and the workpiece. If the chip is trapped between the cutting tooth and workpiece surface, it will be pressed against the surface which make it re-deposited and stick to the surface. The re-deposition of material destroys the surface quality [37].

The surface roughness profile and the corresponding roughness parameters for AISI 12L14, AISI 1045, Al 7075, and brass are presented in Appendix A. These figures show the surface roughness before, during, and after broaching.

6-5   Effects of Broaching on the Subsurface Microhardness and Subsurface Microstructure of the Machined Surface

The Vickers hardness (HV) was utilized for measuring the microhardness beneath the broached surface. Following figures show the effects of broaching operation on microhardness and microstructure of the subsurface layers.
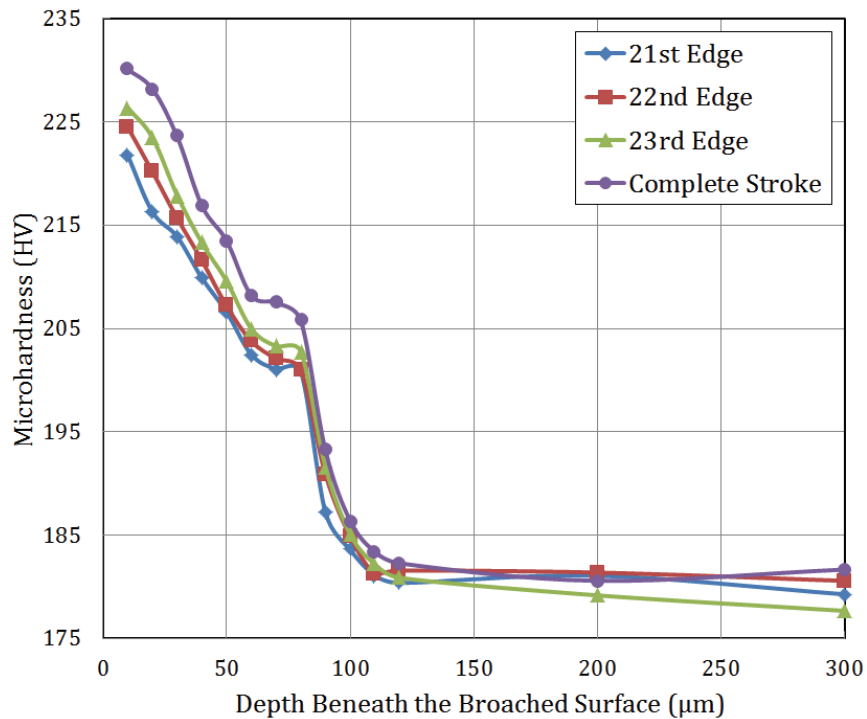
Figure 6-2: Variation of microhardness beneath the broached surface of AISI 12L14
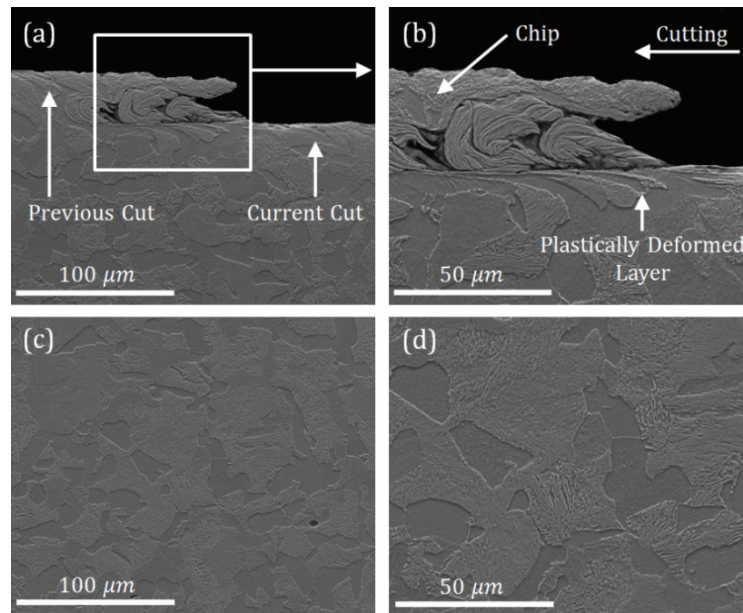
Figure 6-3: SEM image for AISI 12L14 (a, b) subsurface around the chip root and (c, d) far beneath the broached surface with different magnifications for 23rd edge
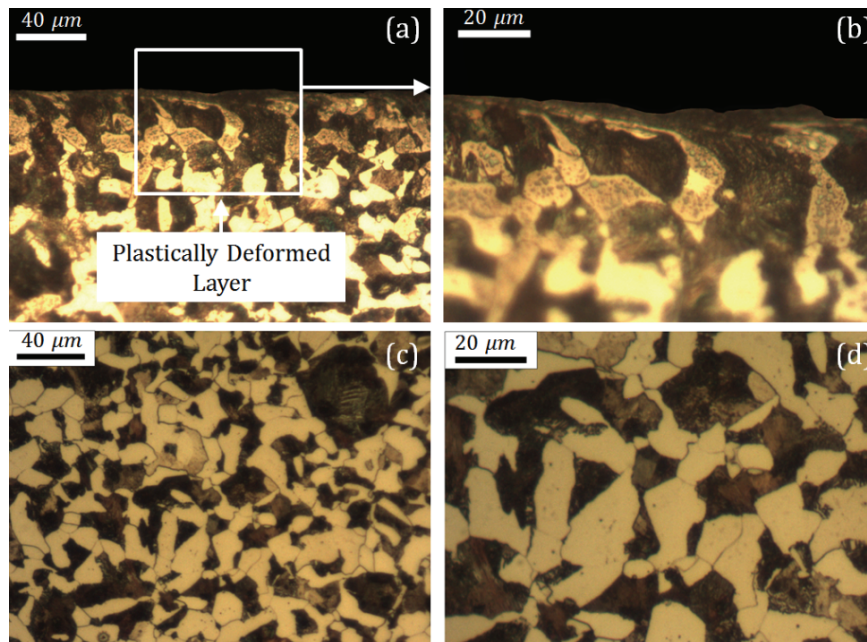
Figure 6-4: Subsurface microstructure for AISI 12L14 (a, b) near the broached surface (c, d) far beneath the broached surface
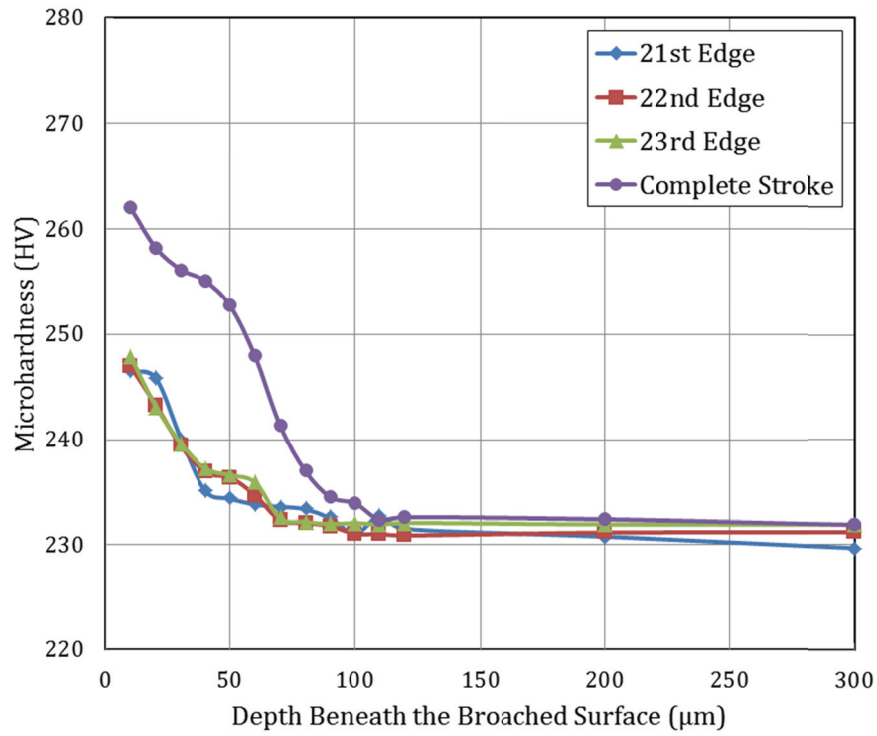
Figure 6-5: Variation of microhardness beneath the broached surface of AISI 1045
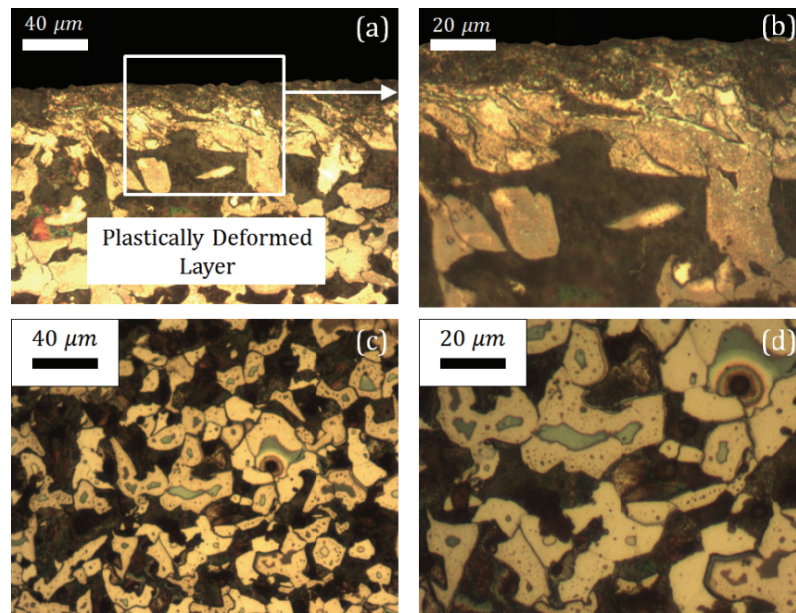
Figure 6-6: Subsurface microstructure for AISI 1045 (a, b) near the broached

surface (c, d) far beneath the broached surface
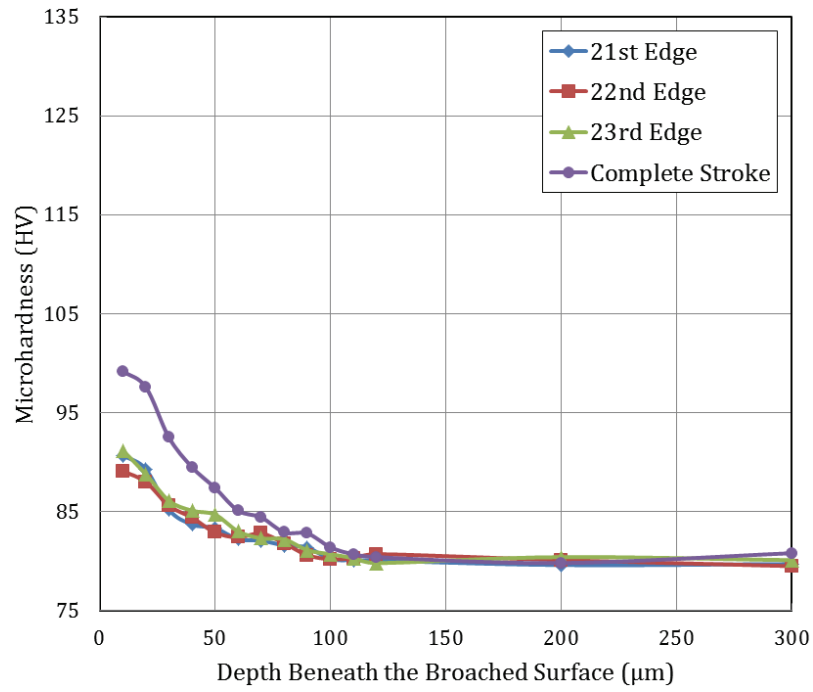
Figure 6-7: Variation of microhardness beneath the broached surface of Al 7075
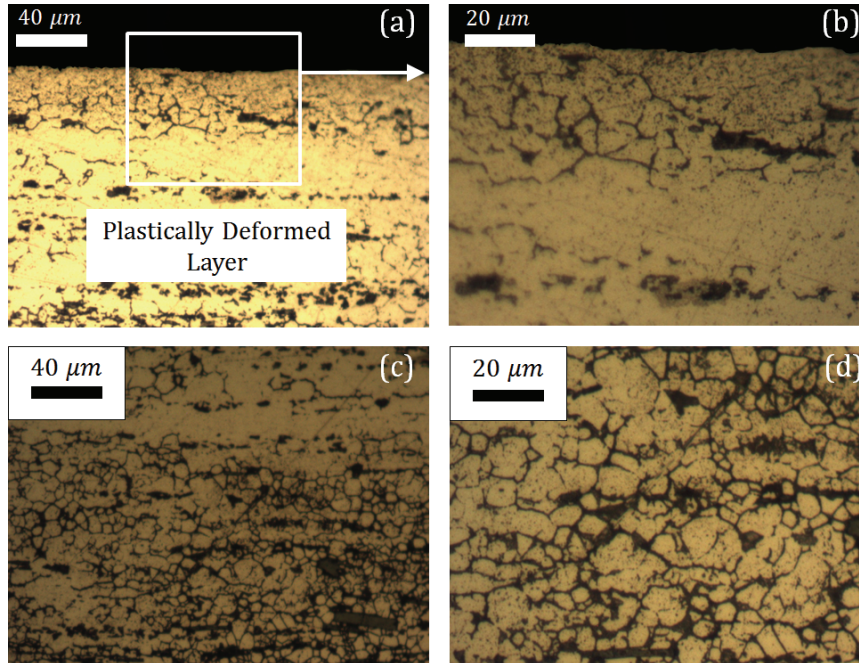
Figure 6-8: Subsurface microstructure for Al 7075 (a, b) near the broached surface

(c, d) far beneath the broached surface
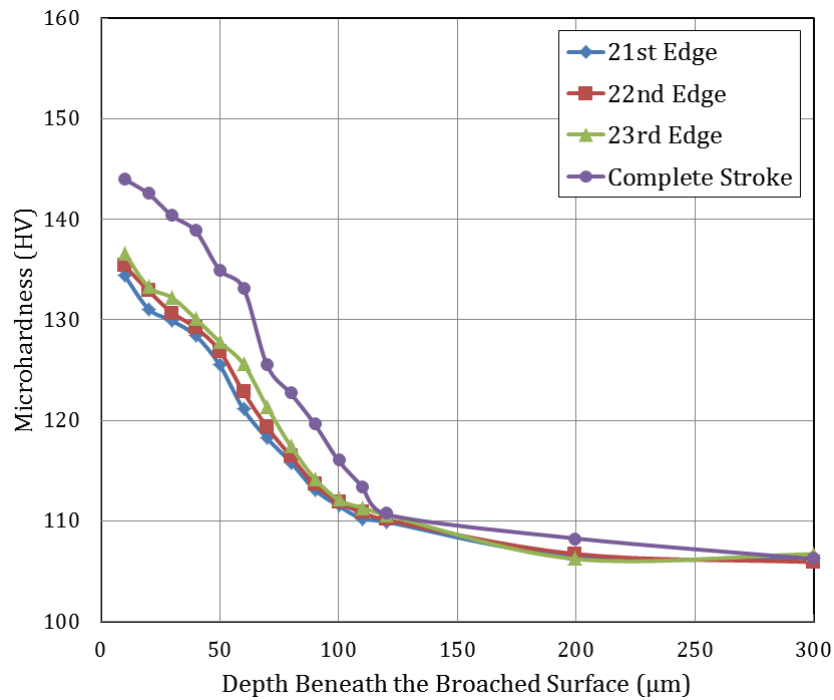
Figure 6-9: Variation of microhardness beneath the broached surface of Brass

Figure 6-2, Figure 6-5, Figure 6-7, and Figure 6-9 show the microhardness beneath the broached surface for AISI 12L14, AISI 1045, Al 7075 and brass for interrupted cut and full cut respectively. Each point represents the average of five data points which are measured at different locations along the same depth beneath the surface. As can be seen, although successive teeth introduce more plastic deformation which is demonstrated by the higher microhardness reading, the depth of the plastically deformed layer was kept unchanged. It can be noted from the above mentioned figures that there is no significant change between the microhardness beneath the broached surface by successive teeth; however, the microhardness beneath the broached surface increases at the end of the cut when

the broaching tool completely leaves the workpiece. This can be related to the effects of finishing teeth at the end broaching tool. Having no rise per tooth, the finishing teeth of a broaching tool do not perform cutting action. These teeth are utilized to improve the surface finish, control the geometric and form tolerances, and induce compressive residual stress to increase the surface and subsurface hardness to improve the fatigue life of the broached part especially if the part is going to be used under dynamic loading.

It can be noted from microhardness figures that in relatively harder material (AISI 12L14 and AISI 1045) more than 80 μm beneath the surface is severely affected by broaching operation while in softer material (Al 7075 and brass specially Al 7075) the depth of aggressively affected part is less than 70 μm. In softer material, the surface layer which is being cut by the current teeth is acting like a cushion and dampens the effect of plastic deformation and consequently decreases the depth of cold-working. The cold-worked layer is then removed by the successive teeth and the loop repeats again. In contrast, the surface layer of the harder material resists against the plastic deformation induced by the cutting edges; hence, other layers beneath the surface are compressed relatively higher than that of the softer materials. For this reason, the depth of cold-worked layer increases in steels (AISI 12L14 and AISI 1045).

To verify the findings shown in figures Figure 6-2, Figure 6-5, and Figure 6-7, SEM and regular examination of the depth of cold-working and severity of the grain deformation were carried out. As it has been previously mentioned, the

magnitude of the cutting forces in broaching is comparatively higher than that in other machining operations for the same uncut chip thickness. As a result, the depth of cold-working is relatively larger (see figures Figure 6-3, Figure 6-4, Figure 6-6, and Figure 6-8). As can be seen, severe plastic deformation or elongation of the grains of the work material took place in the direction of the cutting. The depth of cold-working measured in these tests is the same as the ones determined by the microhardness tests.

6-6   Summary

The depth of cold-working which defines the distortions during heat treatment as well as the reliability of the parts is a function of several parameters like uncut chip thickness, cutting edge radius, material properties of the workpiece and the geometry of the finishing teeth for standard broaching tool geometry. As such the extent of the most severe plastic deformation can be an accurate indicator in the selection of the proper radius of the cutting edge of the broaching tool as well as the selection of the parameters of the subsequent heat treatment.

Chapter 7:   Optimized Design of Broaching Tools

7-1   Preamble

Among the cutting tools that are utilized in industry broaching tools are one the most expensive ones. Hence, a proper design of the broaching tools has the highest priority in broaching process planning and design. Every single feature of these expensive tools must be accurately designed to increase the productivity, promote the part quality and reduce the cost. In this chapter, a new approach is proposed for optimal design of the broaching tools considering several types of physical and geometrical process constraints.

7-2   Design Variables

The mathematical model for the geometry of broaching tool as well as the force model for estimating the cutting force during broaching operation was presented in chapters 2 and 5 respectively. An optimized design procedure will be developed in this chapter to identify the geometric features of the broaching tool

for maximum reliability. It must be noted that the geometry of broaching tool is unknown at the beginning of design process. The known parameters are the final geometry of the workpiece, geometry of the profile in the workpiece to allow the broaching tool goes through which is normally a hole and finally material properties of the workpiece. Geometric features of the broaching tool such as rake angle, clearance angle, pitch, land, tooth height and rise per tooth must be designed optimally to achieve the desired tool geometry for maximum performance.

Similar to any optimization problem, several design variables must be taken into consideration while optimized design of a broaching tool is a matter of interest. As it has been formerly stated by Kokturk [2] these variables are interconnected, and their governing equations are sometimes implicit and nonlinear. In previously published work discussing about broaching optimization [2, 39-41, 75, 76] the geometric variables such as pitch length (P), rake angle (α), clearance angle (β), land (f_b), gullet radius (r_1, r_2), and tooth height (h_b) that create the side profile of a broaching tool have been selected according to the commonly used values in industry. It has also been mentioned that further study is necessary in order to optimize these variables.

The above mentioned geometric variables are going to be studied in detail. Pitch which is the distance between two successive teeth directly defines the length of the broaching tool. In association with the length of the workpiece, the pitch length also controls the number of the simultaneously engaged teeth with the workpiece. The optimum tool length is attained by compromising between smaller

pitch which results in shorter length and higher stiffness at the cost of increasing the required power to overcome higher cutting forces due to having more teeth in cut at the same time. The same problem occurs while the rake angle or clearance angle must be optimized. Increasing the rake angle sharpens the tool and decreases the cutting forces but it adversely affects the tooth strength. Big clearance angle is also favourable since it decreases the rubbing between back of the tool and workpiece; however, it has the same negative effect as increasing the rake angle on the tooth strength. Gullet space is another important parameter that must be determined to provide enough space for accommodating the chips during the cutting action. The role of gullet space becomes more significant during internal broaching when the chips are trapped between broaching tool and workpiece until the tooth leaves the workpiece. The gullet geometry must have a rounded and smoothed profile to curl up the chip [16]. Tooth rise plays the role of feed motion in broaching operation and directly determines the chip thickness and consequently the cutting force, tooth stress and required power.

7-3   Optimization Procedure

To optimally design a broaching tool, an objective function must be defined and all of the above mentioned parameters such as pitch length (P), rake angle (α), clearance angle (β), land (f_b), gullet radius (r_1, r_2), and tooth height (h_b) need to be determined in order to satisfy the objective function. These parameters are constrained by several limiting factors which must be taken into consideration.

These constraints can be either machine tool restrictions like power and dimension or process and tool limitation like maximum allowable stress on the tooth.

7-3-1 Objective Function

The objective function is normally formulated based on the requirement of the broaching operation. It can be either achieving higher process stability by having a tool with the shortest possible length, reaching maximum productivity by maximizing the metal removal rate, or targeting both of them simultaneously. Tool length and metal removal rate (MRR) can be presented mathematically as follows:

$$L = (N - 1)P$$

$$MRR = \left(\frac{l_w \times rpt \times w \times N}{l_w + (N - 1)P}\right) \times V$$

(7-1)

where, (L) is tool length, (N) is the number of teeth on the broaching tool, (P) is the pitch length, (l_w) is the length of cut which is the length of the part or profile to be broached, (rpt) is the rise per tooth which is normally determined by the chip thickness, (w) is the width of the profile to be broached, and (V) is the cutting speed. As a result, the objective functions can be defined as:

$$Min\ L = Min\ [(N - 1)P]$$

$$Max\ MRR = Max\left[\left(\frac{l_w \times rpt \times w \times N}{l_w + (N - 1)P}\right) \times V\right]$$

(7-2)

Although both of the objective functions presented in equation 7-2 have a deep impact on the stability and productivity of the broaching process, satisfying both of them simultaneously is a challenging and time consuming job. In this thesis, maximizing MRR to promote the process productivity has been selected as an objective function and all of the necessary constraints are defined to satisfy this objective function.

7-3-2 Constraints

7-3-2-1   Tool Length

A broaching operation is performed by a broaching machine which holds the broaching tool and pushes or pulls it through the workpiece body to perform the cutting action. Each broaching machine has dimensional limitations and consequently a broaching tool which exceeds a certain limit cannot be accommodated by the machine. For this reason, the broaching tool must be designed considering this limiting factor. The tool length constraint can be expressed as follows [2]:

$$L_{tool} \leq L_{ram} \tag{7-3}$$

where (L_{tool}) is the length of the broaching tool and (L_{ram}) is the maximum length that can be accommodated by the ram of the broaching machine.

7-3-2-2   Gullet Space

As it was previously mentioned, the gullet space is an important feature of a broaching tool which holds the chip until the tool leaves the workpiece. Based on the geometric features of the broaching tool which was presented in chapter 3 (see figure 3-4), the gullet space can be mathematically approximated by equation 7-4. Figure 7-1 shows the gullet space and its contributing geometric features.
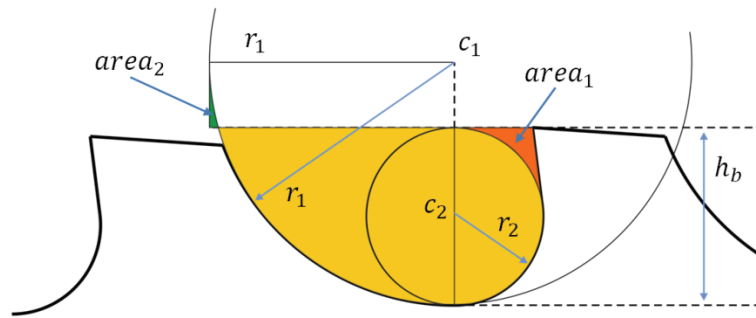
Figure 7-1: Gullet space

$$V_{gullet} = \left[\left(\frac{\pi r_1^2}{4} + \frac{\pi r_2^2}{2} \right) - (r_1 - h_b) \times r_1 \right] \times w \qquad (7\text{-}4)$$

where (r_1) is the bigger radius of the gullet, (r_2) is the smaller radius of the gullet, (h_b) is the tooth height, and (w) is the width of the profile to be broached. As can be seen from Figure 7-1, equation 7-4 is a pessimistic approximation of the gullet where $(area_1)$ is not considered toward the final volume of the gullet while $(area_2)$ which is not a part of gullet space is subtracted from the real space. This pessimistic approximation ensures that the calculated gullet space is smaller than the real space which is a positive point and brings a factor of safety into the calculations.

In order to provide enough space for the chip during the cutting action, it was recommended by Monday [16] that gullet space must be almost three times bigger than the cut chip volume. This constraint is represented by the following inequality:

$$\frac{V_{chip}}{V_{gullet}} \leq 0.35 \tag{7-5}$$

7-3-2-3   Chip Load and Tooth Stresses

Chip load and imposed stress on the tooth are directly related. Tooth stress is increased by increasing the chip load while decreasing the chip load will decrease the tooth stress. The chip load in broaching operation is directly determined by the rise per tooth. The normal stress acting on the tool rake face is shown in Figure 7-2.
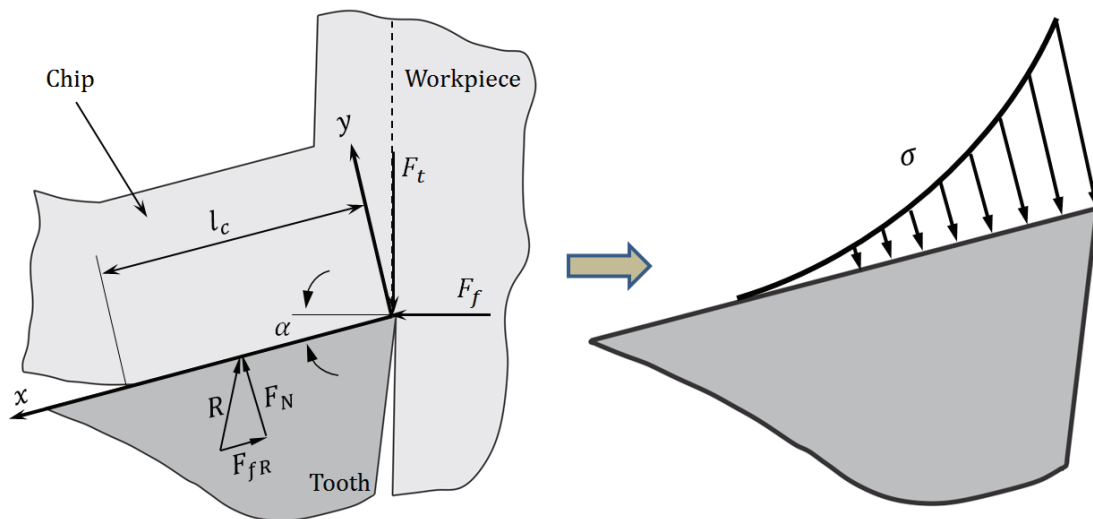
Figure 7-2: Distribution of contact stress on the tooth rake face

In Figure 7-2, (F_t) can be determined using equation 5-1. The component of force along the feed direction (along rise per tooth) (F_f) can be approximated as $(0.3F_t)$. Once the two components of force are determined, the friction angle (β_a) and friction coefficient (μ) can be calculated using equation 7-6 (see figure 5-1).

$$\beta_a = \alpha + \tan^{-1}\frac{F_f}{F_t}$$

$$\mu = \tan\beta_a$$

(7-6)

The friction force can be calculated using equation 5-6 which was previously presented in chapter 5. The normal force (F_N) is also revealed by applying the following equation:

$$F_N = \left(\sqrt{F_t^2 + F_f^2}\right)\cos\beta_a$$

$$F_{fR} = \left(\sqrt{F_t^2 + F_f^2}\right)\sin\beta_a$$

(7-7)

A detailed description of parameters in equation 7-7 was presented in chapter 5. Once the cutting force and tangential force are converted to the normal and frictional forces, the contact stress distribution on the tooth is then revealed using the proposed equation by Astakhov and Outeiro [77].

$$\sigma(x) = \frac{2F_N}{\pi b_{1t} l_c (1 - 2\rho_s)}\left(\frac{l_c - x}{x}\right)^{\frac{1}{2}-\rho_s}$$

(7-8)

where (l_c) is the contact length between chip and rake face (see equation 5-6), (b_{1t}) is the true chip width (width of the profile to be cut), (F_N) is the normal

force between chip and rake face, and (v_s) is Poisson's ratio. The (ρ_s) in equation

7-8 is calculated by [77]:

$$\rho_s = \frac{1}{\pi}\tan^{-1}\mu\frac{\kappa_s - 1}{\kappa_s + 1}$$

$$\kappa_s = 3 - 4v_s$$

(7-9)

The boundary conditions for the contact stress distribution presented in

equation 7-8 are as follows:

$$if\ x < 0\ or\ x \geq l_c \ \rightarrow \ \sigma(x) = 0$$

(7-10)

Using the contact stress distribution and geometry of the tooth, the tooth can

be solved as a cantilever beam exposed to a distributed load and maximum normal

and shear stresses will be determined.
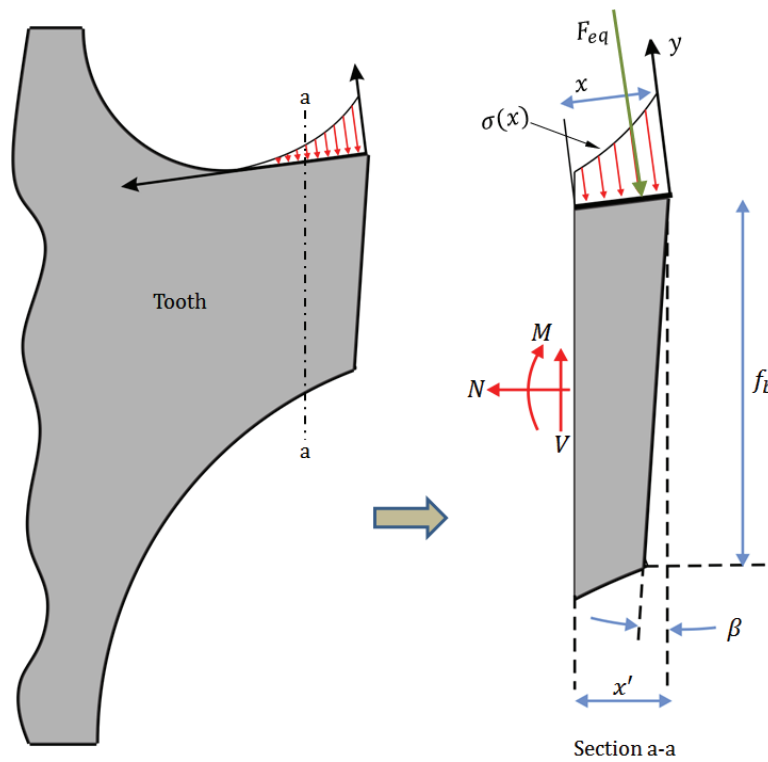
Figure 7-3: Solving the teeth as a cantilever beam subjected to distributed load

In order to solve the teeth as cantilever beam, three different sections must be made (see figure 3-5). The relation between the position of section (a-a) which is presented by (x') and the amount of contact stress action on that section of the teeth can be expressed by:

$$x' = x \times \cos \alpha \tag{7-11}$$

At each section the corresponding force to the distributed contact stress can be calculated as follows:

$$\sigma(x) = \frac{F(x)}{A_0^{l_c}} \rightarrow F(x) = \sigma(x) \times A_0^{l_c} = \sigma(x) \times l_c \times b_{1t} \tag{7-12}$$

As a result

$$F(x) = \frac{2F_N}{\pi b_{1t} l_c (1 - 2\rho_s)} \left(\frac{l_c - x}{x}\right)^{\frac{1}{2} - \rho_s} \times (l_c \times b_{1t})$$

$$\tag{7-13}$$

$$= \frac{2F_N}{\pi(1 - 2\rho_s)} \left(\frac{l_c - x}{x}\right)^{\frac{1}{2} - \rho_s}$$

Then the equivalent force must be determined and placed at the centroid of the area beneath the distributed force curve.

$$F_{eq} = \int_0^x F(x)dx = \frac{2F_N}{\pi(1 - 2\rho_s)} \int_0^x \left(\frac{l_c - x}{x}\right)^{\frac{1}{2} - \rho_s} dx \tag{7-14}$$

It must be noted that contact stress function and consequently the force functions are singular at the cutting edge where $(x = 0)$. For this reason, the lower boundary of the integration must be set equal to a very small number. In this thesis, this boundary is set equal to the nose radius ($5\mu m = 5 \times 10^{-6}m$). This integration can be solved using MATALB symbolic toolbox. In this thesis, the integration was solved using MATLAB software. Once (F_{eq}) and its acting point for the tooth section are determined, the equilibrium equations for the tooth section can be written as follows:

$$\sum F = 0$$
$$\sum M = 0$$

(7-15)

By solving equation 7-15, normal force (N), shear forces (V), and bending moment (M)acting on the tooth cross section and consequently the internal stress for a small element of the beam (tooth) will be revealed.

Maximum normal or shear stress on the tooth can be used as a design criteria and the rise must be selected in a way that the tooth will not be exposed to the stresses more than the maximum allowable normal or shear stresses. It must be mentioned that the chip load has also a lower limit to prevent the rubbing between tool and workpiece.

7-3-2-4 Total Cut Volume

Total cut chip volume must be equal to the volume of the geometry to be cut.

7-3-2-5 Maximum Pitch Length

Because of some dynamic problems during the process, generally at least two teeth should be cutting at the same time. Thus, the pitch length has an upper limit which is determined by the length of cut as seen in equation 7-15.

$$Pitch \leq \frac{length\ of\ cut}{2} \tag{7-16}$$

7-3-2-6 Power

The power required to perform the cutting action should not exceed the maximum machine power. This constraint can be presented as:

$$Power_{total} \leq Available\ machine\ power \tag{7-17}$$

7-4 Broaching tool optimization

The presented optimization procedure was applied to the spline broaching tool and the corresponding workpiece geometry which has been described in chapter 5 (see figures Figure 5-8 and Figure 5-9 and Table 5-2). The predefined constraints and the result of optimization are presented in Table 7-1and Table 7-2.

Table 7-1: Predefined constraints

Limits	Rake angle	Clearance angle	pitch	Rise/tooth	Power
Lower	5°	1°	3 mm	0.01 mm	500 Watt
Upper	20°	4°	17 mm	0.4 mm	

Table 7-2: Optimization results

	Rake angle	Clearance angle	pitch	Rise/tooth
Original Tool	15°	3°	10 mm	0.03 mm
Optimized tool (AISI1045 and AISI 12L14)	5°	4°	10 mm	0.15 mm
Optimized tool (Al7075 and Brass)	5°	1.5°	14.5 mm	0.25 mm

The optimum rake angle which is suggested by optimization algorithm for both harder (AISI 12L14 and AISI 1045) and softer (Al 7075 and Brass) workpiece material is almost 5° while the rake angle of the utilized tool is 15°. It is reasonable because the cutting tooth was modeled as a cantilevered beam and the small rake angle makes the tool tip thicker and consequently stronger. The suggested optimum clearance angle for AISI 12L14 and AISI 1045 is 4° while the optimum clearance angle for Al 7075 and Brass is 1.5°. The difference between the optimum clearance angles can be interpreted based on the suggested optimum rise per tooth for each category of materials. The suggested optimum rise per tooth for AISI 12L14 and AISI 1045 is 0.15 mm while for the Al 7075 and Brass which are relatively easier to cut 0.25 mm is suggested by the optimization algorithm. The higher rise per tooth results in higher cutting forces, for this reason the algorithm

automatically adjusted the clearance angles and proposed a smaller clearance angle for Al 7075 and Brass. This makes the tool tip thicker and stronger.

The bigger rise per tooth also results in the bigger chips and consequently more gullet space is required to accommodate the chips. As can be seen from Table 7-2, a bigger pitch length is suggested for Al 7075 and Brass.

The proposed optimum parameters are different from the parameters of the existing broaching tool. This difference can be due to some other design aspects which have been considered by the tool designer. One of those considerations can be the safety factor for the tool. In the proposed optimization procedure, the maximum normal stress on the rake face is allowed to increase up to its maximum limit (1000 MPa for ASP HSS tools); however, in a real case a safety factor is always considered to prevent the tool from chipping or breakage. The safety factor shows its importance specifically in rise per tooth where the optimized design procedure shows that a rise per tooth of 0.15 mm and 0.25 mm are applicable depends on the material to be cut while in reality the rise per tooth is considered much smaller. The safety factor must be determined based on the tool material, workpiece material and working condition of the tool and it can be easily added to the optimization model by dividing the maximum allowable stress for the tool to the safety factor. The other geometric parameters are justified accordingly by the model. It must be clearly stated that although the MRR was selected as the objective function, our ultimate goal is to find the corresponding geometric features of the broaching tool to achieve that maximum MRR.

7-5 Summary

The productivity and part quality in every machining operation is directly determined by machine reliability and cutting tool durability. Tool design which consequently defines the cutting conditions plays an important role in broaching where a cutting tool is uniquely designed for specific purpose. A mathematical optimization procedure was presented in this chapter to describe the process of optimized tool design for the broaching tool. Metal removal rate (MRR) which determines the productivity of each machining process is selected as an objective function and other geometric features of a broaching tool such as rake angle, clearance angle, pitch and rise per tooth have been determined accordingly to satisfy the objective function. The presented model is able to optimally design any broaching tool based on the given set of requirements.

Chapter 8:   Conclusions and Road Map for Future Works

8-1   Preamble

The main objective of this thesis is focussed on the simulation of broaching operations and the broaching tool design. The simulations that have been incorporated include the mathematical formulation of broaching tool geometry, modelling of the cutting process in broaching operation, investigating the effects of broaching operation on the integrity of machined surface and finally optimized design of the broaching tools. This chapter contains a summary and conclusions of the presented work, brief description of the main contributions, and outline of the road map for future works.

8-2   Summary and Conclusions

The first step in modelling of each cutting process is to know the geometry of cutting tool utilized to perform the task. A mathematical formulation of broaching

115

tool geometry is presented to define the geometry of the side profile for broaching tools. Majority of previously published papers discussing broaching operation and the utilized cutting tool in this process, have focused on the front profile which directly determines the final desired geometry of the workpiece. However, side profile have a deep impact on the cutting tool geometry and process parameters where some of the important geometric features of the cutting tool like rake angle, clearance angle, land, and rise per tooth are built into the side profile. The mathematical model which is presented in this thesis formulates the geometric features of the side profile and it can be used toward further simulations.

The second step in modelling of each cutting process is defining the geometry of engagement between the cutting tool and the workpiece. These parameters are normally hard to calculate for broaching operation where the front profile of broaching tools varies base on the broad range of profiles that can be produced by broaching. Calculation of the chip load (the engagement area between tool and workpiece) and tool-workpiece contact length (the length of engaged part of each tooth with the workpiece) using parametric representation of cutting edge was presented in this thesis. The presented parametric approach can be used in the modelling of tool-workpiece interaction for any arbitrary profile of cutting tool. The proposed model was also verified utilizing 3D ACIS modeller in order to confirm the achieved results.

The third and one of the most important steps in simulation of each cutting process is predicting the generated forces during cutting. An energy-based model,

based on quantifying the contribution of different power components spent in the cutting system, has been presented to predict the cutting forces during broaching operation. The results of simulations followed by experimental validations showed that the amount of cutting forces in broaching is comparatively higher than other conventional machining operation due to the higher number of cutting edges simultaneously engaged in cutting. This makes the virtual modelling of cutting forces very important where real experimentations would be very costly and time-consuming.

Combining the geometrical and force models which were presented early in this thesis; a mathematical optimization procedure was introduced to optimally design the broaching tools. Metal removal rate (MRR) was selected as an objective function and other geometric features of a broaching tool such as rake angle, clearance angle, pitch and rise per tooth have been determined accordingly.

The effects of broaching operation on the integrity of machined surface have been also investigated in this thesis. Surface roughness, subsurface microhardness and subsurface microstructure were selected among integrity parameters and the effects of broaching on these parameters have been studied. The results of the surface integrity tests can be summarized into the following conclusions:

1- The results of the surface roughness testing before, during and after broaching shows that although each successive cutting edge has its own share in the improvement of machined surface, the main improvement is achieved by finishing teeth where no cutting action is performed. For this reason, appropriate

design of the finishing teeth will have a deep impact on the final roughness of the workpiece.

2- The results of subsurface microhardness and subsurface microstructure testing show that the subsurface layer of the machined surface is affected by broaching operation. For similar cutting condition and tool geometry, depth of the cold-working for harder material (AISI 12L14 and AISI 1045) is higher than softer material (Al7075 and brass).

8-3   Road Map for the Future Works

The future research works in this area can be focussed on the following items:

1- Combining the geometric, force, and optimization model into one integrated, user interactive software package. The input of this software can be requested final profile of the workpiece as well as its mechanical properties and the output will be front and side profile, number of teeth, and overall length of the broaching tool.

2- Developing a finite element model to simulate the broaching operation and investigate the surface damage and depth of plastic deformation.

References

[1] H.A. Kishawy, A. Hosseini, B. Moetakef-Imani, V.P. Astakhov, An energy based analysis of broaching operation: Cutting forces and resultant surface integrity, CIRP Annals-Manufacturing Technology, 61 (2012) 107-110.

[2] U. Kokturk, Optimization of broaching tool design, in, M. Sc. Thesis, Industrial Engineering, Sabanci University, Istanbul, Turkey, 2004.

[3] G. He, Y. Zhang, Experimental Investigations of the Surface Integrity of Broached Titanium Alloy, CIRP Annals-Manufacturing Technology, 34 (1985) 491-494.

[4] W. König, M. Klinger, R. Link, Machining hard materials with geometrically defined cutting edges—field of applications and limitations, CIRP Annals-Manufacturing Technology, 39 (1990) 61-64.

[5] J.P. Davim, Surface Integrity in Machining, Springer, 2010.

[6] M.C. Shaw, Metal cutting principles, Oxford University Press Oxford, 2005.

[7] D.A. Stephenson, J.S. Agapiou, Metal cutting theory and practice, CRC, 2005.

[8] E. Budak, Y. Altintas, E. Armarego, Prediction of milling force coefficients from orthogonal cutting data, Journal of engineering for industry, 118 (1996) 216-224.

[9] P. Lee, Y. Altintaş, Prediction of ball-end milling forces from orthogonal cutting data, International Journal of Machine Tools and Manufacture, 36 (1996) 1059-1072.

[10] Y. Altintas, S. Engin, Generalized modeling of mechanics and dynamics of milling cutters, CIRP Annals-Manufacturing Technology, 50 (2001) 25-30.

[11] S. Engin, Y. Altintas, Mechanics and dynamics of general milling cutters.: Part I: helical end mills, International Journal of Machine Tools and Manufacture, 41 (2001) 2195-2212.

[12] S. Engin, Y. Altintas, Mechanics and dynamics of general milling cutters.: Part ii: inserted cutters, International Journal of Machine Tools and Manufacture, 41 (2001) 2213-2231.

[13] S. Merdol, Y. Altintas, Mechanics and dynamics of serrated cylindrical and tapered end mills, Journal of manufacturing science and engineering, 126 (2004) 317-326.

[14] V.P. Astakhov, Geometry of Single-point Turning Tools and Drills: Fundamentals and Practical Applications, Springer, 2010.

[15] N. Yussefian, B. Moetakef-Imani, H. El-Mounayri, The prediction of cutting force for boring process, International Journal of Machine Tools and Manufacture, 48 (2008) 1387-1394.

[16] C. Monday, Broaching, Machinery Pub, 1960.

[17] E.W. Kokmeyer, Better broaching operations, Society of Manufacturing Engineers, 1984.

[18] B. Imani, M. Sadeghi, M. Elbestawi, An improved process simulation system for ball-end milling of sculptured surfaces, International Journal of Machine Tools and Manufacture, 38 (1998) 1089-1107.

[19] B. Imani, Model Based Die Cavity Machining Simulation Methodology, in, Ph. D. thesis, McMaster University, Hamilton, ON, 1998.

[20] D. Zhang, A. Bowyer, CSG set-theoretic solid modelling and NC machining of blend surfaces, in: Proceedings of the second annual symposium on Computational geometry, ACM, 1986, pp. 236-245.

[21] W. Wang, Solid modeling for optimizing metal removal of three-dimensional NC end milling, Journal of Manufacturing Systems, 7 (1988) 57-65.

[22] Y. Takeuchi, T. Idemura, T. Sata, 5-axis control machining and grinding based on solid model, CIRP Annals-Manufacturing Technology, 40 (1991) 455-458.

[23] Y. Altintas, A. Spence, J. Tlusty, End milling force algorithms for CAD systems, CIRP Annals-Manufacturing Technology, 40 (1991) 31-34.

[24] A.D. Spence, Solid modeller based milling process simulation, in, University of British Columbia, 1992.

[25] R. Boogert, H. Kals, F. Van Houten, Tool paths and cutting technology in computer-aided process planning, The International Journal of Advanced Manufacturing Technology, 11 (1996) 186-197.

[26] M. Sadeghi, H. Haghighat, M. Elbestawi, A solid modeler based ball-end milling process simulation, The International Journal of Advanced Manufacturing Technology, 22 (2003) 775-785.

[27] R. Fleisig, A. Spence, Techniques for accelerating B-rep based parallel machining simulation, Computer-Aided Design, 37 (2005) 1229-1240.

[28] S.D. Merdol, Y. Altintas, Virtual cutting and optimization of three-axis milling processes, International Journal of Machine Tools and Manufacture, 48 (2008) 1063-1071.

[29] A. Hosseini, H.A. Kishawy, B-spline based general force model for broaching, Transaction of the North American Manufacturing Research Institution of SME, 38 (2010) 9-15.

[30] A. Hosseini, H.A. Kishawy, H. El-Mounayri, A solid modeler based simulation of chip load in broaching operation, Transaction of the North American Manufacturing Research Institution of SME, 39 (2011) 217-223.

[31] P. Gilormini, E. Felder, L. Tronchet, F. Leroy, F. Le Maitre, A comparative analysis of three machining processes: broaching, tapping and slotting, CIRP Annals-Manufacturing Technology, 33 (1984) 19-22.

[32] J. Sutherland, E. Salisbury, F. Hoge, A model for the cutting force system in the gear broaching process, International Journal of Machine Tools and Manufacture, 37 (1997) 1409-1421.

[33] V. Sajeev, L. Vijayaraghavan, U. Rao, An analysis of the effects of burnishing in internal broaching, International Journal of Mechanical Engineering Education, 28 (2000) 163-173.

[34] V. Sajeev, L. Vijayaraghavan, U. Rao, Effect of tool-work deflections on the shape of a broached hole, International Journal of Mechanical Engineering Education, 28 (2000) 88.

[35] E. Budak, Broaching process monitoring, in: Proceedings of Third International Conference on Metal Cutting and High Speed Machining, Metz-France, 2001, pp. 251-260.

[36] D.A. Axinte, N. Gindy, Tool condition monitoring in broaching, Wear, 254 (2003) 370-382.

[37] D.A. Axinte, N. Gindy, K. Fox, I. Unanue, Process monitoring to assist the workpiece surface quality in machining, International Journal of Machine Tools and Manufacture, 44 (2004) 1091-1108.

[38] W.R. Terry, R. Karni, Y.J. Huang, Concurrent tool and production system design for a surface broach cutting tool: a knowledge-based systems approach, The International Journal of Production Research, 30 (1992) 219-240.

[39] O. Ozturk, E. Budak, Modelling of Broaching for Improved tool design, in: Proc. of the IMECE, 2003, pp. 16-21.

[40] O. Ozturk, Modelling of broaching process, in, M. Sc. Thesis, Industrial Engineering, Sabanci University, Istanbul, Turkey, 2003.

[41] U. Kokturk, E. Budak, Optimization of broaching tool design, in: Proceedings of the Intelligent Computation in Manufacturing Engineering–4 Conference, CIRP ICME'04, Sorrento, 2004.

[42] M. Field, J.F. Kahles, Review of surface integrity of machined components, Defense Technical Information Center., 1971.

[43] J.T. Black, R.A. Kohser, DeGarmo's materials and processes in manufacturing, Wiley, 2011.

[44] M. Field, J.F. Kahles, W.P. Koster, Surface finish and surface integrity, ASM Handbook., 16 (1989) 19-36.

[45] D. Jang, T. Watkins, K. Kozaczek, C. Hubbard, O. Cavin, Surface residual stresses in machined austenitic stainless steel, Wear, 194 (1996) 168-173.

[46] D. Lucca, E. Brinksmeier, G. Goch, Progress in assessing surface and subsurface integrity, CIRP Annals-Manufacturing Technology, 47 (1998) 669-693.

[47] M. Field, Surface integrity–A new requirement for improving reliability of aerospace hardware, in: 18th Annual National SAMPE Symposium Los Angeles, 1973.

[48] R. M'saoubi, J. Outeiro, B. Changeux, J. Lebrun, A. Morao Dias, Residual stress analysis in orthogonal machining of standard and resulfurized AISI 316L steels, Journal of materials processing technology, 96 (1999) 225-233.

[49] Y. Matsumoto, F. Hashimoto, G. Lahoti, Surface integrity generated by precision hard turning, CIRP Annals-Manufacturing Technology, 48 (1999) 59-62.

[50] M. El-Axir, A method of modeling residual stress distribution in turning for different materials, International Journal of Machine Tools and Manufacture, 42 (2002) 1055-1063.

[51] X. Yang, C.R. Liu, A new stress-based model of friction behavior in machining and its significant impact on residual stresses computed by finite element method, International Journal of Mechanical Sciences, 44 (2002) 703-723.

[52] J. Rech, A. Moisan, Surface integrity in finish hard turning of case-hardened steels, International Journal of Machine Tools and Manufacture, 43 (2003) 543-550.

[53] F.D. Jones, D.T. Hamilton, C.L. Lucas, Broaching, The Industrial press, 1914.

[54] *Miller Broach, Inc.* 2009 [cited 2012; Available from: http://www.millerbroach.com/.

[55] H. El-Hofy, Fundamentals of Machining Processes: Conventional and Nonconventional Processes, CRC, 2006.

[56] Y. Altintas, Manufacturing automation: metal cutting mechanics, machine tool vibrations, and CNC design, Cambridge university press, 2012.

[57] L.A. Piegl, W. Tiller, The NURBS book, Springer Verlag, 1997.

[58] C.-K. Shene. *CS3621 Introduction to Computing with Geometry Course Notes*.

1998   [cited   2012;   Available   from:

http://www.cs.mtu.edu/~shene/COURSES/cs3621/NOTES/.

[59] D. Manocha, S. Krishnan, Algebraic pruning: a fast technique for curve and

surface intersection, Computer Aided Geometric Design, 14 (1997) 823-845.

[60] M.E. Merchant, Mechanics of the metal cutting process. I. Orthogonal cutting

and a type 2 chip, Journal of applied physics, 16 (1945) 267-275.

[61] H. Ernst, M.E. Merchant, Chip formation, friction and finish, Cincinnati milling

machine Company, 1941.

[62] V.P. Astakhov, X. Xiao, A methodology for practical cutting force evaluation

based on the energy spent in the cutting system, Machining Science and

Technology, 12 (2008) 325-347.

[63] H.J. Fu, R. DeVor, S. Kapoor, A mechanistic model for the prediction of the

force system in face milling operations, in, University of Illinois at Urbana-

Champaign, 1982.

[64] V.P. Astakhov, S. Shvets, The assessment of plastic deformation in metal

cutting, Journal of materials processing technology, 146 (2004) 193-202.

[65] A. Boresi, R. Schmidt, Advanced mechanics of materials, John Wiley & Sons,

(2003).

[66] V.P. Astakhov, Tribology of metal cutting, Elsevier Science Limited, 2006.

[67] V.P. Astakhov, Metal cutting mechanics, CRC, 1998.

[68] A.D. Deutschman, W.J. Michels, C.E. Wilson, Machine design; theory and practice, Macmillan, 1975.

[69] A. Javidi, U. Rieger, W. Eichlseder, The effect of machining on the surface integrity and fatigue life, International Journal of fatigue, 30 (2008) 2050-2055.

[70] A. Sharman, D. Aspinwall, R. Dewes, D. Clifton, P. Bowen, The effects of machined workpiece surface integrity on the fatigue life of γ-titanium aluminide, International Journal of Machine Tools and Manufacture, 41 (2001) 1681-1685.

[71] A. Sadat, Effect of high cutting speed on surface integrity of AISI 4340 steel during turning, Materials Science and Technology, 6 (1990) 371-375.

[72] J.P. Davim, Machining of metal matrix composites, Springer, 2011.

[73] P. Benardos, G.C. Vosniakos, Predicting surface roughness in machining: a review, International Journal of Machine Tools and Manufacture, 43 (2003) 833-844.

[74] T. Sata, M. Li, S. Takata, H. Hiraoka, C. Li, X. Xing, X. Xiao, Analysis of surface roughness generation in turning operation and its applications, CIRP Annals-Manufacturing Technology, 34 (1985) 473-476.

[75] E.C. Ozelkan, O. Ozturk, E. Budak, Identifying parameters of a broaching design using non-linear optimisation, International Journal of Modelling, Identification and Control, 12 (2011) 244-252.

[76] E. Özelkan, Ö. Öztürk, E. Budak, Optimization of broaching design, (2007).

[77] V. Astakhov, J. Outeiro, Modeling of the contact stress distribution at the tool-chip interface, Machine Science and Technology, 9 (2005) 85-99.

Appendix A: 3D Surface Roughness Graphs
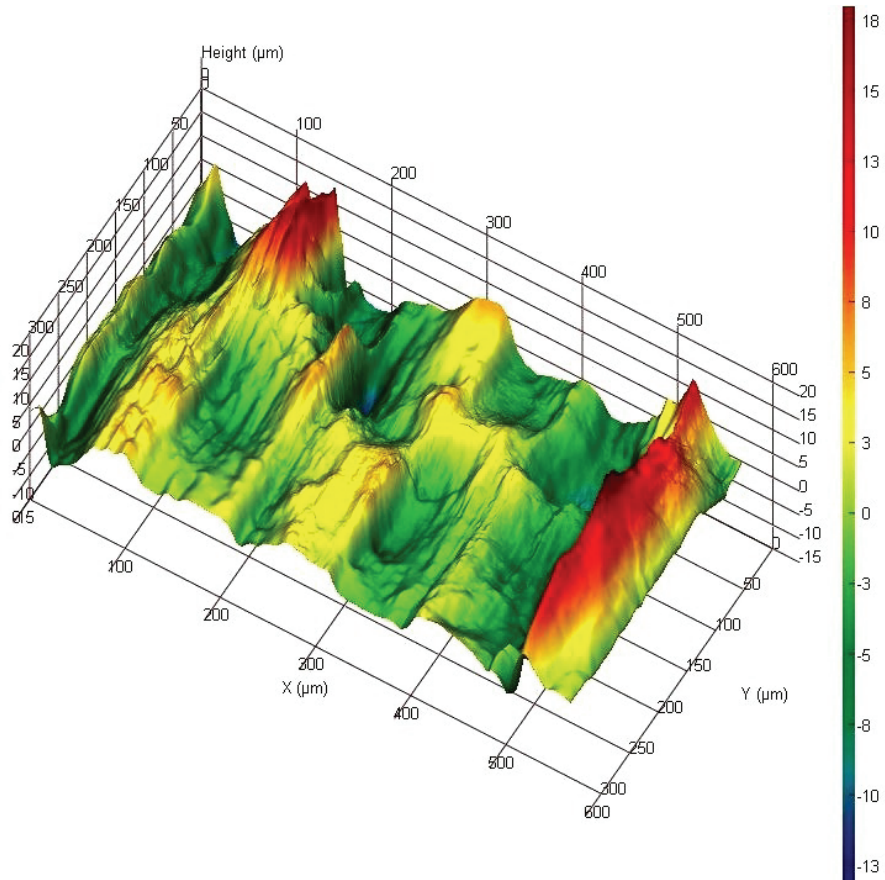
Figure A-1: Surface roughness for AISI 12L14 before broaching

Table A-1: Roughness parameter values for AISI 12L14 before broaching

Cut − off length x 500 μm	Cut − off length y 500 μm
$S_a = 3.18 \ \mu m$	$S_t = 32.4 \ \mu m$
$S_q = 4.21 \ \mu m$	$S_z = 14.5 \ \mu m$
$S_{sk} = 0.448$	$S_{ds} = 1528.33 \ summits/mm^2$
$S_{ku} = 3.18$	$S_{dr} = 4.95 \ \%$
$S_v = -13.9 \ \mu m$	$S_{ci} = 1.74$
$S_p = 18.55 \ \mu m$	

Figure A-2: Surface roughness for AISI 12L14 interrupted broaching (21st teeth)

Table A-2: Roughness parameter values for AISI 12L14 interrupted broaching (21st

teeth)

$Cut - off\ length\ x\ 500\ \mu m$	$Cut - off\ length\ y\ 500\ \mu m$
$S_a = 2.6\ \mu m$	$S_t = 39.29\ \mu m$
$S_q = 3.7\ \mu m$	$S_z = 14.47\ \mu m$
$S_{sk} = -0.55$	$S_{ds} = 2452.91\ summits/mm^2$
$S_{ku} = 6.17$	$S_{dr} = 5\ \%$
$S_v = -19.7\ \mu m$	$S_{ci} = 1.32$
$S_p = 19.59\ \mu m$	

Figure A-3: Surface roughness for AISI 12L14 interrupted broaching (22nd teeth)

Table A-3: Roughness parameter values for AISI 12L14 interrupted broaching

(22nd teeth)

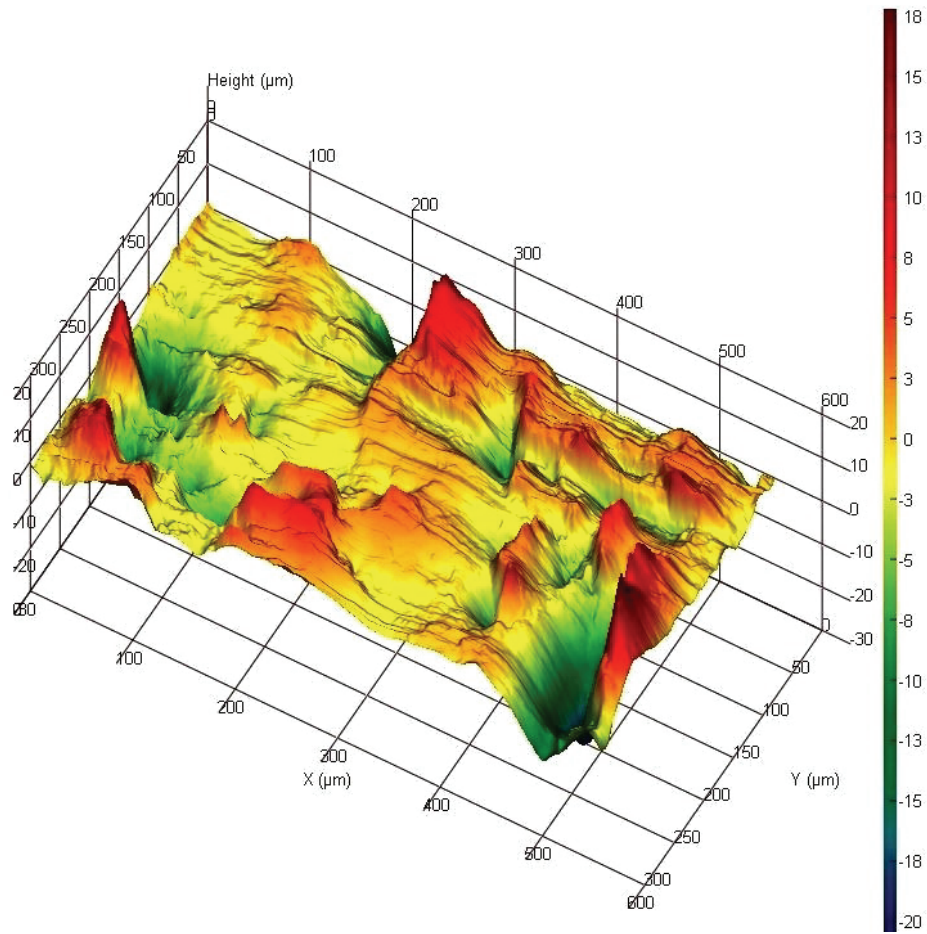| $Cut-off\ length\ x\ 500\ \mu m$	$Cut-off\ length\ y\ 500\ \mu m$
$S_a = 2.95\ \mu m$	$S_t = 36.82\ \mu m$
$S_q = 3.98\ \mu m$	$S_z = 14.93\ \mu m$
$S_{sk} = 0.212$	$S_{ds} = 1682.81\ summits/mm^2$
$S_{ku} = 4.64$	$S_{dr} = 4.13\ \%$
$S_v = -15.8\ \mu m$	$S_{ci} = 1.36$
$S_p = 20.99\ \mu m$	

Figure A-4: Surface roughness for AISI 12L14 interrupted broaching (23rd teeth)

Table A-4: Roughness parameter values for AISI 12L14 interrupted broaching

(23rd teeth)

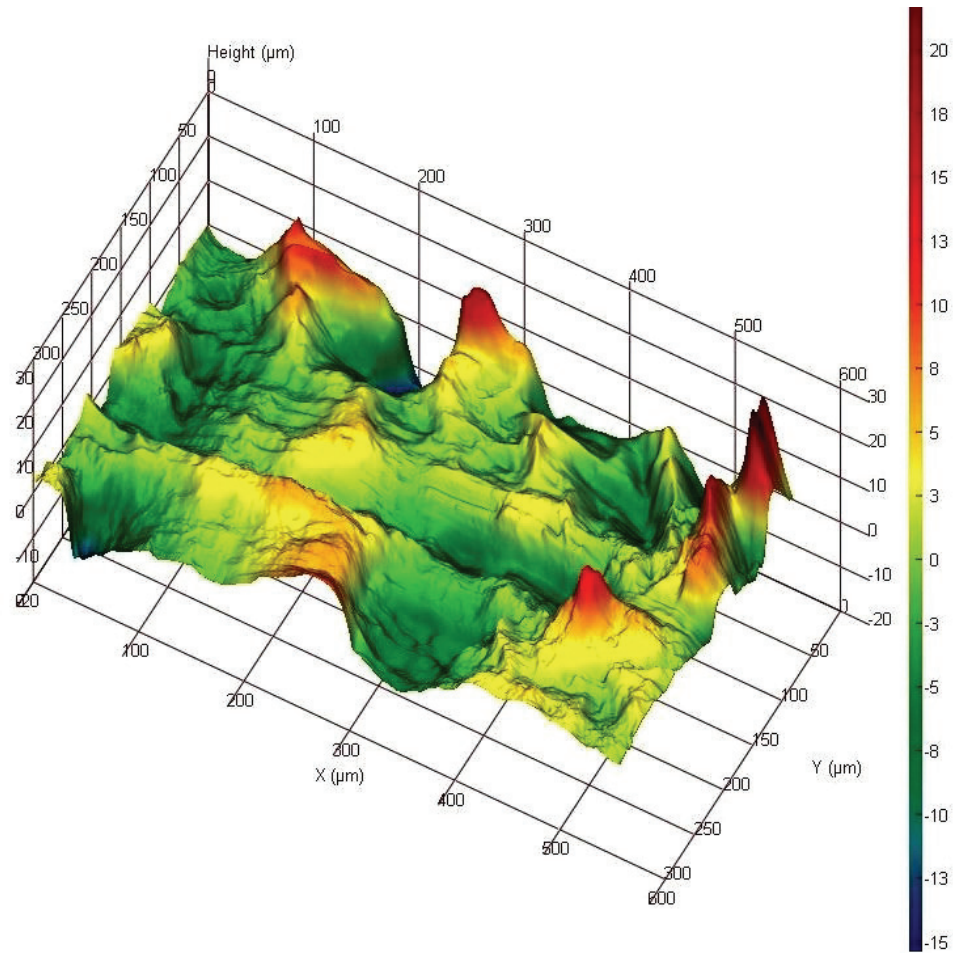| $Cut-off\ length\ x\ 500\ \mu m$	$Cut-off\ length\ y\ 500\ \mu m$
$S_a = 1.8\ \mu m$	$S_t = 28.7\ \mu m$
$S_q = 2.42\ \mu m$	$S_z = 9.97\ \mu m$
$S_{sk} = -0.374$	$S_{ds} = 2384.46\ summits/mm^2$
$S_{ku} = 5.59$	$S_{dr} = 2.53\ \%$
$S_v = -14.9\ \mu m$	$S_{ci} = 1.21$
$S_p = 13.83\ \mu m$	
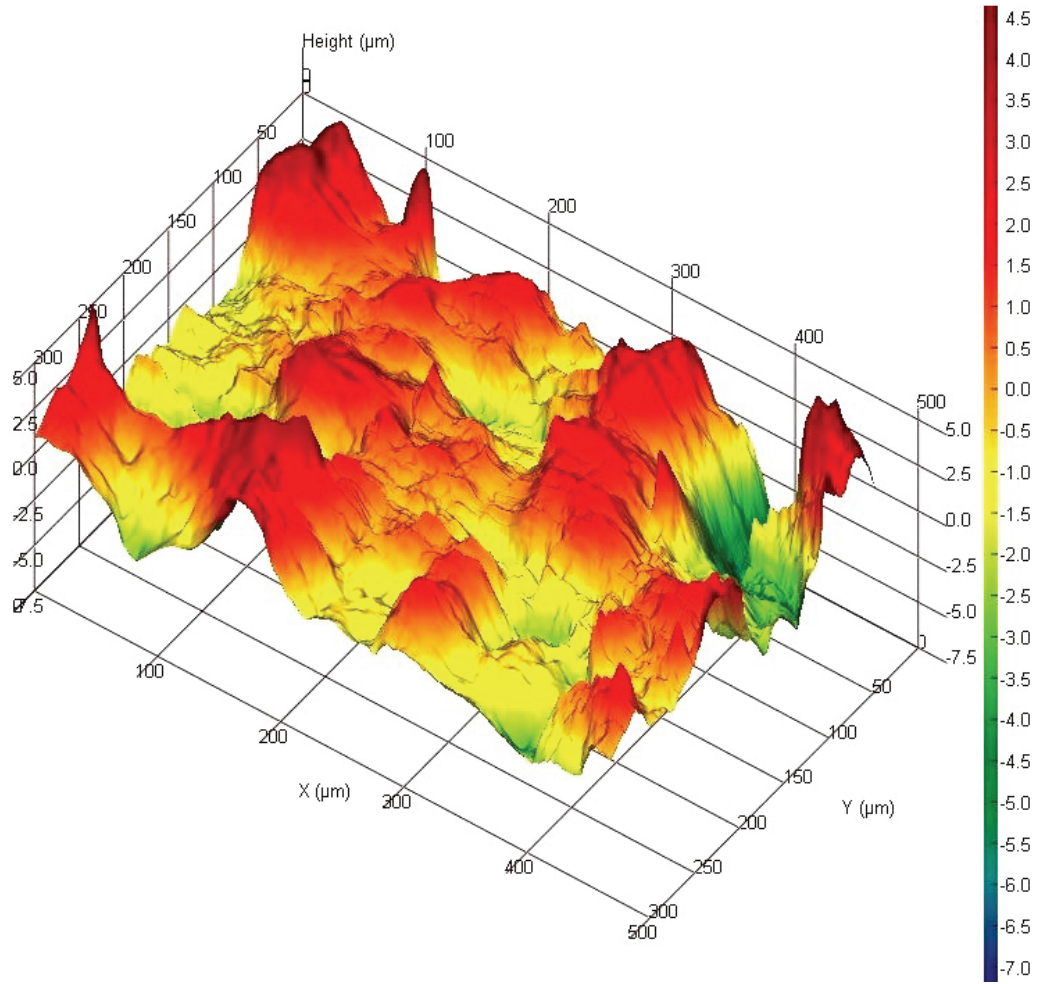
Figure A-5: Surface roughness for AISI 12L14 after broaching

Table A-5: Roughness parameter values for AISI 12L14 after broaching

$Cut - off\ length\ x\ 500\ \mu m$	$Cut - off\ length\ y\ 500\ \mu m$
$S_a = 1.24\ \mu m$	$S_t = 12.23\ \mu m$
$S_q = 1.63\ \mu m$	$S_z = 5.91\ \mu m$
$S_{sk} = -0.313$	$S_{ds} = 2666.05\ summits/mm^2$
$S_{ku} = 3.95$	$S_{dr} = 1.04\ \%$
$S_v = -6.79\ \mu m$	$S_{ci} = 1.39$
$S_p = 5.43\ \mu m$	

Figure A-6: Surface roughness for AISI 1045 before broaching

Table A-6: Roughness parameter values for AISI 1045 before broaching

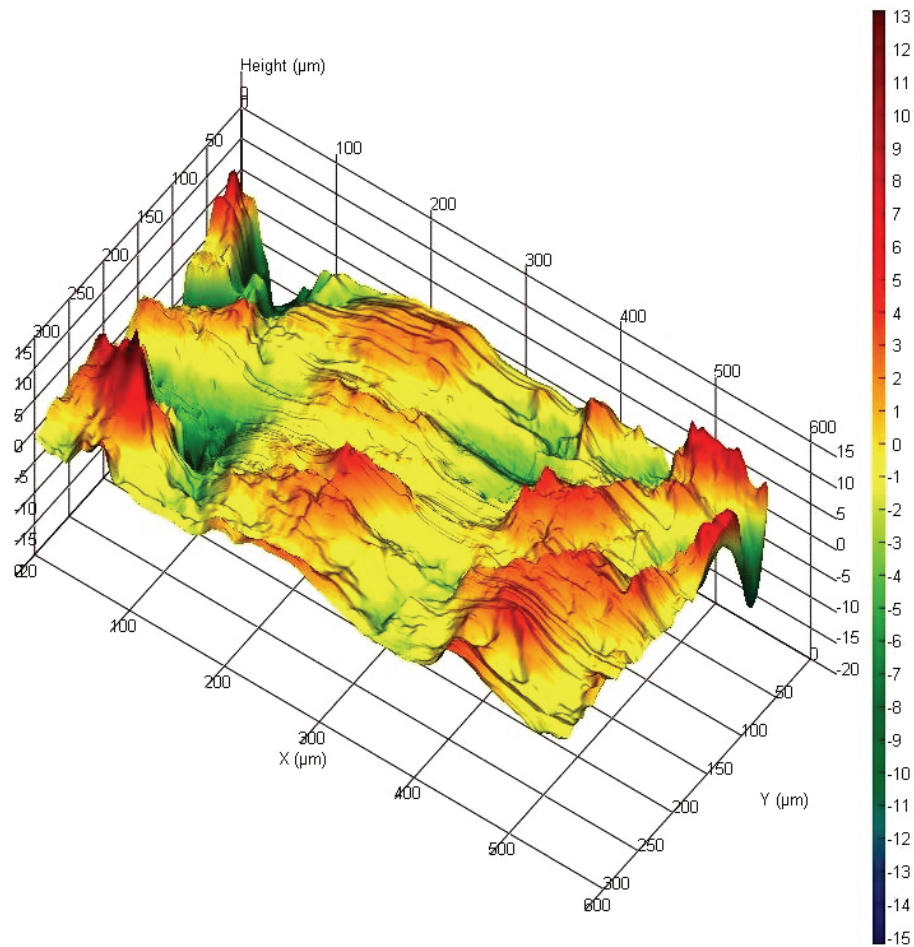| $Cut-off\ length\ x\ 500\ \mu m$	$Cut-off\ length\ y\ 500\ \mu m$
$S_a = 3.09\ \mu m$	$S_t = 27.11\ \mu m$
$S_q = 3.82\ \mu m$	$S_z = 13.79\ \mu m$
$S_{sk} = -0.314$	$S_{ds} = 3164.86\ summits/mm^2$
$S_{ku} = 2.73$	$S_{dr} = 5.69\ \%$
$S_v = -15.3\ \mu m$	$S_{ci} = 1.28$
$S_p = 11.85\ \mu m$	

Figure A-7: Surface roughness for AISI 1045 interrupted broaching (21st teeth)

Table A-7: Roughness parameter values for AISI 1045 interrupted broaching (21st

teeth)

Cut − off length x 500 μm	Cut − off length y 500 μm
$S_a = 3.9\ \mu m$	$S_t = 59.54\ \mu m$
$S_q = 5.09\ \mu m$	$S_z = 19.28\ \mu m$
$S_{sk} = -0.211$	$S_{ds} = 798.89\ summits/mm^2$
$S_{ku} = 4.2$	$S_{dr} = 5.05\ \%$
$S_v = -34.8\ \mu m$	$S_{ci} = 1.41$
$S_p = 24.7\ \mu m$	

Figure A-8: Surface roughness for AISI 1045 interrupted broaching (22nd teeth)

Table A-8: Roughness parameter values for AISI 1045 interrupted broaching (22nd

teeth)

$Cut - off\ length\ x\ 500\ \mu m$	$Cut - off\ length\ y\ 500\ \mu m$
$S_a = 1.37\ \mu m$	$S_t = 13.36\ \mu m$
$S_q = 1.77\ \mu m$	$S_z = 6.24\ \mu m$
$S_{sk} = 0.0292$	$S_{ds} = 2452.14\ summits/mm^2$
$S_{ku} = 3.52$	$S_{dr} = 1.3\ \%$
$S_v = -7.26\ \mu m$	$S_{ci} = 1.47$
$S_p = 6.11\ \mu m$	

Figure A-9: Surface roughness for AISI 1045 interrupted broaching (23rd teeth)

Table A-9: Roughness parameter values for AISI 1045 interrupted broaching (23rd

teeth)

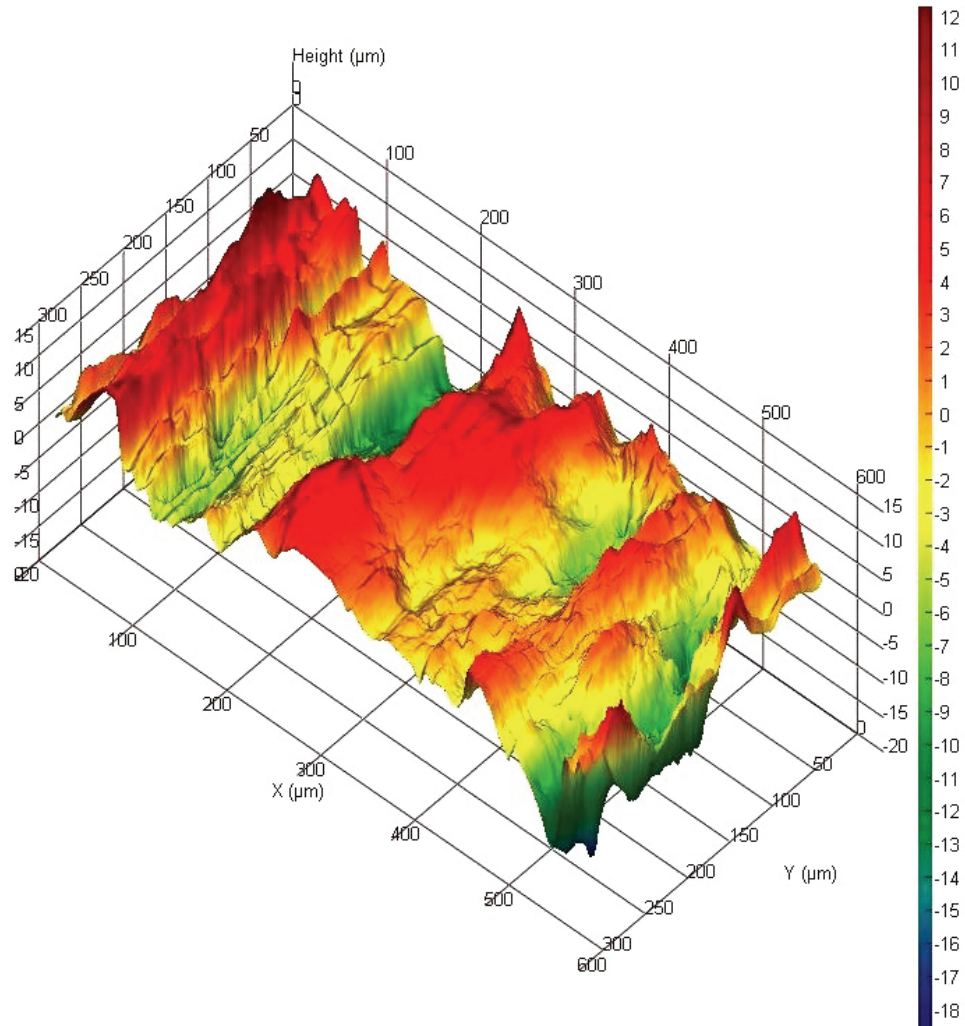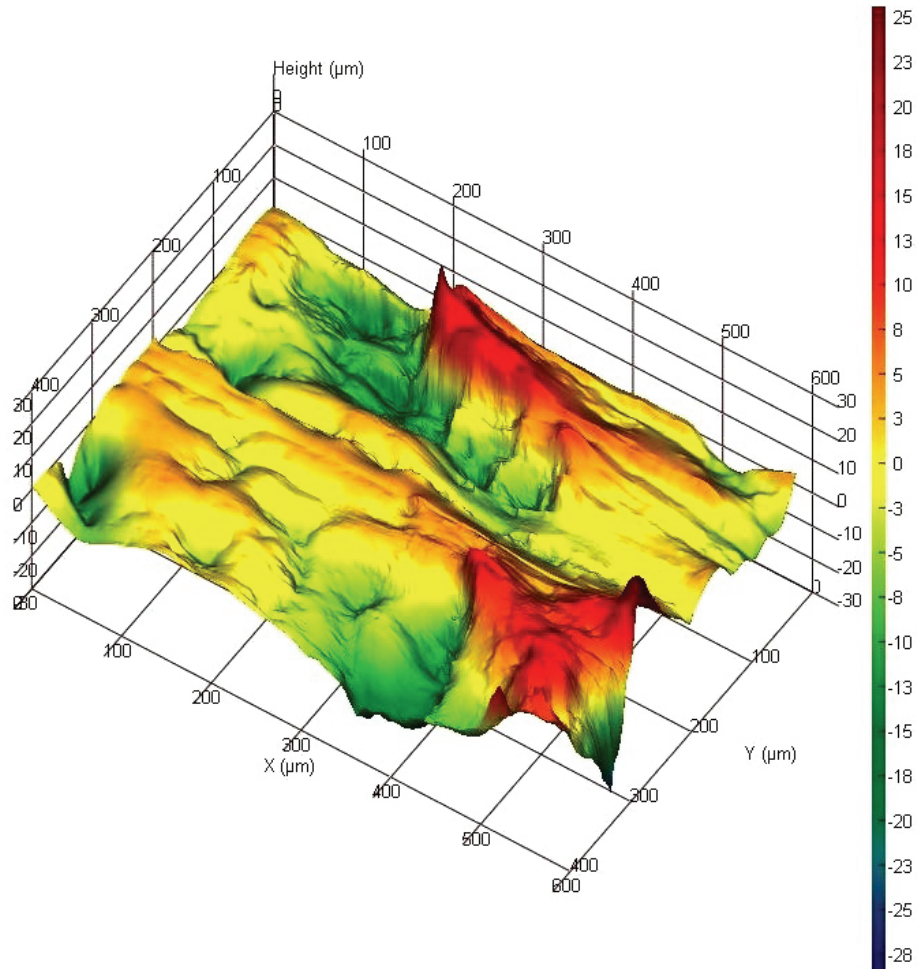| $Cut-off\ length\ x\ 500\ \mu m$	$Cut-off\ length\ y\ 500\ \mu m$
$S_a = 2.99\ \mu m$	$S_t = 37.28\ \mu m$
$S_q = 4.08\ \mu m$	$S_z = 16.8\ \mu m$
$S_{sk} = 0.442$	$S_{ds} = 1701.12\ summits/mm^2$
$S_{ku} = 5.3$	$S_{dr} = 5.12\ \%$
$S_v = -15.4\ \mu m$	$S_{ci} = 1.29$
$S_p = 21.91\ \mu m$	
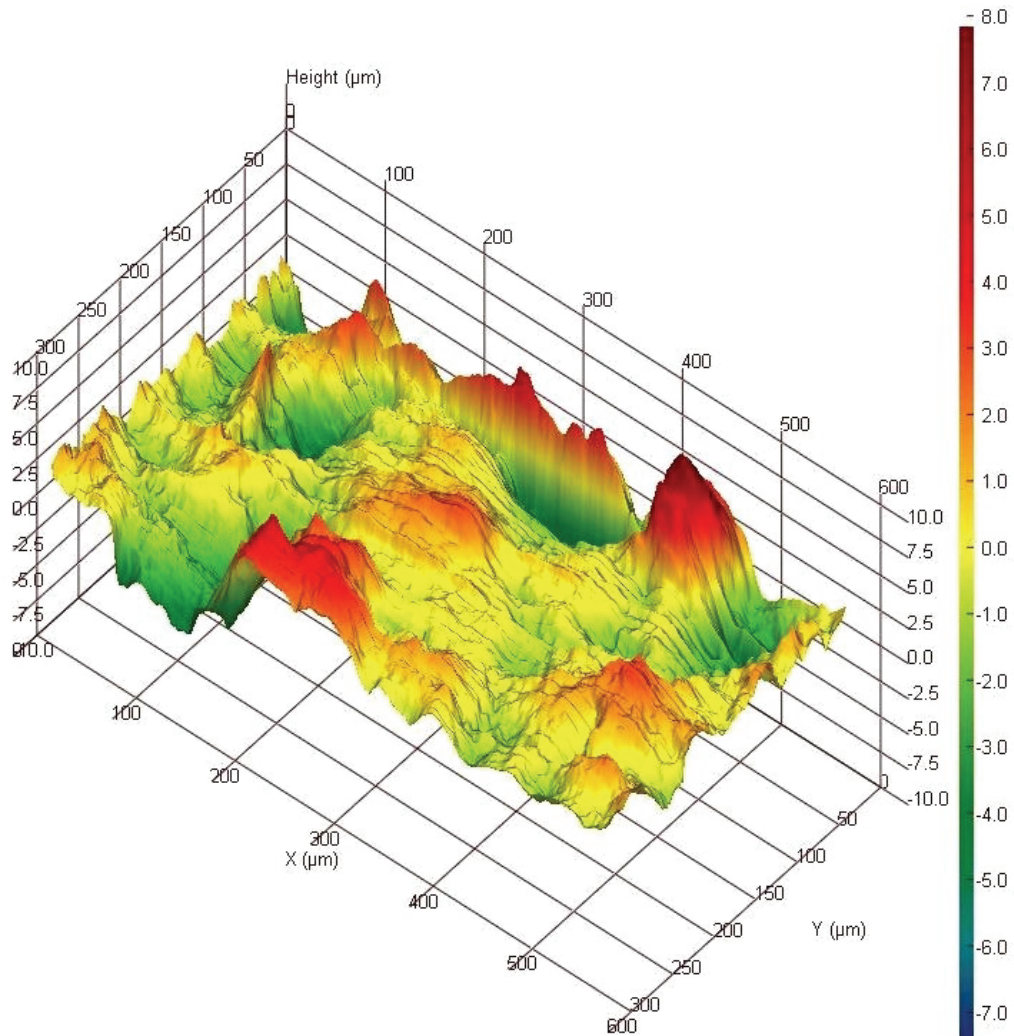
Figure A-10: Surface roughness for AISI 1045 after broaching

Table A-10: Roughness parameter values for AISI 1045 after broaching

Cut $-$ off length x 500 μm	Cut $-$ off length y 500 μm
$S_a = 1.2\ \mu m$	$S_t = 15.93\ \mu m$
$S_q = 1.64\ \mu m$	$S_z = 6.23\ \mu m$
$S_{sk} = 0.122$	$S_{ds} = 3071.81\ summits/mm^2$
$S_{ku} = 5.15$	$S_{dr} = 1.51\ \%$
$S_v = -7.88\ \mu m$	$S_{ci} = 1.45$
$S_p = 8.05\ \mu m$	

Figure A-11: Surface roughness for Al 7075 before broaching

Table A-11: Roughness parameter values for Al 7075 before broaching

Cut − off length x 500 μm	Cut − off length y 500 μm
$S_a = 1.3\ \mu m$	$S_t = 9.43\ \mu m$
$S_q = 1.7\ \mu m$	$S_z = 4.45\ \mu m$
$S_{sk} = 0.661$	$S_{ds} = 9656.56\ summits/mm^2$
$S_{ku} = 3.43$	$S_{dr} = 2.72\ \%$
$S_v = -4.16\ \mu m$	$S_{ci} = 1.74$
$S_p = 5.27\ \mu m$	

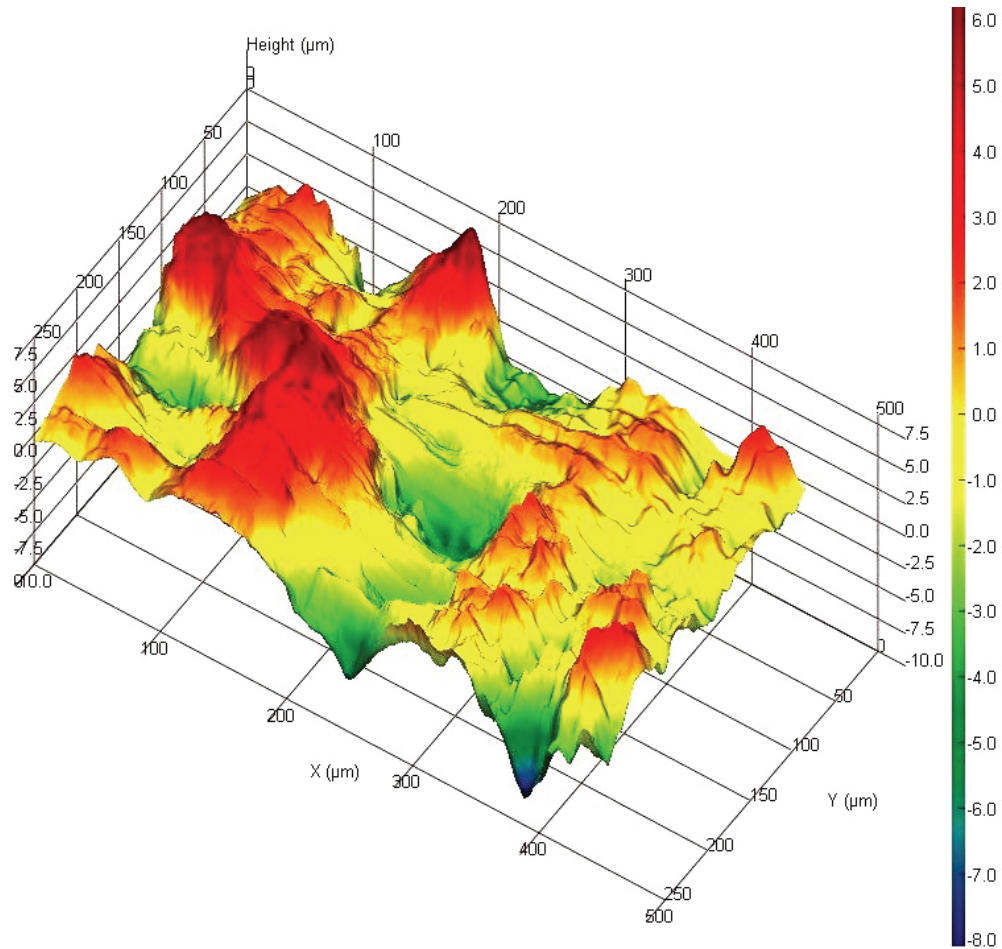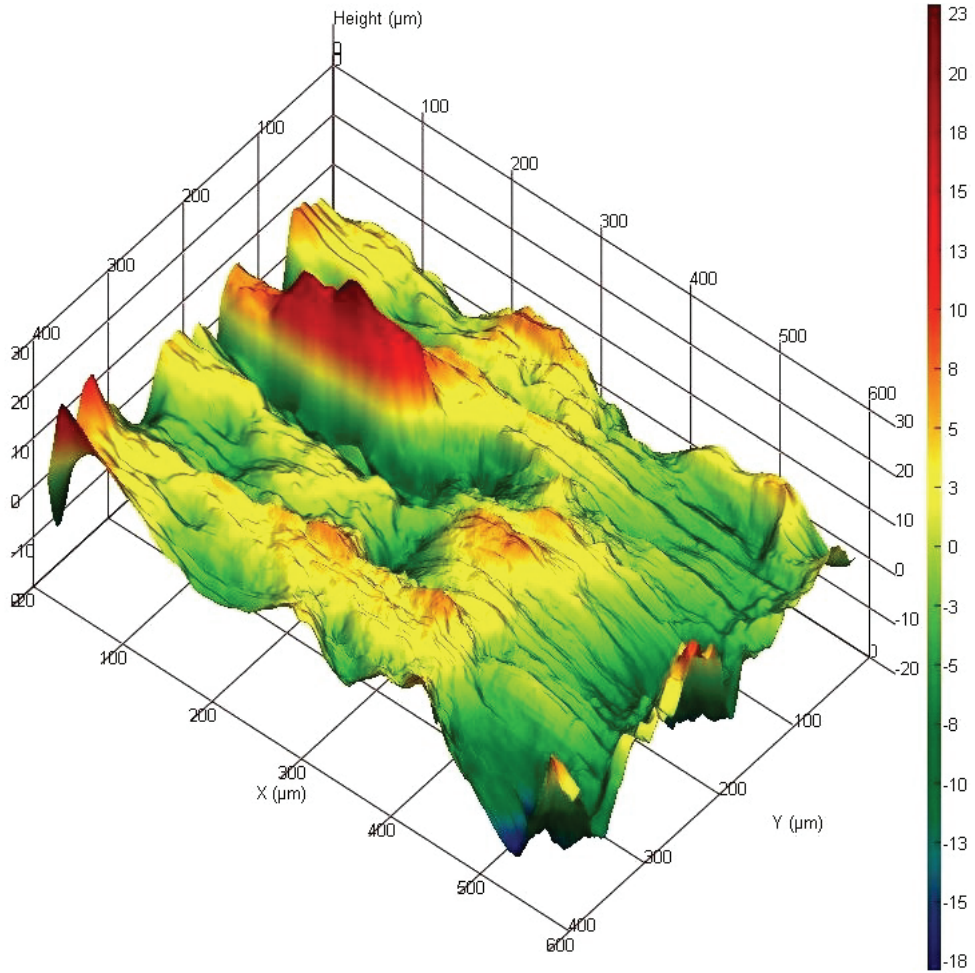Figure A-12: Surface roughness for Al 7075 interrupted broaching (21st teeth)

Table A-12: Roughness parameter values for Al 7075 interrupted broaching (21st

teeth)

Cut − off length x 500 μm	Cut − off length y 500 μm
$S_a = 1.4\ \mu m$	$S_t = 11.65\ \mu m$
$S_q = 1.78\ \mu m$	$S_z = 6.12\ \mu m$
$S_{sk} = -0.583$	$S_{ds} = 16457.81\ summits/mm^2$
$S_{ku} = 3.38$	$S_{dr} = 4.24\ \%$
$S_v = -6.21\ \mu m$	$S_{ci} = 1.35$
$S_p = 5.43\ \mu m$	

Figure A-13: Surface roughness for Al 7075 interrupted broaching (22nd teeth)

Table A-13: Roughness parameter values for Al 7075 interrupted broaching (22nd

teeth)

$Cut-off\ length\ x\ 500\ \mu m$	$Cut-off\ length\ y\ 500\ \mu m$
$S_a = 1.66\ \mu m$	$S_t = 15.19\ \mu m$
$S_q = 2.19\ \mu m$	$S_z = 6.81\ \mu m$
$S_{sk} = -0.119$	$S_{ds} = 7886.37\ summits/mm^2$
$S_{ku} = 3.89$	$S_{dr} = 5.71\ \%$
$S_v = -7.82\ \mu m$	$S_{ci} = 1.45$
$S_p = 7.37\ \mu m$	

Figure A-14: Surface roughness for Al 7075 interrupted broaching (23rd teeth)

Table A-14: Roughness parameter values for Al 7075 interrupted broaching (23rd

teeth)

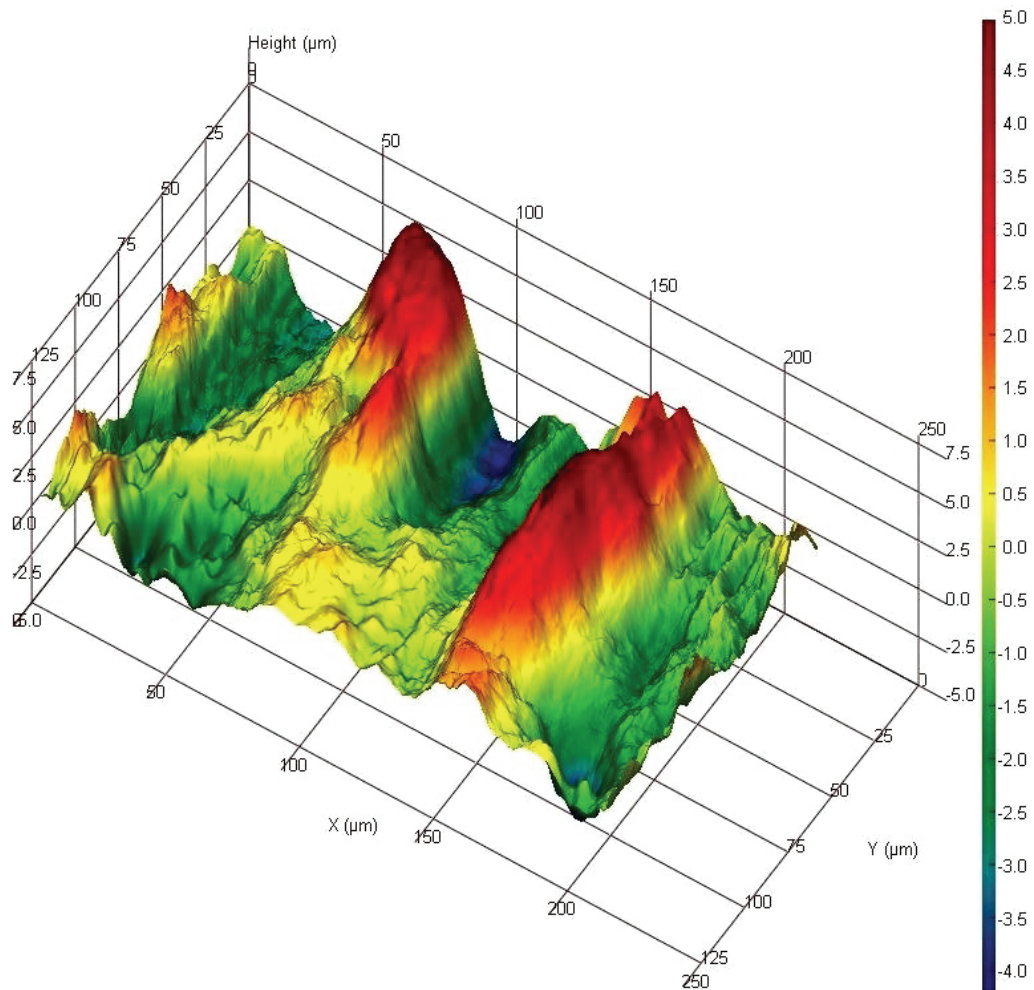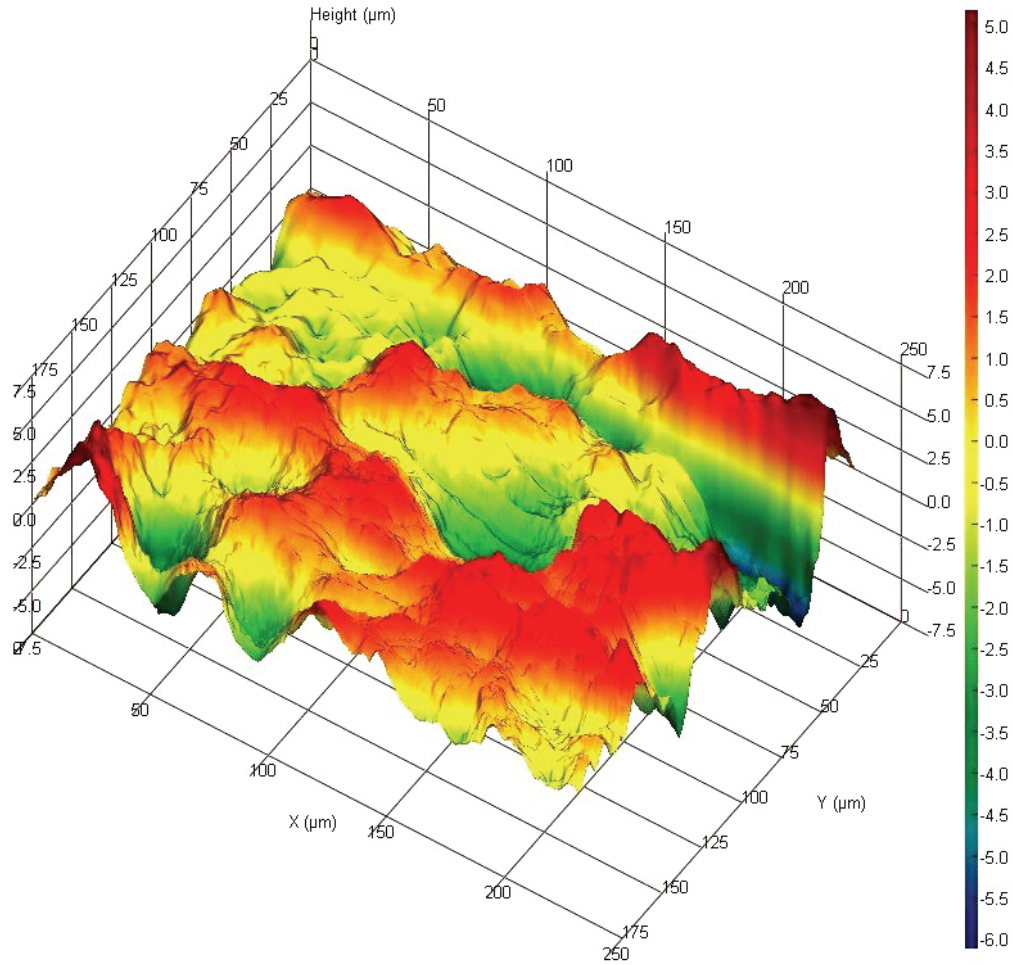| $Cut-off\ length\ x\ 500\ \mu m$	$Cut-off\ length\ y\ 500\ \mu m$
$S_a = 0.803\ \mu m$	$S_t = 11.82\ \mu m$
$S_q = 1.1\ \mu m$	$S_z = 4.61\ \mu m$
$S_{sk} = -0.713$	$S_{ds} = 15098.68\ summits/mm^2$
$S_{ku} = 6.04$	$S_{dr} = 2.22\ \%$
$S_v = -7.03\ \mu m$	$S_{ci} = 1.37$
$S_p = 4.79\ \mu m$	
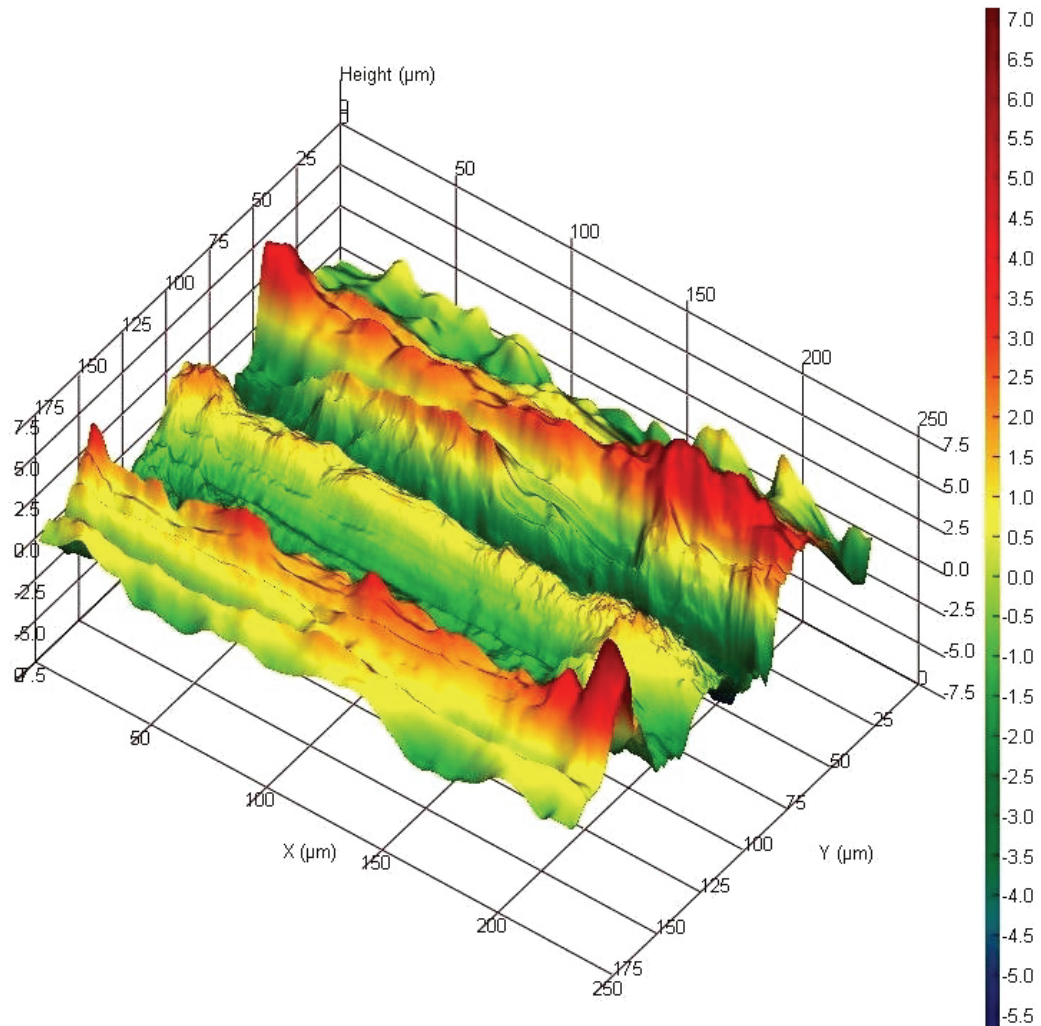
Figure A-15: Surface roughness for Al 7075 after broaching

Table A-15: Roughness parameter values for Al 7075 after broaching

Cut − off length x 500 μm	Cut − off length y 500 μm
$S_a = 1.36 \ \mu m$	$S_t = 13.29 \ \mu m$
$S_q = 1.68 \ \mu m$	$S_z = 6.15 \ \mu m$
$S_{sk} = 0.117$	$S_{ds} = 6360.49 \ summits/mm^2$
$S_{ku} = 3.16$	$S_{dr} = 4.19 \ \%$
$S_v = -6.11 \ \mu m$	$S_{ci} = 1.34$
$S_p = 7.16 \ \mu m$	

Figure A-16: Surface roughness for brass before broaching

Table A-16: Roughness parameter values for brass before broaching

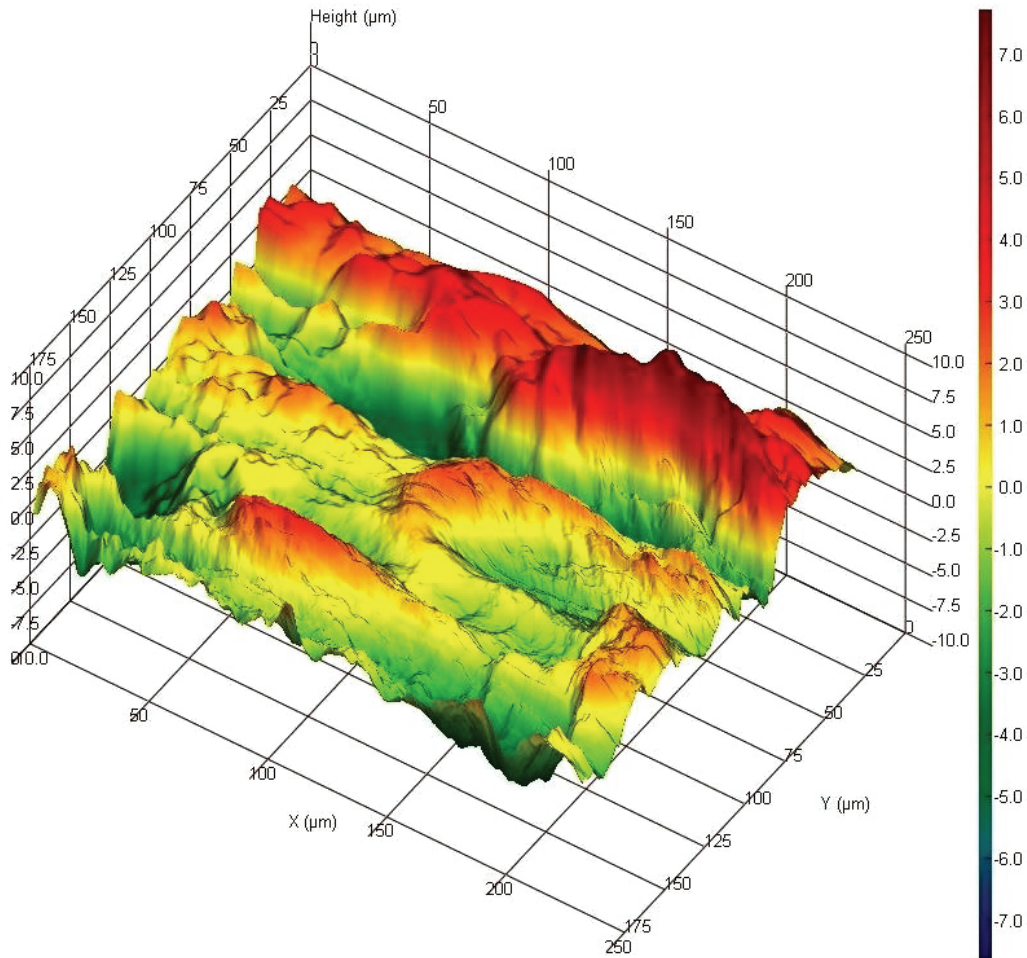| Cut − off length x 500 μm	Cut − off length y 500 μm
$S_a = 0.808\ \mu m$	$S_t = 6.96\ \mu m$
$S_q = 0.996\ \mu m$	$S_z = 3.49\ \mu m$
$S_{sk} = -0.221$	$S_{ds} = 18133.07\ summits/mm^2$
$S_{ku} = 3.02$	$S_{dr} = 1.29\ \%$
$S_v = -3.75\ \mu m$	$S_{ci} = 1.45$
$S_p = 3.21\ \mu m$	
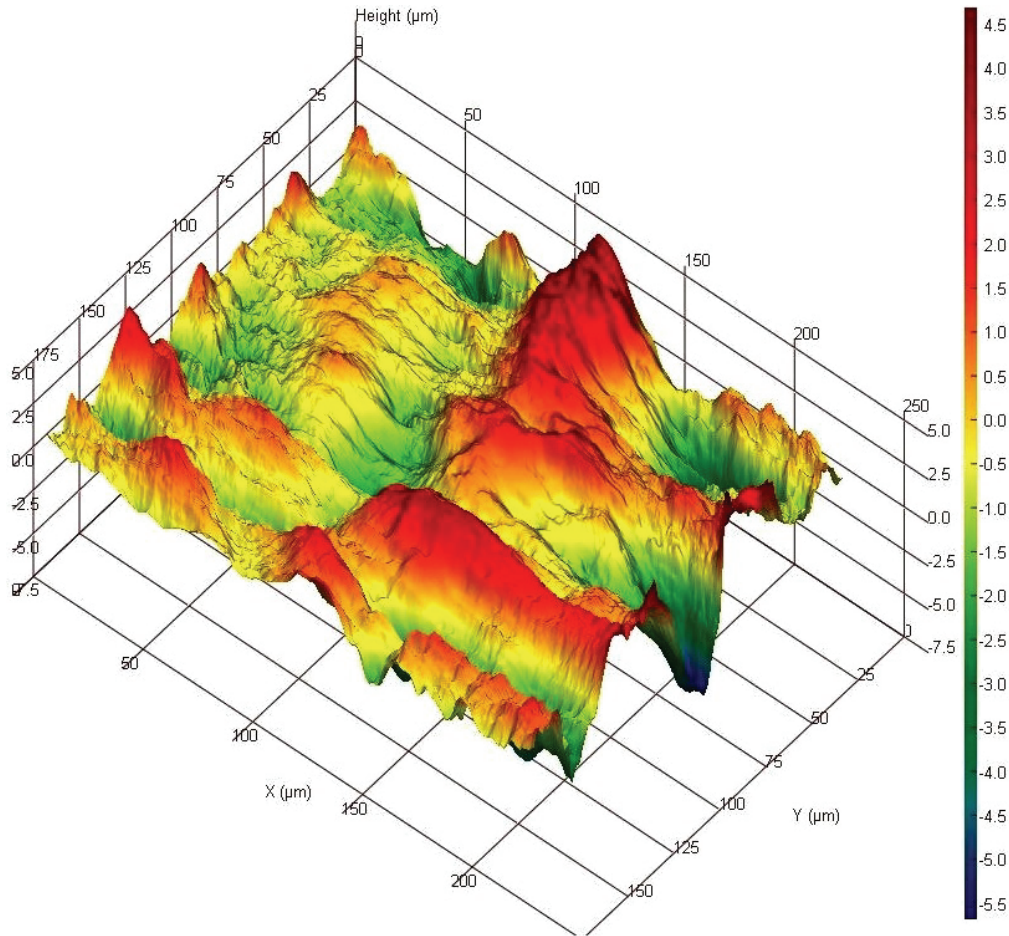
Figure A-17: Surface roughness for brass interrupted broaching (21st teeth)

Table A-17: Roughness parameter values for brass interrupted broaching (21st

teeth)

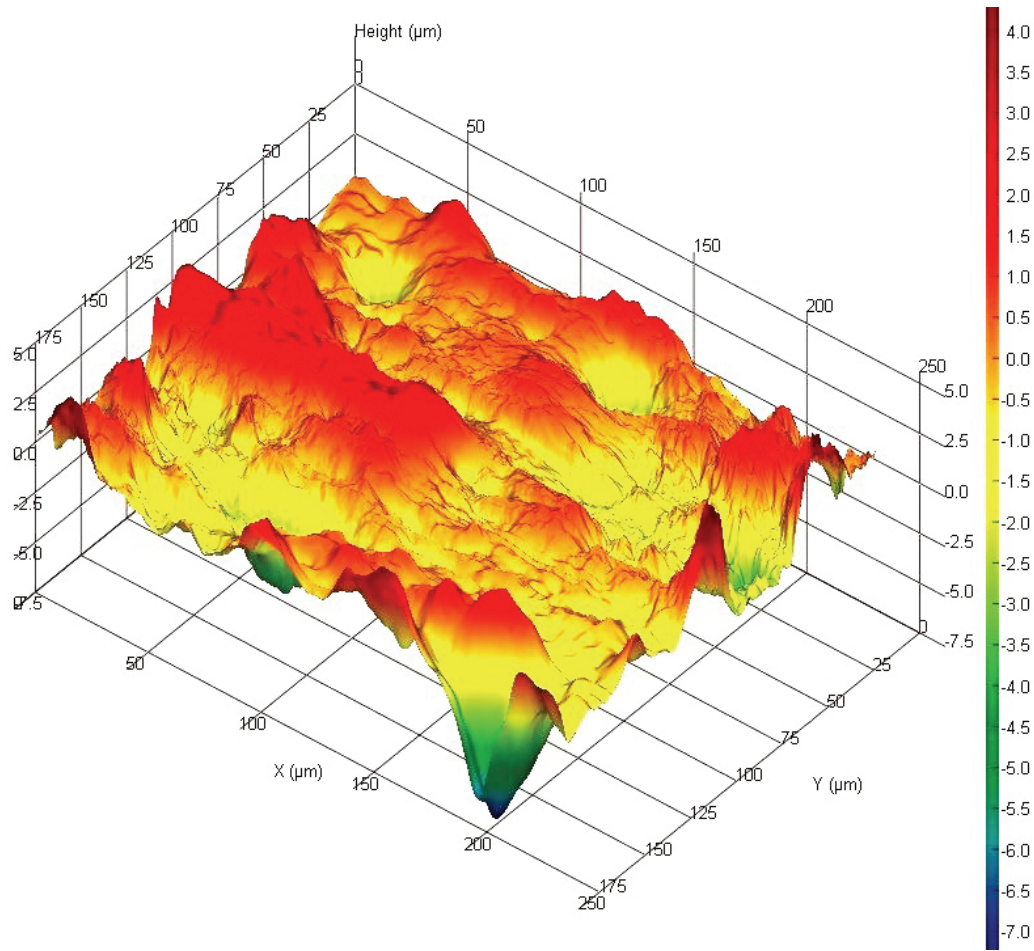| Cut − off length x 500 μm	Cut − off length y 500 μm
$S_a = 1.03 \ \mu m$	$S_t = 10.53 \ \mu m$
$S_q = 1.35 \ \mu m$	$S_z = 4.93 \ \mu m$
$S_{sk} = -0.0486$	$S_{ds} = 14956.49 \ summits/mm^2$
$S_{ku} = 3.91$	$S_{dr} = 3.19 \ \%$
$S_v = -5.67 \ \mu m$	$S_{ci} = 1.58$
$S_p = 4.86 \ \mu m$	
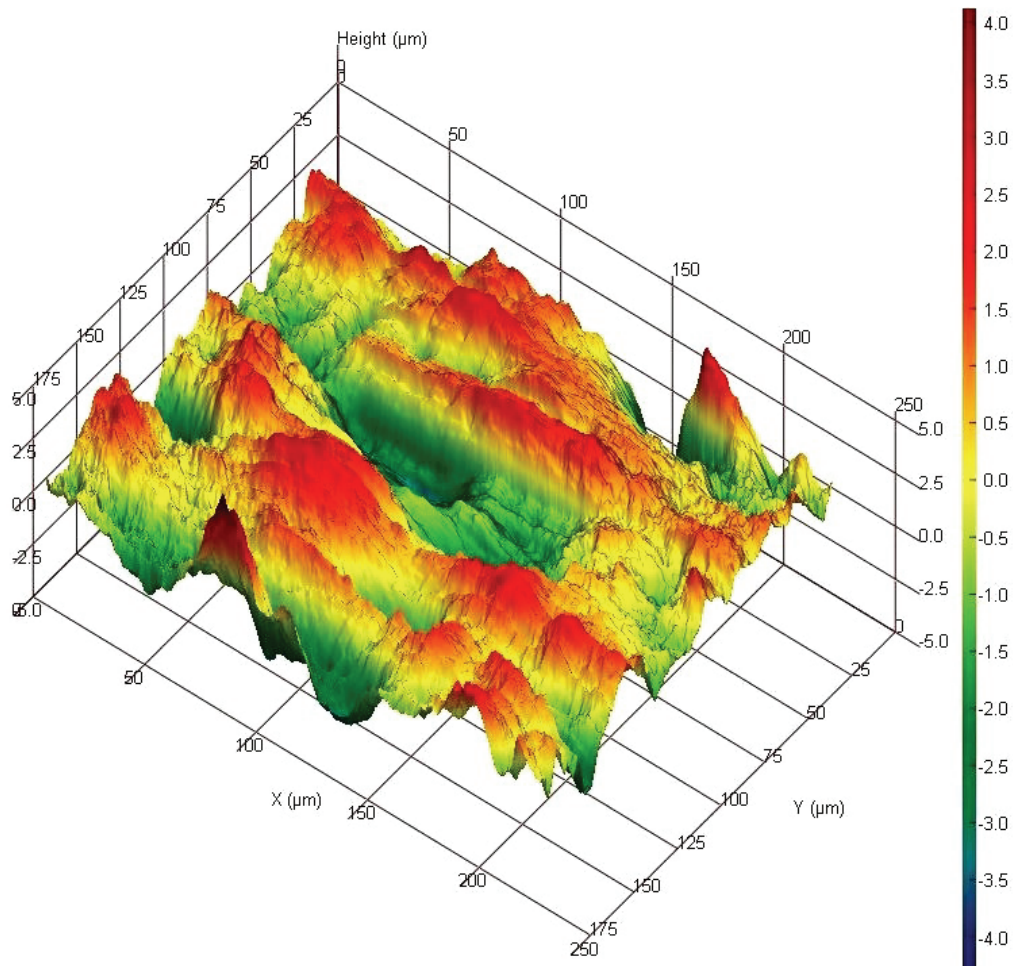
Figure A-18: Surface roughness for brass interrupted broaching (22nd teeth)

Table A-18: Roughness parameter values for brass interrupted broaching (22nd teeth)

$Cut-off\ length\ x\ 500\ \mu m$	$Cut-off\ length\ y\ 500\ \mu m$
$S_a = 0.946\ \mu m$	$S_t = 8.81\ \mu m$
$S_q = 1.17\ \mu m$	$S_z = 4.57\ \mu m$
$S_{sk} = -0.552$	$S_{ds} = 32335.4\ summits/mm^2$
$S_{ku} = 2.95$	$S_{dr} = 3.67\ \%$
$S_v = -4.46\ \mu m$	$S_{ci} = 1.4$
$S_p = 4.35\ \mu m$	
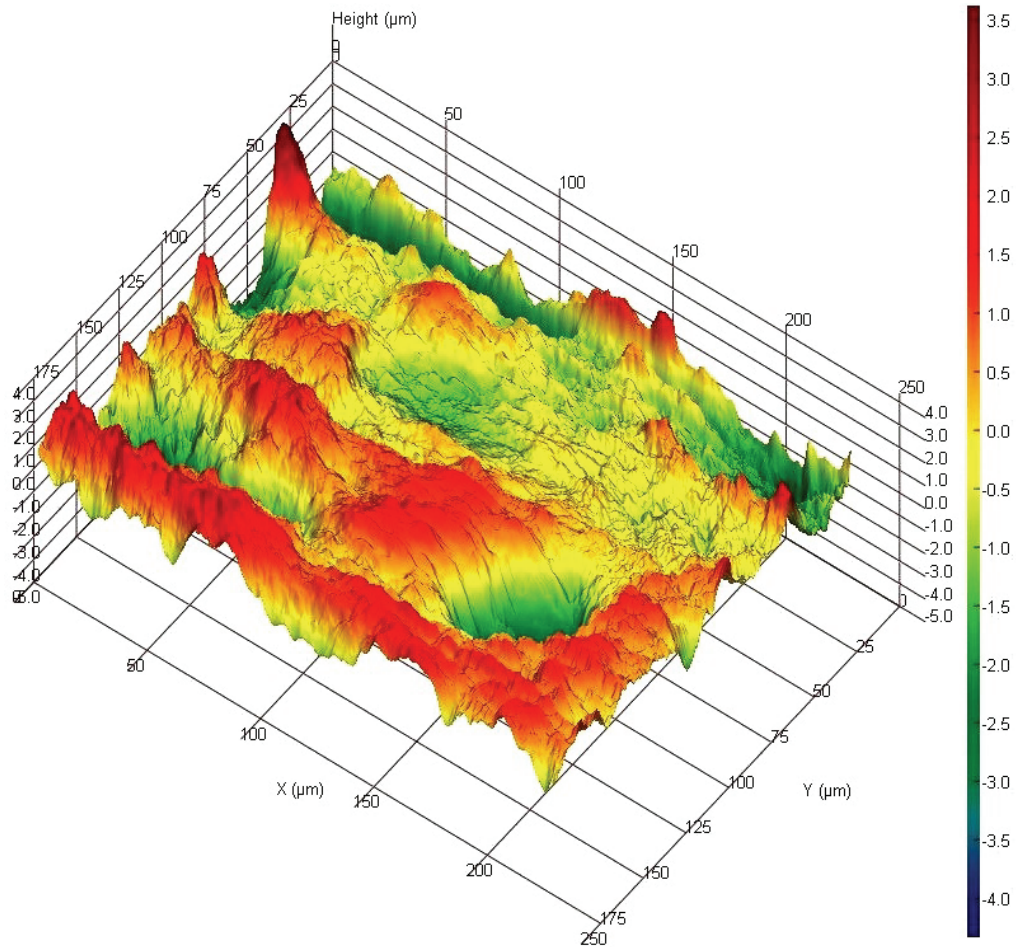
Figure A-19: Surface roughness for brass interrupted broaching (23rd teeth)

Table A-19: Roughness parameter values for brass interrupted broaching (23rd teeth)

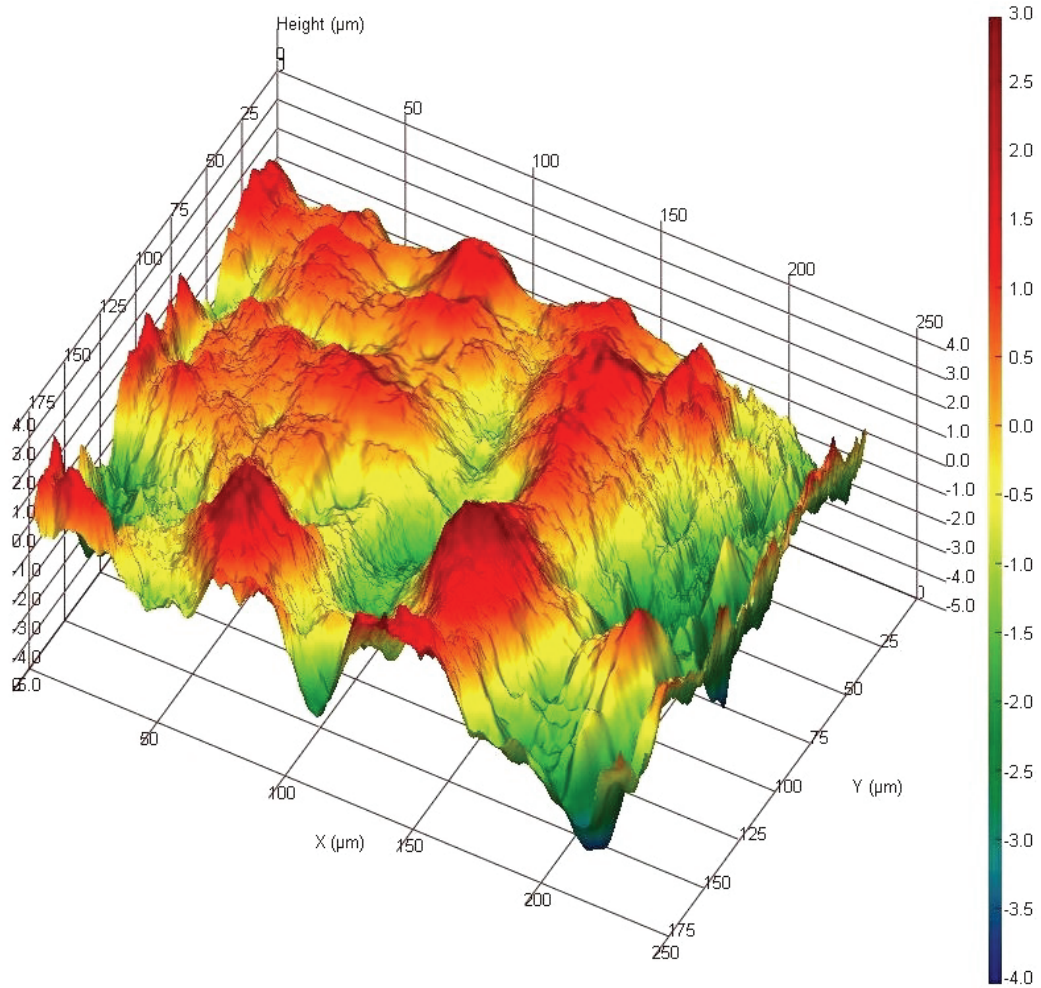| Cut − off length x 500 μm	Cut − off length y 500 μm
$S_a = 0.774\ \mu m$	$S_t = 8.23\ \mu m$
$S_q = 1.01\ \mu m$	$S_z = 3.86\ \mu m$
$S_{sk} = -0.733$	$S_{ds} = 31339.23\ summits/mm^2$
$S_{ku} = 3.95$	$S_{dr} = 2.23\ \%$
$S_v = -4.32\ \mu m$	$S_{ci} = 0.153$
$S_p = 3.92\ \mu m$	
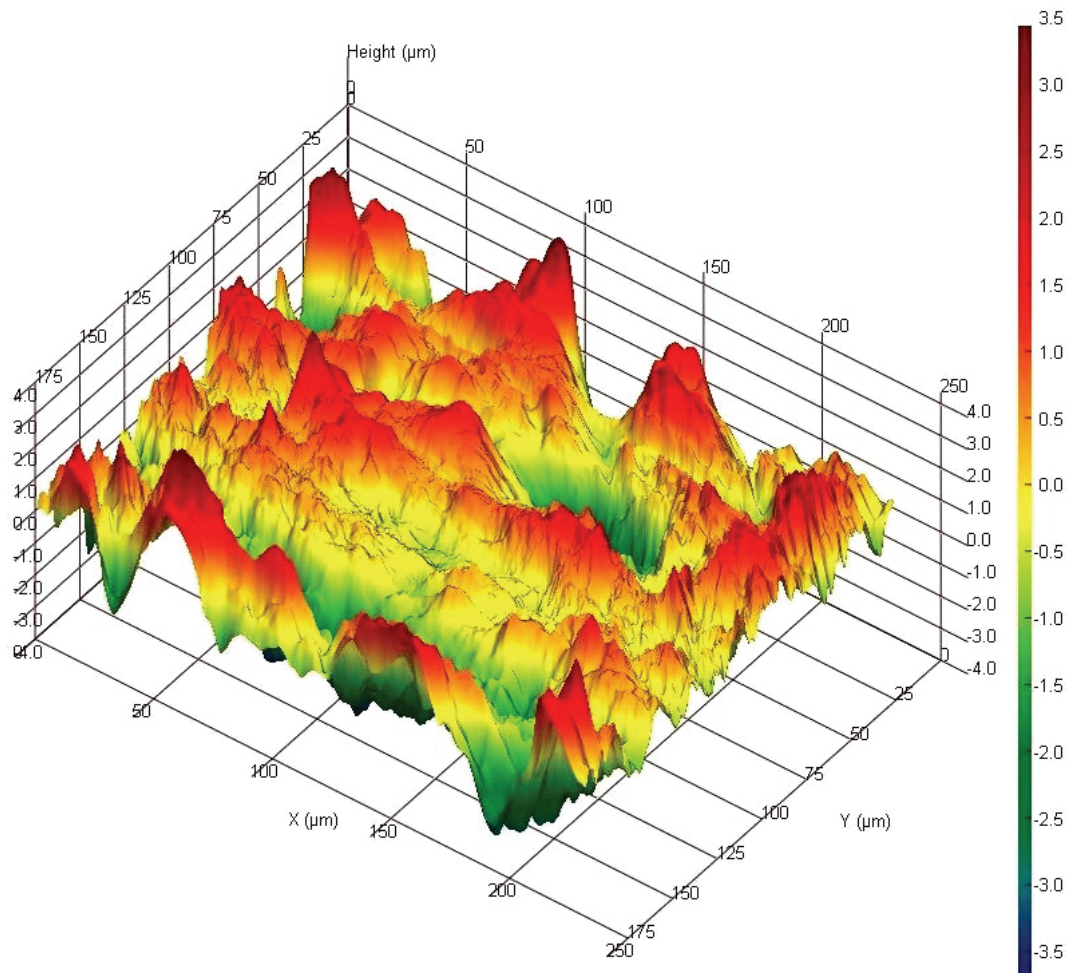
Figure A-20: Surface roughness for brass after broaching

Table A-20: Roughness parameter values for brass after broaching

Cut − off length x 500 μm	Cut − off length y 500 μm
$S_a = 0.806\ \mu m$	$S_t = 7.51\ \mu m$
$S_q = 1.04\ \mu m$	$S_z = 4.45\ \mu m$
$S_{sk} = -0.546$	$S_{ds} = 20580.97\ summits/mm^2$
$S_{ku} = 3.43$	$S_{dr} = 2.94\ \%$
$S_v = -3.95\ \mu m$	$S_{ci} = 1.41$
$S_p = 3.56\ \mu m$	

Appendix B: Copyright Permission Letters

Some contents of the presented thesis are completely adopted or partially revised from the papers that have been previously published or submitted for publication in scientific journals. These works have been done under the supervision of my research supervisor, Professor H.A. Kishawy, who is also the co-author.

The list of above mentioned papers and the copyright permissions from the corresponding publishers are as follows:

1- **Hosseini, A.,** Kishawy, H.,A., and El-Mounayri, H., "*A Solid Modeler Based Simulation of Chip Load in Broaching Operation*", Transaction of NAMRI/SME, Vol.39, pp. 217-223, 2011.

2- **Hosseini, A.,** and Kishawy, H.,A., "*B-spline Based General Force Model for Broaching*", Transaction of the NAMRI/SME, Vol.38, pp. 9-15, 2010.

3- Kishawy, H.,A., **Hosseini, A.,** Moetakef-Imani, B., Astakhov, V.,P., "*An Energy Based Analysis of Broaching Operation: Cutting Forces and Resultant Surface Integrity*", Annals of the CIRP - Manufacturing Technology, Vol. 61/I, pp. 107–110, 2012.

4- **Hosseini, A.,** Kishawy, H.,A., *"Prediction of Cutting Forces in Broaching Operation"*, Journal of Advanced Manufacturing Systems, (Accepted for publication), 2013.

Copyright Permission Letter

February 25, 2013

To whom it may concern

I am preparing my Ph.D. thesis entitled "Model Based Simulation of Broaching Operation: Cutting Mechanics, Surface Integrity and Process Optimization" for submission to the Office of Graduate Studies at the University of Ontario Institute of Technology (UOIT) in Oshawa, Ontario, Canada. I am seeking your permission to include a manuscript version of the following papers as a chapter in the thesis:

1- **Hosseini, A.,** Kishawy, H.,A., and El-Mounayri, H., *"A Solid Modeler Based Simulation of Chip Load in Broaching Operation"*, Transaction of NAMRI/SME, Vol.39, pp. 217-223, 2011.

2- **Hosseini, A.,** and Kishawy, H.,A., *"B-spline Based General Force Model for Broaching"*, Transaction of the NAMRI/SME, Vol.38, pp. 9-15, 2010.

Canadian graduate theses are reproduced by the Library and Archives of Canada (formerly National Library of Canada) through a non-exclusive, world-wide license to reproduce, loan, distribute, or sell theses. I am also seeking your permission for the material described above to be reproduced and distributed by the LAC(NLC). Further details about the LAC(NLC) thesis program are available on the LAC(NLC) website (www.nlc-bnc.ca).
Full publication details and a copy of this permission letter will be included in the thesis.

Yours sincerely,
Sayyed Ali Hosseini

Permission is granted for:
(a) The inclusion of the material described above in your thesis.
(b) For the material described above to be included in the copy of your thesis that is sent to the Library and Archives of Canada (formerly National Library of Canada) for reproduction and distribution.

Name: _Ellen J. Kehoe_   Title: _Senior Editor_
Signature: _Ellen J. Kehoe_   Date: _3-4-13_

Copyright Permission Letter

February 25, 2013

To whom it may concern

I am preparing my Ph.D. thesis entitled "Model Based Simulation of Broaching Operation: Cutting Mechanics, Surface Integrity and Process Optimization" for submission to the Office of Graduate Studies at the University of Ontario Institute of Technology (UOIT) in Oshawa, Ontario, Canada. I am seeking your permission to include a manuscript version of the following paper as a chapter in the thesis:

1- Kishawy, H.,A., **Hosseini, A.,** Moetakef-Imani, B., Astakhov, V.,P., *"An Energy Based Analysis of Broaching Operation: Cutting Forces and Resultant Surface Integrity"*, Annals of the CIRP - Manufacturing Technology, Vol. 61/I, pp. 107–110, 2012.

Canadian graduate theses are reproduced by the Library and Archives of Canada (formerly National Library of Canada) through a non-exclusive, world-wide license to reproduce, loan, distribute, or sell theses. I am also seeking your permission for the material described above to be reproduced and distributed by the LAC(NLC). Further details about the LAC(NLC) thesis program are available on the LAC(NLC) website (www.nlc-bnc.ca).
Full publication details and a copy of this permission letter will be included in the thesis.

Yours sincerely,
Sayyed Ali Hosseini

Please See the Attached Letter

Permission is granted for:
(a) The inclusion of the material described above in your thesis.
(b) For the material described above to be included in the copy of your thesis that is sent to the Library and Archives of Canada (formerly National Library of Canada) for reproduction and distribution.

Name: _____   Title: _____

Signature: _____   Date: _____

ELSEVIER LICENSE
TERMS AND CONDITIONS

Feb 25, 2013

This is a License Agreement between Sayyed Ali Hosseini ("You") and Elsevier ("Elsevier") provided by Copyright Clearance Center ("CCC"). The license consists of your order details, the terms and conditions provided by Elsevier, and the payment terms and conditions.

All payments must be made in full to CCC. For payment instructions, please see information listed at the bottom of this form.

Supplier	Elsevier Limited The Boulevard,Langford Lane Kidlington,Oxford,OX5 1GB,UK
Registered Company Number	1982084
Customer name	Sayyed Ali Hosseini
Customer address	2000 Simcoe Street North
	Oshawa, ON L1H7K4
License number	3096110035129
License date	Feb 25, 2013
Licensed content publisher	Elsevier
Licensed content publication	CIRP Annals - Manufacturing Technology
Licensed content title	An energy based analysis of broaching operation: Cutting forces and resultant surface integrity
Licensed content author	Hossam A. Kishawy,Ali Hosseini,Behnam Moetakef-Imani,Viktor P. Astakhov
Licensed content date	2012
Licensed content volume number	61
Licensed content issue number	1
Number of pages	4
Start Page	107
End Page	110
Type of Use	reuse in a thesis/dissertation
Portion	full article
Format	both print and electronic
Are you the author of this Elsevier article?	Yes
Will you be translating?	No
Order reference number	
Title of your thesis/dissertation	Model Based Simulation of Broaching Operation: Cutting Mechanics, Surface Integrity and Process Optimization

Expected completion date	Apr 2013
Estimated size (number of pages)	170
Elsevier VAT number	GB 494 6272 12
Permissions price	0.00 USD
VAT/Local Sales Tax	0.0 USD / 0.0 GBP
Total	0.00 USD

Terms and Conditions

INTRODUCTION

1. The publisher for this copyrighted material is Elsevier. By clicking "accept" in connection with completing this licensing transaction, you agree that the following terms and conditions apply to this transaction (along with the Billing and Payment terms and conditions established by Copyright Clearance Center, Inc. ("CCC"), at the time that you opened your Rightslink account and that are available at any time at http://myaccount.copyright.com).

GENERAL TERMS

2. Elsevier hereby grants you permission to reproduce the aforementioned material subject to the terms and conditions indicated.

3. Acknowledgement: If any part of the material to be used (for example, figures) has appeared in our publication with credit or acknowledgement to another source, permission must also be sought from that source. If such permission is not obtained then that material may not be included in your publication/copies. Suitable acknowledgement to the source must be made, either as a footnote or in a reference list at the end of your publication, as follows:

"Reprinted from Publication title, Vol /edition number, Author(s), Title of article / title of chapter, Pages No., Copyright (Year), with permission from Elsevier [OR APPLICABLE SOCIETY COPYRIGHT OWNER]." Also Lancet special credit - "Reprinted from The Lancet, Vol. number, Author(s), Title of article, Pages No., Copyright (Year), with permission from Elsevier."

4. Reproduction of this material is confined to the purpose and/or media for which permission is hereby given.

5. Altering/Modifying Material: Not Permitted. However figures and illustrations may be altered/adapted minimally to serve your work. Any other abbreviations, additions, deletions and/or any other alterations shall be made only with prior written authorization of Elsevier Ltd. (Please contact Elsevier at permissions@elsevier.com)

6. If the permission fee for the requested use of our material is waived in this instance, please be advised that your future requests for Elsevier materials may attract a fee.

7. Reservation of Rights: Publisher reserves all rights not specifically granted in the

combination of (i) the license details provided by you and accepted in the course of this licensing transaction, (ii) these terms and conditions and (iii) CCC's Billing and Payment terms and conditions.

8. License Contingent Upon Payment: While you may exercise the rights licensed immediately upon issuance of the license at the end of the licensing process for the transaction, provided that you have disclosed complete and accurate details of your proposed use, no license is finally effective unless and until full payment is received from you (either by publisher or by CCC) as provided in CCC's Billing and Payment terms and conditions. If full payment is not received on a timely basis, then any license preliminarily granted shall be deemed automatically revoked and shall be void as if never granted. Further, in the event that you breach any of these terms and conditions or any of CCC's Billing and Payment terms and conditions, the license is automatically revoked and shall be void as if never granted. Use of materials as described in a revoked license, as well as any use of the materials beyond the scope of an unrevoked license, may constitute copyright infringement and publisher reserves the right to take any and all action to protect its copyright in the materials.

9. Warranties: Publisher makes no representations or warranties with respect to the licensed material.

10. Indemnity: You hereby indemnify and agree to hold harmless publisher and CCC, and their respective officers, directors, employees and agents, from and against any and all claims arising out of your use of the licensed material other than as specifically authorized pursuant to this license.

11. No Transfer of License: This license is personal to you and may not be sublicensed, assigned, or transferred by you to any other person without publisher's written permission.

12. No Amendment Except in Writing: This license may not be amended except in a writing signed by both parties (or, in the case of publisher, by CCC on publisher's behalf).

13. Objection to Contrary Terms: Publisher hereby objects to any terms contained in any purchase order, acknowledgment, check endorsement or other writing prepared by you, which terms are inconsistent with these terms and conditions or CCC's Billing and Payment terms and conditions. These terms and conditions, together with CCC's Billing and Payment terms and conditions (which are incorporated herein), comprise the entire agreement between you and publisher (and CCC) concerning this licensing transaction. In the event of any conflict between your obligations established by these terms and conditions and those established by CCC's Billing and Payment terms and conditions, these terms and conditions shall control.

14. Revocation: Elsevier or Copyright Clearance Center may deny the permissions described in this License at their sole discretion, for any reason or no reason, with a full refund payable to you. Notice of such denial will be made using the contact information provided by you. Failure to receive such notice will not alter or invalidate the denial. In no event will Elsevier or Copyright Clearance Center be responsible or liable for any costs, expenses or damage incurred by you as a result of a denial of your permission request, other than a refund of the

amount(s) paid by you to Elsevier and/or Copyright Clearance Center for denied permissions.

LIMITED LICENSE

The following terms and conditions apply only to specific license types:

15. **Translation**: This permission is granted for non-exclusive world **English** rights only unless your license was granted for translation rights. If you licensed translation rights you may only translate this content into the languages you requested. A professional translator must perform all translations and reproduce the content word for word preserving the integrity of the article. If this license is to re-use 1 or 2 figures then permission is granted for non-exclusive world rights in all languages.

16. **Website**: The following terms and conditions apply to electronic reserve and author websites:
Electronic reserve: If licensed material is to be posted to website, the web site is to be password-protected and made available only to bona fide students registered on a relevant course if:
This license was made in connection with a course,
This permission is granted for 1 year only. You may obtain a license for future website posting,
All content posted to the web site must maintain the copyright information line on the bottom of each image,
A hyper-text must be included to the Homepage of the journal from which you are licensing at http://www.sciencedirect.com/science/journal/xxxxx or the Elsevier homepage for books at http://www.elsevier.com , and
Central Storage: This license does not include permission for a scanned version of the material to be stored in a central repository such as that provided by Heron/XanEdu.

17. **Author website** for journals with the following additional clauses:

All content posted to the web site must maintain the copyright information line on the bottom of each image, and the permission granted is limited to the personal version of your paper. You are not allowed to download and post the published electronic version of your article (whether PDF or HTML, proof or final version), nor may you scan the printed edition to create an electronic version. A hyper-text must be included to the Homepage of the journal from which you are licensing at http://www.sciencedirect.com/science/journal/xxxxx . As part of our normal production process, you will receive an e-mail notice when your article appears on Elsevier's online service ScienceDirect (www.sciencedirect.com). That e-mail will include the article's Digital Object Identifier (DOI). This number provides the electronic link to the published article and should be included in the posting of your personal version. We ask that you wait until you receive this e-mail and have the DOI to do any posting.

Central Storage: This license does not include permission for a scanned version of the material to be stored in a central repository such as that provided by Heron/XanEdu.

18. **Author website** for books with the following additional clauses:

Authors are permitted to place a brief summary of their work online only.
A hyper-text must be included to the Elsevier homepage at http://www.elsevier.com . All
content posted to the web site must maintain the copyright information line on the bottom of
each image. You are not allowed to download and post the published electronic version of
your chapter, nor may you scan the printed edition to create an electronic version.

Central Storage: This license does not include permission for a scanned version of the
material to be stored in a central repository such as that provided by Heron/XanEdu.

19. **Website** (regular and for author): A hyper-text must be included to the Homepage of the
journal from which you are licensing at http://www.sciencedirect.com/science/journal
/xxxxx. or for books to the Elsevier homepage at http://www.elsevier.com

20. **Thesis/Dissertation**: If your license is for use in a thesis/dissertation your thesis may be
submitted to your institution in either print or electronic form. Should your thesis be
published commercially, please reapply for permission. These requirements include
permission for the Library and Archives of Canada to supply single copies, on demand, of
the complete thesis and include permission for UMI to supply single copies, on demand, of
the complete thesis. Should your thesis be published commercially, please reapply for
permission.

21. **Other Conditions**:

v1.6

**If you would like to pay for this license now, please remit this license along with your
payment made payable to "COPYRIGHT CLEARANCE CENTER" otherwise you will be
invoiced within 48 hours of the license date. Payment should be in the form of a check
or money order referencing your account number and this invoice number
RLNK500964535.
Once you receive your invoice for this order, you may pay your invoice by credit card.
Please follow instructions provided at that time.**

**Make Payment To:
Copyright Clearance Center
Dept 001
P.O. Box 843006
Boston, MA 02284-3006**

**For suggestions or comments regarding this order, contact RightsLink Customer
Support: customercare@copyright.com or +1-877-622-5543 (toll free in the US) or
+1-978-646-2777.**

**Gratis licenses (referencing $0 in the Total field) are free. Please retain this printable
license for your reference. No payment is required.**

Copyright Permission Letter

February 25, 2013

To whom it may concern

I am preparing my Ph.D. thesis entitled "Model Based Simulation of Broaching Operation: Cutting Mechanics, Surface Integrity and Process Optimization" for submission to the Office of Graduate Studies at the University of Ontario Institute of Technology (UOIT) in Oshawa, Ontario, Canada. I am seeking your permission to include a manuscript version of the following paper as a chapter in the thesis:

1- Hosseini, A., Kishawy, H.,A., *"Prediction of Cutting Forces in Broaching Operation"*, Journal of Advanced Manufacturing Systems, (Accepted for publication), 2013.

Canadian graduate theses are reproduced by the Library and Archives of Canada (formerly National Library of Canada) through a non-exclusive, world-wide license to reproduce, loan, distribute, or sell theses. I am also seeking your permission for the material described above to be reproduced and distributed by the LAC(NLC). Further details about the LAC(NLC) thesis program are available on the LAC(NLC) website (www.nlc-bnc.ca).
Full publication details and a copy of this permission letter will be included in the thesis.

Yours sincerely,
Sayyed Ali Hosseini

Please See the Attached Email

Permission is granted for:
(a) The inclusion of the material described above in your thesis.
(b) For the material described above to be included in the copy of your thesis that is sent to the Library and Archives of Canada (formerly National Library of Canada) for reproduction and distribution.

Name: _____   Title: _____

Signature: _____   Date: _____

Sayyed Ali Hosseini

From: Gopalan Mukundan <gmukundan@chrysler.com>
Sent: February-25-13 4:40 PM
To: Sayyed Ali Hosseini
Subject: RE: Copyright Permission Request

Ali,

Yes, you can do that.

With Personal Regards,

Mukundan
ICT NAFTA Head Product Design, Engineering, Powertrain & Product Planning
Chrysler Group LLC
CIMS 483 01 19
Tel: +1 248 838 4901
Tieline: 8 821 4901

From: Sayyed Ali Hosseini [mailto:SayyedAli.Hosseini@uoit.ca]
Sent: Monday, February 25, 2013 4:18 PM
To: Gopalan Mukundan
Cc: Hossam Kishawy
Subject: Copyright Permission Request

Dear Dr Mukundan

I am preparing my Ph.D. thesis entitled "Model Based Simulation of Broaching Operation: Cutting Mechanics, Surface Integrity and Process Optimization" for submission to the Office of Graduate Studies at the University of Ontario Institute of Technology (UOIT) in Oshawa, Ontario, Canada. I am seeking your permission to include a manuscript version of my following paper (accepted for publication) as a chapter in the thesis:

1- Hosseini, A., Kishawy, H.,A., "Prediction of Cutting Forces in Broaching Operation", Journal of Advanced Manufacturing Systems, (Accepted for publication), 2013.

Attached, Please find the Copyright permission form.
I would be appreciated if you could fill it out and return it to me at your earliest convenience.
I really appreciate your time and your very kind consideration.
Sincerely Yours,
…………………………………………………………………………….
Ali Hosseini
PhD Candidate
Department of Mechanical Engineering
University of Ontario Institute of Technology
Oshawa, ON, Canada